CUK-H05299+16-V7166096

DYNAMICS OF THE LOWER TROPOSPHERE :

A DIAGNOSTIC CRITIQUE OF PRE–MONSOON AND MONSOON SCENARIOS

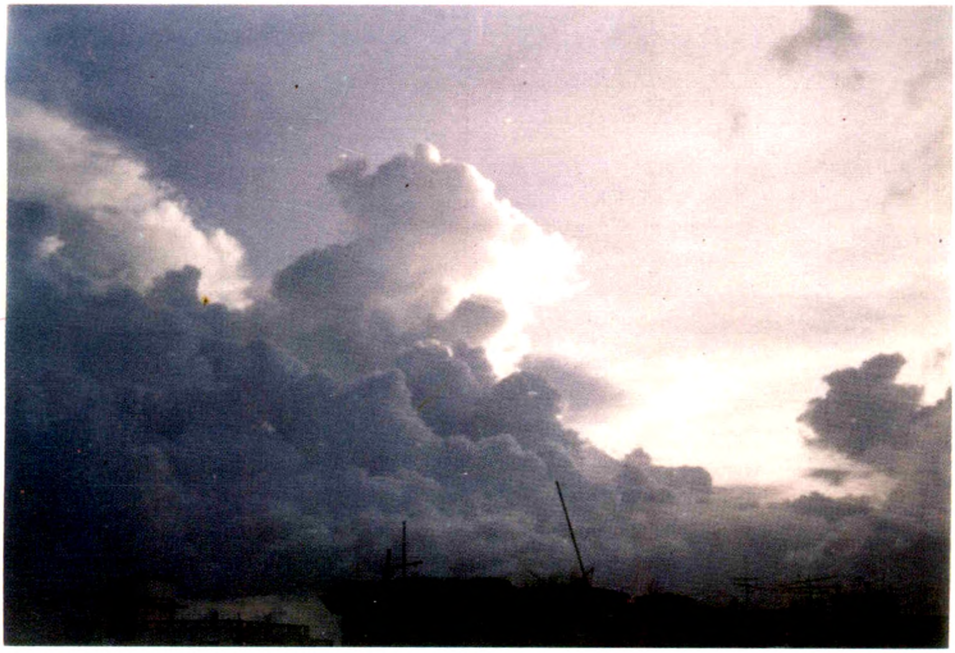

D.K. SINHA
G.K. SEN
M. CHATTERJEE

UNIVERSITY OF CALCUTTA
CALCUTTA
1996

DYNAMICS OF THE LOWER TROPOSPHERE :
A DIAGNOSTIC CRITIQUE OF PRE-MONSOON AND MONSOON SCENARIOS

16

DYNAMICS OF THE LOWER TROPOSPHERE :
A DIAGNOSTIC CRITIQUE OF PRE-MONSOON AND MONSOON SCENARIOS

Dilip K. Sinha
Goutam K. Sen
Meenakshi Chatterjee

Centre for Atmospheric Sciences
University of Calcutta

CALCUTTA UNIVERSITY
CENTRAL LIBRARY

UNIVERSITY OF CALCUTTA
CALCUTTA
1996

About the Authors

Sinha, D.K.	**Ghose Professor of Applied Mathematics, University of Calcutta and Coordinator, Centre for Atmospheric Sciences, University of Calcutta (on lien). Currently, Vice-Chancellor, Visva-Bharati, Shantiniketan, 731235.**
Sen, G.K.	**Research Scientist, Centre for Atmospheric Sciences, University of Calcutta, 92, A.P.C. Road, Calcutta 700 009.**
Chatterjee, M.	**Research Associate, Centre for Atmospheric Sciences, University of Calcutta, 92, A.P.C. Road, Calcutta 700 009.**

Price

India : Rs. 150.00; Foreign : $ 25.00

G166096

Printed by Sri Pradip Kumar Ghosh, Superintendent, Calcutta University Press,
48, Hazra Road, Calcutta : 700 019.

Contents

Page

Preface

List of Symbols and Acronyms

Chapter 1. Prologue **1–8**

1.1 The Indian Summer Monsoon 1

1.2 The Monsoon Trough 2

1.3 The Atmospheric Boundary Layer 4

1.4 The Monsoon Trough Boundary Layer Experiment 6

Chapter 2. Handling Data : A Prelude to Mathematical Modelling **9–12**

2.1 The Computation of Richardson Numbers 9

2.2 Generation and Initialization of Fine Mesh Data 12

Chapter 3. Understanding The Physical Processes in The Atmospheric Boundary Layer Through Mathematical Modelling **13–26**

3.1 The Non-local Closure Model : Transilient Turbulence Theory 15

3.2 The Second Order Local Closure Model 20

3.3 The Linear Wave Model 22

Chapter 4. Pre-Monsoon Scenarios : Model Results **27–46**

4.1 Intercomparison of ABL Fluxes During The Pre-Monsoon Period 29

4.2 Internal Gravity Waves in the Pre-Monsoon Troposphere Part I : The Effect of Phase Speed on Stability 32

4.3 Internal Gravity Waves in the Pre-Monsoon Troposphere Part II : Their Role in Storm Development. 35

4.4 Numerical Simulation of the Lower Tropospheric Structure : During a Nor'wester. 43

Chapter 5. Monsoon Scenarios : Model Results **47–53**

5.1 Understanding the Turbulence Structure of The Monsoon Trough Boundary-Layer Part I. : Results from the T3 model 48

5.2 Understanding the Turbulence Structure of the Monsoon Trough Boundary Layer Part II : The Role of Pressure Covariance and Dissipation 51

Bibliography 54

Preface

Atmospheric Sciences, in recent times, has acquired a variety of strands. The scenario of pursuits in this field is fast changing. While observational findings continue to be the mainstay of such endeavours, there is a greater urge than ever before to move well beyond such exercises. Needless to add that computational facilities coupled with modelling have augmented the status of understanding in various aspects of such investigations.

The Indian setting invariably offers meteorological phenomena, which have, since antiquity, drawn the attention of several investigators. For example, the study of monsoons is an integral part of our fabric of civilization. The phase of MONEX, in recent times, has brought out several characteristic features of the monsoon hitherto unknown. As a follow up, the Monsoon Trough Boundary Layer Experiment or MONTBLEX has been conceived as a coupling between the monsoon trough and apposite boundary layer features. This, of course, has been rightly accorded top priority. The experimental outfits brought in its trail a host of data and characteristics, which need to be made use of for capturing the essence of the dynamical processes in such phenomena. Obviously, this may lead to a wide canvas and hence, a significant step would be to look at them from a diagnostic point of view. This is precisely what this book seeks to do.

The methodologies adopted here are based on frequently used ways of reckoning characteristic features of boundary layers. Whatever might be the limitations in regard to the adequacy and reliability of the data, we have sought to present a fairly understandable level of the dynamics of the phenomena and the structure of turbulence of the boundary layer over the north Indian plains during the pre–monsoon and monsoon phases.

The layout of this book is structured in five chapters. There is a rationale behind sequencing these chapters which becomes discernible at a first glance. There is also an attempt to have each chapter as a prelude to the next one which deals with some conceptual framework. An apparently offbeat area in Chapter 4 is that of Internal Gravity Waves which is something distinctive this treatise has to offer, there being no erstwhile attempt to look at Nor'westers from this standpoint. Another hallmark of the book is the use of the Transilient Turbulence Theory and Second Order Local Closure, not widely used in the Indian context.

An important spinoff of this work is the study of Nor'westers. Nonlinearities do not seem to have been taken up in greater depth in such scenarios. It is to be hoped that the investigations here on Nor'westers will trigger off fresh approaches, with a conceptual aspect, which will strengthen the fairly voluminous and dominantly observational studies on Nor'westers that already exist.

Calcutta
25th January 1996

D.K.S.
G.K.S.
M.C.

Acknowledgement

The contents of this book are the outcome of the research investigations carried out in the project 'On Aspects of Model Studies from MONTBLEX' funded by the **Department of Science and Technology (DST), Government of India**. We gratefully acknowledge the DST for this support.

We also wish to express our gratitude to the **India Meteorological Department (IMD), Government of India** and the **Indian Institute of Tropical Meteorology (IITM)**, Pune, for supplying us with the data used for these studies.

Several individuals helped us by their cooperation, valuable suggestions and discussions, at various stages. We extend our heartfelt thanks to them. In particular, we thank Dr.(Mrs.) Malti Goel (DST), Dr. N. Sen Roy, Dr. G.S. Mandal, Dr. M.K. Guha and Dr. H.N. Srivastava (IMD), Dr. K.G. Vernekar and Dr. S. Shivaramakrishnan (IITM), Dr. Y. Ramanathan, Dr. D.K. Rakshit (Jadavpur University), Dr. U.C. Mohanty (IIT, Delhi), Prof. R. Narasimha, Dr. A. Prabhu and Dr.(Mrs.) Kusuma G. Rao (IISc., Bangalore) and the Staff Members of the Computer Centre, IITM, Pune.

It is indeed a pleasure to acknowledge gratefully the encouragement and impetus that Dr.J.S.A. Green of the University of East Anglia provided during his visit to our Centre in 1991, for pursuing these boundary layer studies.

We specially thank Prof. P.K. Das for his constant encouragement.

We thank Prof. R.N. Basu, Vice-Chancellor, Calcutta University for consenting to the publication of this book.

Finally, we express our warmest appreciation to Shri Pradip Kumar Ghosh, Superintendent, Calcutta University Press and all members of his staff who bore with us with immense patience and cooperated extensively for bringing out this treatise.

List of Symbols & Acronyms

asl	above surface level
A, A_i, A_{0i}	abbreviative constants
ABL	Atmospheric Boundary Layer
AMTEX	Air Mass Transformation Experiment
c	phase velocity
c_{ij}	elements of transilient matrix
C	constants in solution of
C	Transilient matrix
C_D	drag coefficient
CISK	Conditional Instability of the Second Kind
D	constants used in fitting α (z) profile
D_Y	dimensionless, nonlocal dissipation parameter
$D^*(z)$	normalized wave induced divergence
DST	Department of Science & Technology, Government of India
e	turbulence kinetic energy
E	constants used in fitting α (z) profile
f	Coriolis parameter; function of a variable
F	function of a variable
F_k	nonlocal flux at height $k \Delta z$
$F_{k/m}$	nonlocal transport spectral components at height $k \Delta z$
FGGE	First GARP Global Experiment
g	acceleration due to gravity; suffix for geostrophic wind components
GARP	Global Atmospheric Research Programme
GATE	GARP Atlantic Tropical Experiment
i	grid or layer index
IGW	Internal Gravity Wave
IIOE	International Indian Ocean Experiment
IMD	India Meteorological Department
ISMEX	Indo Soviet Monsoon Experiment
ITCZ	Inter Tropical Convergence Zone
j_{max}	total number of vertical grid points/observation levels
k	meridional wave number; grid or layer index
k_0	Von Karman constant
k_i	complex constant
k_{ri}, k_{ji}	real and imaginary parts of k_i

K	coefficient of eddy diffusivity
l	mixing length; zonal wave number
l_r, l_j, l_k	nonlocal mixing lengths
L_k	nonlocal weight wavelength at height $k \Delta z$
LST	Local Standard Time
m	horizontal wave number; grid index
MONEX	Monsoon Experiment
MONTBLEX	Monsoon Trough Boundary Layer Experiment
N	total number of vertical grid points
N_d	total number of gridpoints in turbulent subdomain
$N(z)$	Brunt – Väisäla frequency
p	pressure
P_o	unperturbed component of pressure
$P_{k/m}$	nonlocal process spectral component at height $k \Delta z$
$P(z)$	amplitude of perturbed pressure
Q_0	residual term in thermodynamic equation
Ri	gradient Richardson number
R_{ij}	nonlocal bulk Richardson number
R_c	Critical Richardson number for onset of turbulence
R_T	Critical Richard number for termination of turbulence
s	suffix denoting near surface values
SBL	Stable Boundary Layer
t	time
Δt	time interval
T_0	nonlocal characteristic time scale
TKE	Turbulence Kinetic Energy
TM	Transilient Matrix
u	zonal (west to east) wind component
u_g	zonal geostrophic wind component
u_0	nonlocal horizontal velocity scale
U_*	friction velocity
$u'w'$	vertical component of kinematic heat flux
U_0	unperturbed zonal wind velocity
$U(z)$	amplitude of perturbed zonal wind velocity
v	meridional (south to north) wind component
$v'w'$	vertical component of kinematic meridional momentum flux
V_0	unperturbed meridional wind velocity
$V(z)$	amplitude of perturbed meridional wind velocity

VIMHEX	Venezuelan International Meteorology and Hydrology Experiment
W	vertical velocity component
W_{ij}	nonlocal weighting factor
W_*	convective velocity scale
$w'e$	vertical turbulent transport of TKE
$w'p'$	pressure covariance
$w'\theta'$	vertical component of kinematic (potential temperature) flux
$w'\theta_v'$	vertical component of buoyancy (vertical potential temperature) flux
$W(z)$	amplitude of perturbed vertical velocity
x	horizontal cartesian coordinate, positive eastwards
X	variable
y	horizontal cartesian coordinate, positive northwards
Y_{ij}	nonlocal mixing potential
z	vertical cartesian coordinate, positive upwards
z_i	height of ABL top
z_0	aerodynamic roughness length
Δz	vertical grid length
Z	variable
α	stability parameter
α (z)	modified Scorer's parameter
δ_{ij}	Kronecker delta fuction
Δ_{ij}	nonlocal difference operator
ϵ	rate of viscous dissipation of TKE
θ	potential temperature
θ_v	virtual potential temperature
Θ	phase of IGW mode
λ	asymptotic value of local mixing length
Λ	characteristic turbulence length scale
μ	constant used in fitting α (z) profile
ξ	variable representing property of state of air
ρ	density of air
σ	frequency of IGW mode
Σ	summation
χ	rate of molecular dissipation of TKE
ω	intrinsic frequency of IGW mode

All throughout the text, primes denote fluctuations from mean quantities and over bars denote averages.

In India, LST = GMT + 0530 hours.

Chapter 1

Prologue

1.1 The Indian Summer Monsoon

The South-West or, summer monsoon, is the most important climatological feature in the Indian sub-continent. Occurring over a hundred day period, from June to mid-September, each year the summer monsoon provides, on an average, seventy percent of the total annual rainfall over entire north and central India and the narrow strip of the Indian penninsula between the Western Ghat mountains and the Arabian Sea. The regular appearance of the summer monsoon over the past thousands of years has made India a primarily agricultural country, with more than sixty percent of her population engaged in agriculture with an economy dominantly dependent on the agricultural produces.

The strength of the monsoon current and the accompanying rainfall shows interannual variability, resulting in below or above normal monsoons in certain years. Both these cases are damaging to agriculture and the Indian economy. Interseasonal fluctuations of the monsoon flow are a characteristic feature during which 'active' periods of copious rainfall alternate with 'break' or dry spells. Normally, the onset of the monsoon over the Kerala coast is around the third week of May and around 15 June over Central India. Late onsets occur in many years, which again disrupts the agricultural calendar. Such vagaries of the monsoon has been known from time immemorial and the urgent need for investigation and identification of the physical processes responsible for the development of the monsoon circulation over India, with the view of predicting its onset and strength, has been strongly felt ever since the setting up of the India Meteorological Department (IMD) in the late nineteenth century.

The occurrence of monsoons in various other parts of the world during the northern and southern hemispheric summers, makes them global phenomena, which has attracted the interest and attention of the international community of meteorologists and atmospheric physicists. There exists a virtual plethora of published research on various facts of the monsoon, particularly after the conclusion of international field experiments, such as, the Global Atmospheric Research Programme or GARP (1967), the International Indian Ocean Experiment or IIOE (1963-65), the Indo-Soviet Monsoon Experiment of ISMEX (1973-1977) and the Monsoon Experiment or MONEX (1979). Very comprehensive reviews of the component features of the summer monsoon can be found in IMD (1960, 1970), Ramage (1971), Rao (1976), Das (1986), Lighthill and Pearce (1977), and others. However, it will not be out of the context to briefly mention the important characteristic features associated with the monsoon circulation and some of the research results emerging from the above experiments, especially from MONEX which are relevant to the subject of this book, namely, the investigation of the premonsoon and monsoon trough boundary layers over India.

The word 'monsoon', implies a consistent and seasonal reversal of winds brought about by the differential heating of land and oceans. This thermal contrast between land and oceans is a result of the differences in their times of response to the heating by the incoming solar radiation. During the northern hemispheric summer, when the sun lies over the Tropic of Cancer, winds blow from the sea to the land, bringing in large amounts of moisture. This results in copious rainfall in regions over which these monsoon winds prevail. During the northern hemispheric winter, the thermal contrast is reversed and the winds blowing from the land to the sea are dry. Simply stated, the monsoon is often conceptualized as a giant sea-breeze circulation. Complexities of the chracteristic features observed in the monsoon on the global, regional and local scales arise due to interactions of the large scale dynamical processes with the diabatic heating field, orography and land and sea surfaces (Inners and Gregory, 1994).

In the planetary scale, monsoons are maintained by east-west oriented Walker type and north-south oriented Hadley type circulations. These are in turn driven by planetary scale heat sources and sinks which also display a south east to northwest orientation with warming over Papua and New Guinea and cooling over northwest India, Pakistan and adjoining countries of Middle East (Wei et al., 1981; Wei and Johnson, 1982; Ackerman and Cox 1982; Blake et al., 1983). These diabatic heat sources and sinks, together with the strong convection in the southeastern part of the Tibetan Plateau has been found to be the major sources of generation of eddy available potential energy which are converted to strong planetary scale motions via the east-west overturnings (Krishnamurti and Kanamitsu, 1981; Pasch, 1983). The conversion of the available potential energy to kinetic energy dominantly takes place in the upper troposphere between ultra-long waves (numbers 1 and 2) and the mean flow (Mohanty et al 1983; Krishnamurti and Kanamitsu 1982) with marked variations in the transfer of energy from year to year. A significant and rapid increase in the kinetic energy just before the onset and during the early stages of the Indian monsoon over Central India has been observed (Mohanty et al., 1982; Krishnamurti and Ramanathan, 1982; Pasch, 1983). Another prominent feature observed during the arrival of the monsoon is the periodic movement of the westerly and easterly jet streams and the near-equatorial trough and the Inter Tropical Convergence Zone (ITCZ).

Satellite evidence indicates the ITCZ as a zone of narrow cloud bands between 5°-15° on either side of the equator. Over the summer monsoon regime, 70°E-90°E, two separate cloud bands, one around 15°N and another slightly south of the equator have been identified, one of which is the near-equatorial trough. Yearly variations in the location of these two troughs are observed. It has been suggested (Datta et al., 1982) that the near equatorial trough and the ITCZ are separate identities both of which move northward during late May to mid July. During years of normal monsoon over India, the ITCZ is located north of the equatorial trough. Erratic and late onsets of the Indian monsoon occurs when the ITCZ lies south of the near equatorial trough. It has been suggested that (Charney, 1969, 1973) cumulus friction allied to Conditional Instability of the Second Kind (CISK) is responsible for the maintenance and dynamics of the ITCZ.

The planetary scale features of the monsoon circulation are closely linked to regional features, although the precise coupling mechanisms between them are not well understood as yet.

The most important regional feature of the Indian summer monsoon are short period fluctuations in rainfall that are observed during the break and active phases. Normally, the duration of each of these periods is about a week, but prolonged breaks occur, specially during weak monsoons and in the second half of duration of normal monsoons (Ramamurthi, 1969). Associated with these alternate break and active phases is the southward and northward movement of the monsoon trough, a low pressure belt oriented east west across India, Pakistan and the middle-east countries.

1.2 The Monsoon Trough

During the pre-monsoon months of April and May, the northwest Indian desert and adjoining areas in Pakistan and middle-east Asia, become extremely heated. A low presure belt, a thermal low, develops over these regions due to the ascent of the heated air. This low level thermal low is a shallow system, extending not higher than the 850 h Pa level (that is, about 1 km above sea level). With the arrival of the summer monsoon, this thermal low becomes elongated and extends right across India, Pakistan and middle-east Asian countries. Meteorologists in India refer to this as the *monsoon trough.* There exists conflicting evidence on the identity of the monsoon trough, the near equatorial trough and the ITCZ during the summer monsoon. Although sufficient evidence exists indicating a north ward movement of the near equatorial trough, the precise mechanism responsible for the coupling of the trough with the thermal low is not clearly known (Das, 1986).

In its normal position, the axis of the Monsoon Trough lies parallel to the southern boundary of the Himalayas and extends from around 85°E - 90°E in northern Bay of Bengal to 70°E-75°E in West Rajasthan and adjoining Pakistan (Figure 1.1)

The eastern end of the trough is the seat of deep moist convection. The principal rain bearing systems of the Indian summer monsoon, the monsoon depressions, form in this northern part of the Bay of Bengal and move westward along the trough, bringing heavy rainfall to the Gangetic planes. On an average, two to three such systems form each month with highest occurrences during July and August. The Western end of the trough, in contrast, is a region of dry convection, with subsidence prevailing from above the near surface layer throughout the entire troposphere. With the gradual advance of the monsoon and the occurence of the monsoon depressions, moisture is drawn westward and even western Rajasthan recieves a good amount of rainfall. Between 75°E-85°E, over Bihar and Uttar Pradesh, the monsoon trough is a region of alternate zones of deep moist or unsaturated processes.

Although the monsoon trough is a quasi-permanent feature of the summer monsoon, oscillations of the axis about its normal position are a characteristic feature which is responsible for the active and break phases mentioned above. During break phases, the axis of the trough shifts northwards and lies close to the Himalayan foothills (Ramamurthi, 1969; Pant et al., 1970). Rise in surface temperatures over the plains south of the trough, decrease in rainfall over these regions and also Central and Western India and a weakening of the Arabian Sea branch of the monsoon are observed during breaks due to lower tropospheric anticyclonic vorticity and subsidence over the Indo-Gangetic plains. North eastern India, however, recieves heavy rainfall during such phases.

Active spells of heavy monsoonal precipitation are associated with the southward shift of the trough axis with the eastern end located low over north Bay of Bengal. Fluctuations in the radiation balance of the earth-atmosphere-ocean system are believed to influence these movements of the trough (Das, 1986). The rise in pressure along the monsoon trough region during breaks has been attributed to low frequency phenomenae with temporal scales of 10-20 days and 30-50 days which are among the dominant low frequency modes of the tropical sea level pressure field (Krishnamurti, 1984). Several investigations on the relations between the active/break cycle of the Indian monsoon and these low frequency oscillations (Yasunari, 1981; Sikka and Gadgil, 1980; Krishamurti et al., 1984), revealed interesting results, based on the FGGE/MONEX data sets. A superposition of the westward propagating ridge lines on the 10-20 day scale (zonal wave numbers 4, 5 and 6) and the eastward propagating ones on the 30-50 day scale (zonal wave numbers 1, 2 and 3) and their 30-50 meridional passage over central India was found to be responsible for an observed break period during 15-25 July 1979 (Krishnamurti et al., 1984). Both types of meridionally moving troughs and ridges originate near the equator, amplify as they approach 10^0N and then dissipate as they approach the Himalayan foothills. At the 850 mb level, the troughs are associated with ascending motion and cloudiness and the ridges, with subsiding motion. In fact, Krishnamurti and Subrahmanyam (1982), Krishnamurti (1984) suggest that the onset, active and break phenomenon of the Indian summer monsoon are related to the passage of these low frequency systems. Earlier investigators have attributed the northward shift of the monsoon trough to, interaction between it and the development and subsequent track of a monsoon depression (Raghavan, 1973); weak middle troposheric or surface lows moving across south India (WMO, 1978); and extension of a middle tropospheric ridge from Indo-China across central India (Dixit and Jones, 1965). Obviously, the exact mechanisms leading to a break situation are not yet fully understood although it is more or less agreed that a unique combination of events precede and accompany break monsoon conditions (Keshavamurty and Awade, 1974).

1.3 The Atmospheric Boundary Layer

The atmospheric boundary layer (ABL) is the lowest 1-2 km of the troposphere that is influenced by the presence of the earth's surface and responds to thermal and dynamical forcings on it. Characteristic temporal scales of this response ranges from a few seconds to an hour. Characteristic spatial scales range from a few millimeteres to several kilometers in the horizontal and from a few meters to around 1 km on an average in the vertical.

The depth of the ABL varies in space and time and is dependent on the intensity of the surface forcings and the conditions prevailing within and above the ABL. Above the ABL lies the stable, free atmospheric layer of the troposphere extending to the tropopause. The ABL can be identified by the presence of an inversion layer across which an abrupt change in the thermodynamic and wind fields is observed. Within the ABL, temperature lapse rates may be locally superadiabatic in which case the ABL is said to have an unstable thermal stratification. Stably stratified ABL's have locally subadiabatic lapse rates. Zero temperature lapse rates result in neutral ABL's. The classification of ABL layers into superadiabatic, adiabatic and subadiabatic, in a non-local sense has been discussed in Stull (1991, 1992).

The most important and interesting physical feature in the ABL is turbulence, generated as a result of surface forcings. Thus, heating and cooling of the earth's surface in response to the incoming solar radiation, frictional drag exerted by the underlying surface on the air above it, evaporation and transpiration, wind shear, raditional cooling, surface inhomogeneties etc. are some the surface forcings that generate turbulence. Vertical transport of mass, momentum, heat, moisture and energy to different layers of the ABL by turbulent eddies is the most important physical process within it. Turbulent transport modifies the mean flow within the ABL which, on a longer time scale, influences the free atmospheric flow above the ABL top.

Forcings outside the ABL, such as thunderstorms, with their intense up and down drafts, downward propagating internal gravity waves generated in dynamically unstable shear layers aloft, advection of air masses having different characteristics and subsidence, also modify the ABL flow characteristics. Within stable boundary layers, buoyancy generated internal gravity waves are a common feature on which, propagating upwards are reflected from the upper levels of the ABL. Modification of the SBL structure due to wave activity, is a frequently observed feature.

The size of the turbulent eddies vary widely, from a few millimeters to several hundred meters. The larger eddies, such as thermals, are organised coherent structures that trigger the formation of boundary layer clouds, usually stratus, stratocumulus and shallow cumulus, near the upper parts of the ABL, just below the inversion. Boundary layer clouds form a very important feature which again modifies the ABL structure and the free atmospheric layer above it. Radiative cooling from the cloud top triggers convection, generating small scale turbulent eddies within the cloud which causes local mixing. Entrainment of dry free atmospheric air at the cloud top and the intensity of the turbulent transport from below play important roles in the evolution of the cloud. The height of the ABL top, the rate of entrainment and the degree of surface forcings, determine to a great extent, the evolution of the mean flow within the ABL. A very interesting discussion on the interactions between ABL clouds and ABL turbulence is given in Randall (1985).

A very intriguing type of ABL, is the stable boundary layer (SBL). The nocturnal boundary layer is an example of an SBL. Turbulence within the SBL is usually very weak and is maintained by mechanical wind shear. The delicate balance between turbulence generated in this way and its supression by buoyancy and dissipation often varies, resulting in SBL's that can be well mixed to those that are non-turbulent. Radiative cooling of the earth's surface is an important forcing in the SBL and can be of the same order of magnitude as the cooling by turbulence (Garatt and Brost, 1981; Andre and Mahrt, 1982). The characteristics of the mean flow within the SBL are complicated and are influenced by topography, buoyancy, friction and entrainment in the lower layers, resulting in katabatic and drainage winds. The nocturnal jet of wind maxima observed near the SBL top is caused by synoptic and mesoscale forcings (Kraus et al., 1985; Stull, 1988). An important component of the Indian summer monsoon, the low level Somali jet is an SBL feature (Stull, 1988). Veering with height is another characteristic of the SBL winds. The SBL top is difficult to identify because of the subadiabatic temperature profile throughout the layer. Even the turbulence within the SBL is rather unusual in the sense that zones of patchy turbulence exist frequently. Observations also indicate that turbulence aloft is often independent of the forcings below. The prevalence of internal gravity wave activity within the SBL has already been mentioned. All these features, added to the difficulty of direct measurements, have made the SBL structure less well understood than its unstable counterpart.

The tropical boundary layer of the low level trade wind circulation regime is characterised by high temperatures and humidity leading to more frequent cloud formations than that observed in mid-latitude ABL's. The ABL top, coincides with the trade wind inversion below which lie the cloud layer, separated by a stable transition layer from the subcloud layer below. Findings from tropical experiments such as IIOE, BOMEX (1969), GATE (1974), AMTEX (1974-75), VIMHEX (1976), indicate that in the tropical boundary layer, particularly over oceans, considerable vertical transports of momentum near the low level jets and counter gradient transports of momentum and heat and thermal energy take place at certain levels (Pennell and Lemone, 1974). The evolution of clouds and their development into tall cumulonimbi is very rapid under favourable conditions frequently ecxisting in the tropical ABL, particularly during the pre-monsoon and monsoon phases. The ITCZ and the near equatorial trough are regions of deep organised cumulus convection which lead to the formation of mesoscale cloud clusters. It is through the individual cumulonimbus clouds and these mesoscale cloud clusters that the ABL air with its high energy content is transported to the upper troposphere (Houze, 1989). Organised cumulus convection within the tropical ABL plays a crucial role in modifying the dynamics of the large scale flow through their control of the budgets of heat, momentum and moisture. In fact, many synoptic scale systems are maintained by the effects of cumulus convection (Bates, 1977). The tropical oceans are the largest sources of heat and the marine boundary layer proceses are influenced by evaporation from the ocean surface, surface wind driven ocean currents and turbulent exchange of fluxes of heat, moisture and momentum at the air-sea interface. The latent heat-energy accumulates in the ABL in the divergent-part of the trade winds and is transported to the ITCZ by the large scale flow where it is released through condensation.

In the Indian context, the land surface processes in the ABL during the pre-monsoon months, play an important role in Nor'wester development. The intense dry convection within the ABL supports the thermal low over the north Indian plains. As the monsoon approches, the transition from shallow convection to deep moist convection occurs, beginning at the eastern end of the monsoon trough. The possibility of a feedback mechanism between the eastern and western ends of the trough through mesoscale orgainsation of clouds, monsoon lows and depressions when the monsoon is well advanced, has been suggested (DST,1990).

The differential heating between land and oceans, which, as has been mentioned earlier, is the primary mechanism for development of the monsoon circulation, is highly dependent on the radiation balance of the earth-atmosphere-ocean system. This in turn is determined by ABL parameters such as the albedo of the land or ocean surface, soil moisture content, snow cover of the Himalayas, sea surface temperatures clouds and aerosol concentrations, (Das, 1986).

Many of the factors controlling the genesis, development and movement of the monsoon depressions, the principal rain bearing systems of the Indian summer monsoon, are esentially ABL processes such as latent and sensible heat transfer from the sea surface, friction and turbulent transports. Regions of latent heat released due to evaporation from the sea surface in the Bay of Bengal favour the formation of incipient depressions which develop into depressions under additional conditions. The precise mechanisms leading to the development of these depressions are not very well understood at present. It has been observed however, that unlike pre-or post-monsoon cyclones, monsoon depressions do not persist long over the oceans. Also, the existence of large scale vertical wind shear, suppresses latent heat accumulation. These facts are thought to be responsible for the relatively lower intensities of these depresions than those observed in cyclones.

The periods of active and break monsoon are characterised by a complete change of the circulation pattern below 500mb. It would be interesting to investigate how the land locked monsoon trough boundary layer responds to these forcings from aloft and the role it plays in maintianing the break period. It has been suggested that due to the wide diurnal variation of the radiative cooling in the tropical atmosphere, important feedback processes between radiative-convective processes possibly exist (Betts, 1978) and their interaction with the large scale dynamics control the north-south movements of the monsoon trough during these phases (DST, 1990). How the monsoon activity recovers from such break phases and the role of the thermodynamic and dynamic changes within the ABL at the beginning and end of a break phase are interesting and important areas for further investigation.

1.4 The Monsoon Trough Boundary Layer Experiment

The Monsoon Trough Boundary Layer Experiment (MONTBLEX) conducted during May to August 1990 over north India and the northern Bay of Bengal was the first national field experiment that addressed several key issues regarding the Indian monsoon, the primary one being investigations of the boundary layer processes within the land locked portion of the monsoon trough. The necessity for conducting such an experiment arose due to the fact that, inspite of the international experiments conducted earlier such as, IIOE (1964), GARP (1967), ISMEX (1973, 1977), MONEX (1979) gaps still existed in our full understanding of various aspects of the monsoon. A brief survey of the objectives of these experiments will clarify the point.

The primary objectives of GARP (1967) were (Das, 1986): (a) the study of large scale fluctuations in the atmosphere that controls changes in weather and (b) examination of the physical basis of climate. The other monsoon experiments, namely, IIOE (1964), ISMEX (1973, 1977) and MONEX (1979) also largely concentrated on the synoptic scale features of the monsoon. During MONEX 79, a programme for studying the ABL over land was included but this covered only the eastern coastal regions of India and over the Arabian sea. Thus in MONEX 79, as well as in the earlier experiments mentioned above the emphasis had been on the study of the marine boundary layer and as such, no data could be collected on the processes within the boundary layer of the land locked monsoon trough (see also DST, 1990).

In order to understand and quantify the processes of interaction of the monsoon trough boundary layer and the large scale flow and their role in organising deep moist convection with periodic reversal to unsaturated shallow convection, a plan for a national field experiment, the **Monsoon Trough Boundary Layer Experiment** or **MONTBLEX** was proposed to be conducted during 15 May to 22 September 1990 under the sponsorship of the Department of Science and Technology, Government of India. Details of the specific tasks and other objectives can be found in DST (1990). The data collecting network consisted of :

1. Surface and instrumented tower measurements of temperature, moisture, wind and momentum fluxes at various points within the monsoon trough where, characteristic features such as dry convection (Jodhpur 26.18^{0}N, 73.04^{0}E), unsaturated convection (Delhi, 28.38^{0}N, 77.12^{0}E) (Varanasi, 25.2^{0}N, 83^{0}E) and deep moist convection (Kharagpur, 22.3^{0}N, 87.2^{0}E) during onset, advance, active, bread and withdrawal periods of the monsoon.

2. Soil temperature and moisture measurements.

3. Estimation of the boundary layer height by SODAR at each of the tower sites.

4. Routine (three hourly) surface synoptic observations at all surface observatories within the monsoon trough region.

5. Six hourly radiosonde/rawinsonde observations at Jodhpur, Delhi, Varanasi, Calcutta throughout the duration of the experiment and at all other stations within the trough region during Intensive Observation Periods (IOP's).

6. Radiometer soundings at all tower sites or close to them for measuring pressure, temperature, long and shortwave radiation.

7. Six hourly Pilot balloon ascents at non-rawinsonde stations during IOP's.

8. Standard surface radiation observations at stations within the monsoon trough region.

9. Tetheredsonde ascents (upto 1 km) in the deep moist part of the monsoon trough at Kharagpur.

10. Mini-radiosonde ascents at all tower sites.

11. Low level aircraft flights (500m and 1000m) over the trough region.

12. Ship observations of surface meterological, micro-meteorological tower, radiosonde, omegasonde XBT profile, STD profile in the marine boundary layer near a monsoon depression.

13. INSAT cloud pictures and outgoing long wave radiation (OLR) over 2.50 lat/long grid within the monsoon trough region, eight times a day.

14. Ceilometer observations of cloud base heights within the trough region whereever possible.

At present,data are archived and available from the MONTBLEX data bank at the Indian Institute of Tropical Meteorology, Pune.

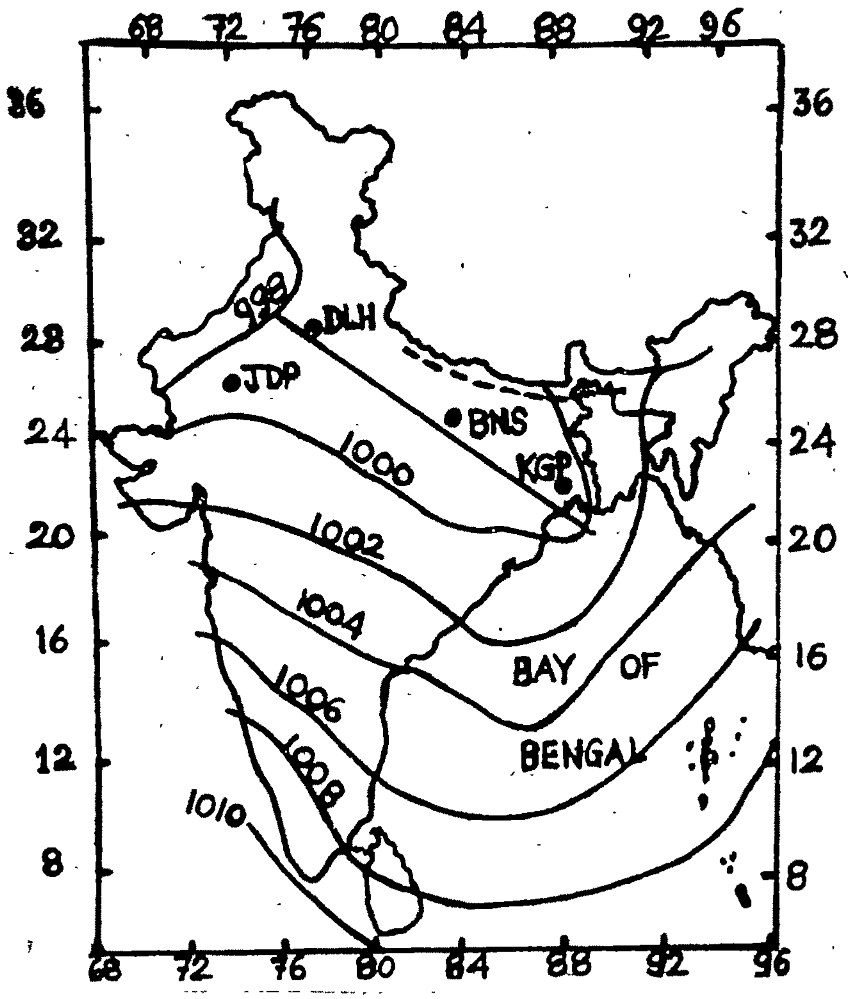

Figure 1.1 : Schematics showing the position of the land-locked monsoon trough over India and location of some MONTBLEX observation platforms in the region. Thick line represents the normal position and dotted line, the position during 'break' periods.
KGP – Kharagpur BNS – Varanasi DLH – Delhi and JDP – Jodhpur

Chapter 2

Handling Data : A Prelude to Mathematical Modelling

The primary objective of analysing meteorological data is the quantified visualization of the structure of the atmosphere at a given location and at a given time. Empirical methods for data analyses are often used, the inherent subjectivity of which frequently leads to disagreement of forecasts issued by meteorologists and also with the observed meteorological situation at the forecast hour.

With the development of the mathematical theory of dynamical meteorology and its success in connecting the theory with actual observations, mathematical models for weather prediction or for diagnosing physical processes in the atmosphere, began to replace the empirical methods and with the great advances in computer technology through the past few decades, led to the development of sophisticated mathematical models for operational forecasts and for research purposes, with an obvious and close feedback between them.

The numerical integration of such models, require the accurate specification of boundary and initial conditions, which have to be provided by the observations from the existing network of meteorological observatories. The model grid in most cases does not coincide with the location of these stations and the observed data have to be interpolated or objectively analysed to provide the basic set of grid point data from which the model is integrated.

Objective analysis of data, disturbs the approximate balance that is observed to exist in the large scale wind and pressure fields and when used directly, causes inaccurate and 'noisy' forecasts. To restore this balance, the grid point data are subjected to the process of initialization, in which the wind and pressure fields are adjusted by means of the steady state simplified versions of the governing equations. This procedure is the static initialization of the objectively analysed data. Other methods of initializing the data, which are widely used at present, include dynamic and normal mode initialization in which the objectively analyzed data are restored to a state of dynamic equilibrium.

Models for investigating meso-scale or smaller scale atmospheric phenomena are extremely sensitive to inaccuracies of the basic data set as they require highly accurate specification of the boundary and initial conditions to produce meaningful results. The spatial and temporal resolutions of these models have to be finer than those required for large scale weather prediction and general circulation models.

This problem of getting basic data over a finely resolved spatial and temporal grid becomes more acute for ABL studies. For ABL models, through which we wish to investigate physical processes in the atmosphere having a temporal scale ranging from a few seconds to an hour and a spatial scale ranging from a few metres to a few kilometers, small scale processes such as turbulence, radiative heat fluxes, condensation and soil-vegetation cover-atmosphere interactions need to be known along with the topography and effects of baroclinicity and non-stationarity.

Even at present, the meteorological observatories follow the conventional network of providing routine surface and upper air radiosonde observations designed principally for synoptic scale operational weather forecasting and do not provide data for ABL studies. Specially designed field experiments have been conducted from time to time to collect data specifically for ABL studies, but these are very expensive to run and provide data for localised regions only.

In order to use them for ABL studies, a method has been developed for generating data that are finely resolved in the vertical and then statically initializing them, from the more readily available, routine, radiosonde data collected by the IMD. This is described in the subsequent sections. This static initialization procedure retains physical properties of the atmospheric layers such as heating/cooling rates etc. and also include the effect of baroclinicity. The method can also be applied to initialize tetheredsonde and slow ascent balloon data to free them from oscilatory modes arising due to the movements of the sondes.

The method also provides an analytical expression for computing the Richardson numbers, which does not involve the computation of gradients, but depends on physical parameters such as the surface roughnesss and the layer heating/cooling rates or other physical properties. The gradient Richardson number, Ri, the most frequently used indicator of the thermal stability of a layer of air, is the ratio of the buoyant production and mechanical shear production terms in the turbulence kinetic energy budget equation and is computed from :

$$\mathrm{Ri}=\frac{g}{\theta_v}\frac{\partial \theta_v}{\partial z}\left[\left(\frac{\partial u}{\partial z}\right)^2+\left(\frac{\partial v}{\partial z}\right)^2\right]^{-1} \qquad (2.1,\ 1)$$

2.1 The computation of Richardson numbers

The steady state equations governing mean flow within the ABL under assumptions of horizontal homogeneity and no subsidence are :

$$f\left(u-u_g\right)=\frac{\partial}{\partial z}\left(\overline{v'w'}\right) \qquad (2.1,\ 2)$$

$$-f\left(v-v_g\right)=\frac{\partial}{\partial z}\left(\overline{u'w'}\right) \qquad (2.1,\ 3)$$

$$0=\frac{\partial}{\partial z}\left(\overline{w'\theta_v'}\right)+Q_o \qquad (2.1,\ 4)$$

$$\text{with}\quad u_g=-\frac{1}{\rho f}\frac{\partial p}{\partial y},\ v_g=\frac{1}{\rho f}\frac{\partial p}{\partial x}$$

where primes denote fluctuating parts of the flow velocity components u,v,w and the virtual potential temperature θ_v;(u_g, v_g)are the geostrophic wind components and f ~ 10^{-5} is the Coriolis parameter of the latitude at Calcutta (22.34° N, 88.24° E).

In (2.1,3), the term Q_o can be considered as a residual term representing tendencies such as layer heating/cooling rates, advection, non-stationarity, radiation, subsidence, etc. For the present case, Q_o is taken as the layer averaged heating/cooling rate computed from successive radiosonde observations.

Another important effect, that of baroclinicity has also been incorporated by using the variation of u_g, v_g with height.

The system of equations, (2.1, 2) → (2.1, 4) are closed using first order local closure, namely, K-theory [Blackadar (1962), Estoque and Bhumralkar (1970)] :

$$\left(\overline{u'w'},\ \overline{v'w'},\ \overline{w'\theta_v'}\right)=K(z)\left(\frac{\partial u}{\partial z},\frac{\partial v}{\partial z},\frac{\partial w}{\partial z}\right) \qquad (2.1,\ 5)$$

$$K(z)=l^2(z)\left[\left(\frac{\partial u}{\partial z}\right)^2+\left(\frac{\partial v}{\partial z}\right)\right]^{1/2} f(\mathrm{Ri}) \qquad (2.1,\ 6)$$

$$\text{where,} \quad f\ (\mathrm{Ri}) = \begin{cases} 1+\alpha\,\mathrm{Ri}, \dfrac{\partial \theta_v}{\partial z} > 0 \text{ (stable)} \\ (1+\alpha\,\mathrm{Ri})^{-1}, \dfrac{\partial \theta_v}{\partial z} < 0 \text{ (unstable)} \end{cases} \tag{2.1, 7}$$

Ri (z) is the gradient Richardson number defined in (2.1, 1) and K (z) is the coefficient of eddy diffusivity.

The mixing length l (z) is determined from Estoque and Bhumralkar (1970):

$$l\,(z) = \frac{k_0(z+z_0)}{1+\dfrac{k_0(z+z_0)}{\lambda}}, \qquad \lambda = 0.0027\frac{(u_g^2+v_g^2)^{1/2}}{f} \tag{2.1, 8}$$

Here $k_o = 0.4$ is the von Karman constant and $z_o = 0.01$m is the roughness length representative of the flat, grassy terrain near the observation site at Calcutta.

Assuming that at the earth surface z = 0, no exchange of turbulent fluxes takes place, we can specify the lower boundary condition as (Stull, 1988):

$$K\ (z) = 0 \text{ at } z = 0 \tag{2.1, 9}$$

Integration of (2.1, 4) from z = 0 to any level z and use of the condition (2.1, 9) provides an expression connecting $\frac{\partial \theta_v}{\partial z}$, $Q_o(z)$ and K (z). Elimination of K (z) between this euqtion and (2.1, 6) and use of (2.1, 1) and (2.1, 8) yields an integral expression connecting $\frac{\partial \theta_v}{\partial z}$, Ri (z), z_o and λ. Integration of this expression between any two layers $[\,z_j, z_{j+1}\,]$ is possible, if Ri(z) is assumed to be constant within this layer. Finally, we obtain,

$$\theta_v^{2/3}(j+l) - \theta_v^{2/3}(j) = F\ (\mathrm{Ri}) \int_{Z_j}^{Z_{j+1}} (Z-k_o z_o)^{2/3}\left(1+\frac{\lambda}{Z}\right)^{4/3} dZ \tag{2.1, 10}$$

$$\text{where, } Z = k_o(z+z_o) \text{ and } F\ (\mathrm{Ri}) = \frac{2}{3}\left[\frac{Q_o^2}{g k_o^5 \lambda^4}\,\frac{\mathrm{Ri}(z)}{f^2\ (\mathrm{Ri})}\right]^{1/3} \tag{2.1, 11}$$

The integral on the right of (2.1, 10) is solved numerically. Depending on the thermal stratification of the layer $[\,z_j, z_{j+1}\,]$, we obtain a cubic equation for Ri (z) for unstable cases and a qudratic equation in Ri (z) for stable cases.

Thus, for the unstable case, using (2.1, 7), in (2.1, 10) one obtains,

$$\mathrm{Ri}^3 - \frac{2}{\alpha}\,\mathrm{Ri}^2 + \frac{1}{\alpha}\mathrm{Ri} - \frac{A}{\alpha^2} = 0 \tag{2.1, 12}$$

and for the stable case,

$$\alpha^2\,\mathrm{Ri}^2 + (2\alpha - A)\,\mathrm{Ri} + 1 = 0 \tag{2.1, 13}$$

where

$$A = \frac{8}{27}\frac{Q_o^2}{g\lambda^4 k_o^5}\left(\frac{I_j}{\Delta\,\theta_j}\right)^3 \tag{2.1, 14}$$

$$\Delta\,\theta_j = \theta_v^{2/3}\,(j+1) - \theta_v^{2/3}\,(j) \tag{2.1, 15}$$

and I_j denotes the value of the integral in (2.1, 10).

Using the well known conditions for the existence of real roots, we obtain a criteria for prescribing α for unstable and stable cases. This are :

a) For unstable cases,

$$\text{(i) if } A > 0\,,\ 0 < \alpha < \frac{4}{27A}$$

$$\text{and (ii) if } A < 0\,,\ \alpha < \frac{4}{27A} \qquad (2.1, 16)$$

and b) For stable cases,

$$\alpha \geq -\frac{1}{4A} \qquad (2.1, 17)$$

In both cases, the smaller of the roots having the appropriate sign (Ri < 0 for unstable and Ri > 0 for stable) is chosen as the Richardson number Ri (z_j) representative of the layer [z_j , z_{j+1}].

Thus Ri (z_j) for all layers j = 1, 2,.. , j_{max}-1 is computed, where z_{jmax} denotes the highest observation level.

2.2 Generation and initiatization of the fine mesh data

The procedure for generating the fine resolution data involves the following steps :

Step 1 : The stability of a layer between two adjacent observation level z_j and z_{j+1} are determined according as $\frac{\partial \theta_V}{\partial z} < 0$ (unstable case) or $\frac{\partial \theta_V}{\partial z} > 0$ (stable case).

Step 2 : Using the appropriate forms of f (Ri) from (2.1, 7) values of Ri (z_j) are computed as outlined in Section 2.1.

Step 3 : Using observed values of θ_V,u,v, at z_j and z_{j+1} as the lower and upper boundary conditions equations (2.1, 2) – (2.1, 4) are integrated numerically to obtain θ_V,u,v, at the mid-level $z_{j+1/2} = 0.5\ [z_j + z_{j+1}]$. This step is carried out for all j = 1,2,.., jmax–1.

Step 4 : Steps 1 to 3 are repeated between the layers [z_j ,$z_{j+1/2}$] and [$z_{j+1/2}$, z_{j+1}] with each vertical interval being successively halved till the desired vertical resolution (50m for the present case) is reached.

To initialize the generated data, we again solve the system of equations (2.1, 2) – (2.1, 5), using as lower and upper boundary conditions, the observed values of θ_V,u,v, at the lowest and highest observation level, till covergence is reached.

The above procedure has been applied to initialize the data generated at 50m intervals from radiosonde observations taken by the IMD at Calcutta, Ranchi (23.23°N, 85.23°E) and Bhubaneswar (20.15°N, 85.52°E) and the observed and initialized profiles of θ_V,u,v, for 0515 GMT on 10 and 22 May 1988 shown in Figures 2.1-2.4. In Figure 2.5, the observed and initialized profile of θ_V,u,v, over Calcutta at 1200 GMT on 22 May has been shown. These initialized data have been used in our investigations of the ABL processes during the pre-monsoon phase described in Chapter 4.

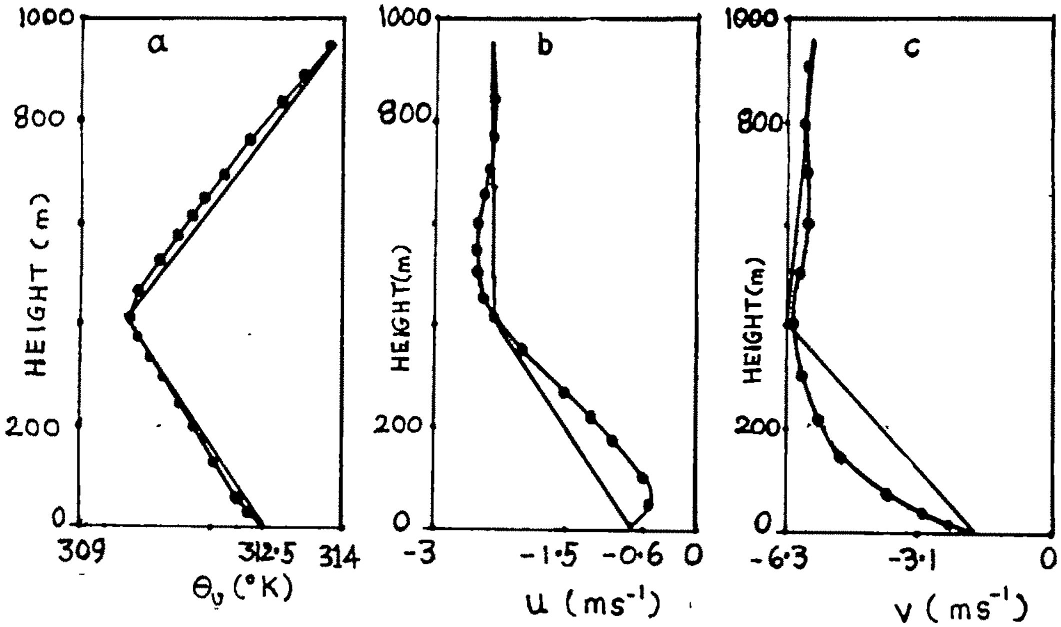

Figure 2.1 : Profiles of a) virtual potential temperature θ_v (°K), b) zonal wind u (ms^{-1}) and c) meridional wind v (ms^{-1}) at Calcutta 0515 GMT, 10 May 1988.
——— Observed ——●—— Generated and initialized data at 50m intervals.

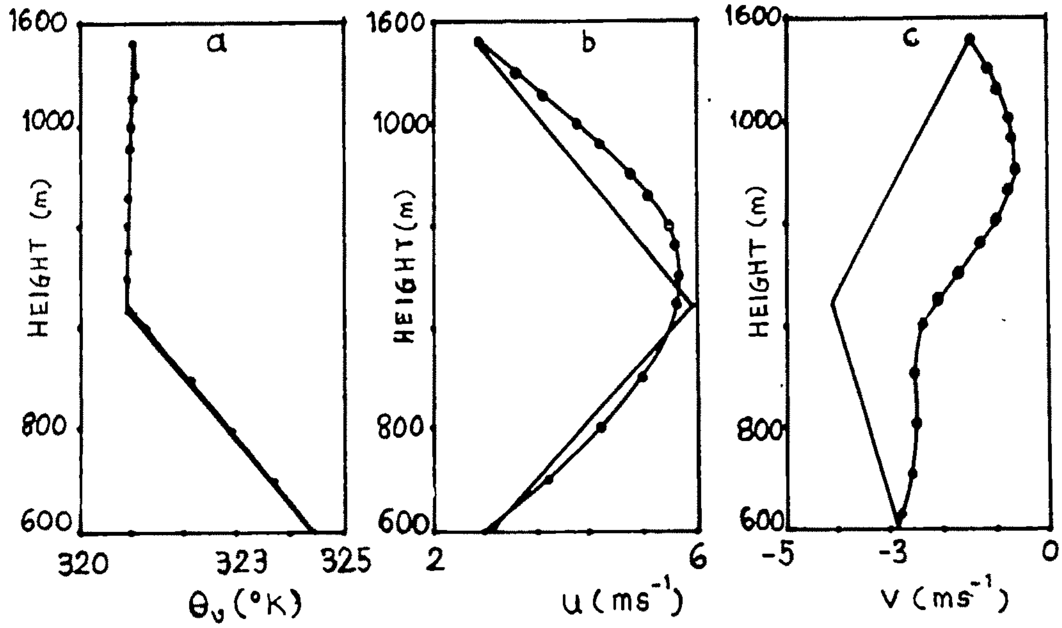

Figure 2.2 : Same as in Fig 2.1, for Ranchi, 0515 GMT, 10 May, 1988

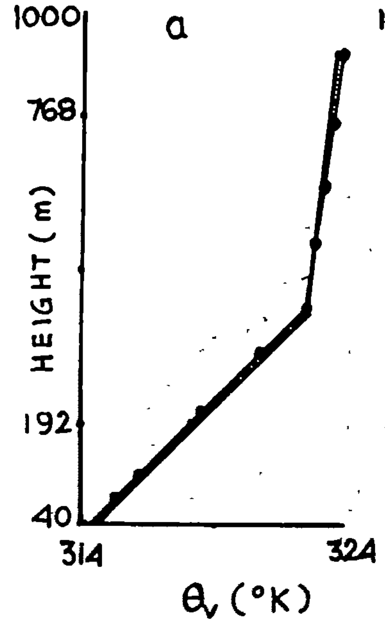

Figure 2.3 : Same as in Fig 2.1, for Bhubaneswar 0515 GMT, 10 May, 1988

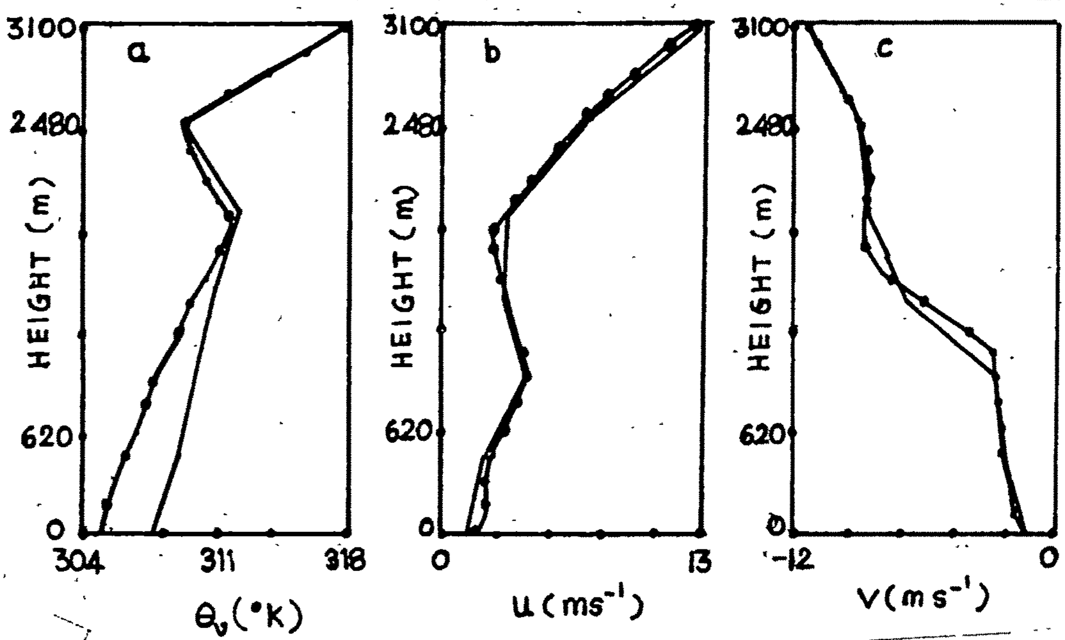

Figure 2.4 : Same as in Fig 2.1, for Calcutta, 0515 GMT, 22 May, 1988

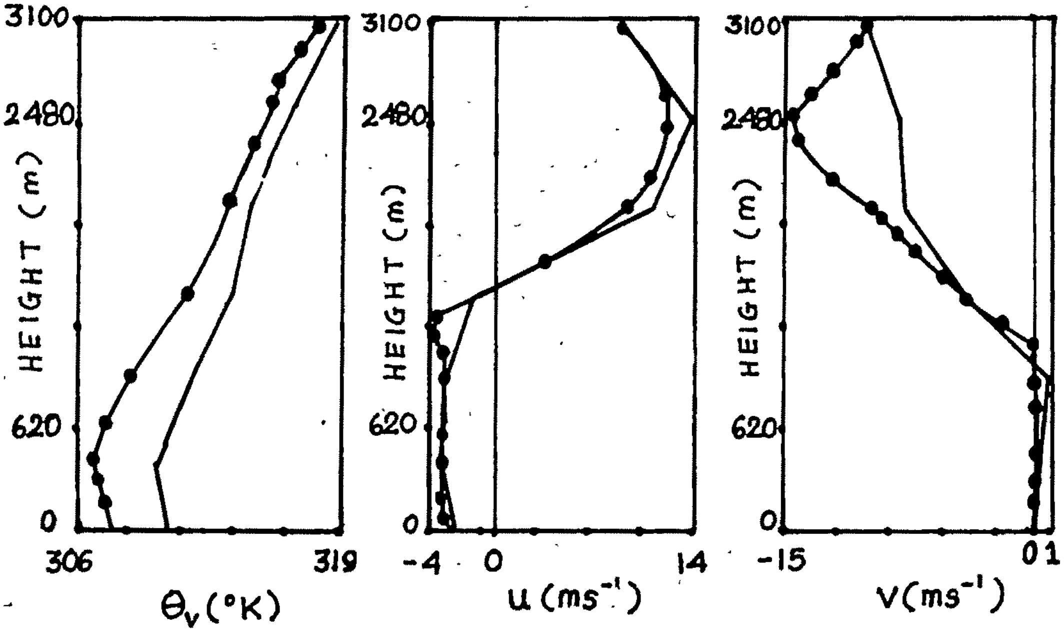

Figure 2.5 : Same as in Fig 2.1, for Calcutta, 1200 GMT, 22 May, 1988

Chapter 3

Understanding the physical processes in the atmospheric boundary layer through mathematical modelling

The wide range or spectrum of the sizes of the turbulent eddies within the ABL is difficult to take into account completely in observational and theoretical investigations attempting indepth studies of the various ABL processes. The sensors usually deployed for this purpose, can provide *in situ* measurments over only a part of the spectrum due to technical limitations. From the standpoint of mathematical modelling, the principal difficulty lies with the solution of the equations governing the ABL flow. These equations are non-linear partial differential equations and in their full form so complex, that analytical solutions are quite impossible. Only in highly idealized cases, exact solutions can be found, but at the expense of considerable deviations from reality. For more realistic solutions, numerical methods have to be used, but even then, simplifying assumptions such as concentrating on a particular range of eddy sizes and employing statistical methods for quantifying turbulence have to be imposed. Adoption of the latter technique results in a set of governing equations which contain, in addition to the mean flow terms, non-linear turbulence terms consisting of statistical moments of various orders between the turbulent components of wind, temperature and moisture fields. Mathematically, these statistics describe turbulent processes such as fluxes, energy, etc. that have become unresolvable by the choice of the range of eddy sizes.

Keller and Friedman (1924) were perhaps the first to point out that this system of governing equations did not form a mathematically closed system : the number of unknowns was always greater than the number of equations used. This resulted in the well known closure methods of parameterizing the unknown turbulent quantities by specifying them in terms of known parameters.

Two principal classes of closure methods are usually used in solving the set of equations governing ABL flow (Stull, 1988). Local closure methods are based on analogy with the process of molecular diffusion and assume that turbulent transport is a diffusive process. The unknown turbulent quantities at any point in space are parameterized in terms of known quantities, such as the observed wind, temperature, humidity, or their gradients at that point. The well known bulk methods and K-theory methods are examples of local closure parameterization. Such methods have been used extensively over a long period of time by investigators and references become too numerous to cite. It seems best to refer to excellent reviews provided in Bhumralkar (1975), Mc Bean et al (1979), Nieuwstadt and Van Dop (1984), Stull (1988) and others.

The non-local closure methods of parameterization are based on the idea that turbulent transport processes are advective, rather than diffusive and the unknown quantities at any point in space are expressed in terms of known quantities and their gradients at various other points in space. Several types of non-local closure theories exist, such as the **Direct Interaction and Two - Point Closure** (Kraichnan, 1959, 1976; Roberts, 1961; Leslie, 1973; Chollet and Lesieur, 1981; Stanisic, 1985); **The Spectral Diffusivity Theory** (Berkowicz and Prahm, 1979, 1984; Prahm et al., 1979; Berkowicz, 1980, 1984; Jenkins, 1985; Imboden, 1981); **Orthonormal Expansions** (Saffman, 1969; Romanoff, 1982, 1989); **Nonlocal or Integral Turbulence Closure** (Eringen, 1972; Fiedler, 1984; Fiedler and Moeng, 1985; Boudreau and Imboden, 1987; Narasimhan and Saivel, 1989). Discrete forms of non-local theory include : **Convective Circulations** (Estoque, 1968; Blackadar, 1979; Zhang and Anthes, 1982); **Turbulence Adjustment** (Klemp and Lilly, 1978; Stull and Hasagawa, 1984); **Markov and Non-Markov Models** (Hostetler and Opitz, 1982; Fortak, 1987). **The Transilient Turbulence Theory** or **T3** developed by Stull (1984, 1986, 1987, 1988) exists in analytical as well as discrete forms. Further details of the T3 can be found in Stull (1992).

None of the closure methods mentioned above, or, the parameterization schemes employed in them are exact. Both have advantages and disadvantages and their applications are dictated by the particular ABL processes being investigated. It has been observed however (Stull, 1988), that non-local closure methods in general and local closure methods of second and higher orders provide more accurate and realistic discriptions of turbulence in the ABL.

The need for using higher order closures for parameterizing turbulent processes within the ABL arose primarily from certain limitations of the K-theory, which became gradually apparent. The coefficient of eddy diffusivity K, is a property of the flow and not a property of the fluid and this dependence of K on the flow structure coupled with the difficulty of determining this dependence is the most serious limitation of the K-Theory approach (Businger, 1984). Thus, use of K-Theory fails to reproduce the ABL structure accurately in shear flows (Zeman, 1981). In highly convective ABL's, in which the length scales of the energy containing eddies become comparable to the depth of the entire layer over which turbulent transfer occurs, unrealistically large and even negative values of K are obtained in the upper layers of the ABL (Deardorff, 1972a, Bhumralkar, 1975). Wyngaard (1984), suggests that K-distributions in these layers are probably influenced by horizontal inhomogeneity, baroclinicity, entrainment through the capping inversion, gravity waves and non-stationarity in addition to which, difficulties in obtaining direct measurments has been the main factor behind the present lack of knowledge regarding K characteristics aloft. K - Theory can account for down - gradient transports only and in highly convective situations where temperature gradients above the surface layer can change sign and remain slightly positive throughout the mixed layer, negative K values occur, implying a countergradient transport (Deardroff, 1966, 1972b). K - theory also fails to describe flows over non-homogeneous surfaces, non-stationary transitions between different regimes (Mc Bean et al., 1979) and cloud-top ABL's (Moeng and Randall, 1984).

Second order closure schemes directly use the prognostic equations for turbulent stresses, with the third order moment terms being parameterized. This approach, which is a logical consequence of first-order closure also offers a method for prescribing K-dynamics (Wyngaard, 1984).

Second order closure schemes have been utilized by several investigators for studying ABL characteristies, for example, Deardorff (1974a, b), Wyngaard and Coté (1974), Wyngaard (1975), Donaldson (1973), André et al (1983), Yamada and Mellor (1975). Reviews of second and higher order closure schemes can be found in Hossain and Rodi (1974), Zeman (1981), Mellor and Yamada (1982), Wyngaard (1984), Moeng and Wyngaard (1989).

Use of higher order schemes markedly improve the lower order variables such as mean wind, temperature and their fluxes, which can be computed more accurately. The higher order schemes necessarily involve a large number of variables which can be tuned easily to obtain increasingly accurate forecasts in ABL and numerical weather prediction models (Stull, 1988). Their main drawback,especially from third order onward schemes, is the huge requirement of computer storage and processing time and the difficulty in obtaining direct measurements of fourth and higher order moments.

Mention has already been made (vide Section 1.3) of the modification of the ABL structure by internal gravity wave (IGW) modes, generated within or outside the ABL or by propagating mesoscale systems, such as thunderstorms. The method of linear stability analysis has been widely used for investigating wave induced momentum and energy transfer and their role in organising cumulus convection and modulating the turbulence state within the ABL. The investigations of Lalas and Einaudi (1976), (1980), Mastrantonio et al (1976), Chimonas and Grant (1984), Hooke and Jones (1986), King et al (1987), Mobbs and Darby (1990) and others are relevant in these contexts.

For the purpose of investigating ABL processes during the pre-monsoon and monsoon periods, we have developed three, diagnostic, one dimensional models based on the methodologies mentioned above. The non-local closure method based on **T3** has been described in Section 3.1, followed by descriptions of the second order closure model in Section 3.2 and the linear wave model in Section 3.3.

3.1 The non-local closure model : Transilient Turbulence Theory

Detailed descriptions of the transilient turbulence theory (**T3**) and its use in investigations of ABL processes can be found in Stull (1984), (1988), (1992) (hereafter referred to as Stull, a,b,c). For convenience we present some salient features of the theory and a brief description of our model.

Basically, **T3** recognises the fact that, larger turbulent eddies are organised, coherent structures which transport turbulent properties (such as momentum, heat, moisture, pollutants etc.) across finite distances in space, in a manner analogous to the process of advection, before the smaller sized eddies begin to do so. **T3**, a first order non-local closure method, thus allows the incorporation of the effects of turbulent mixing not only between adjacent layers of air (as in local closure methods) but also between layers of air separated by finite distances. This is thus an extremely advantageous method of studying ABL phenomena in which large eddies are present (for example, in a highly convective ABL) and also for studying the stable boundary layer, within which phenomena such as patchy turbulence, are present.

In order to translate mathematically the basic idea behind **T3**, we proceed as in Stull (a,b,c) and begin by discretizing the vertical column of air over the observing station into N equal-sized grid boxes of length Δz (meters) each. Grid indices are placed at the box centres, with i denoting a reference (destination) box and j denoting other (source) boxes. (See, Figure 3.1)

At any instant of time t (seconds), all the grid boxes will contain air, having some average property of state $\overline{\xi_i}$ (t) which may physically represent its mass (density), momentum, temperature, humidity etc. After an interval of Δt seconds, turbulence, if generated will cause mixing of air between boxes i and j. It is assumed that within the interval Δt, the air being mixed from the box j retains and carries with it, its original state property $\overline{\xi_j}$ (t) into the box i. If c_{ij} (t, Δt) denotes the fraction of air from box j mixing with air in box i, then after Δt seconds, the state property $\overline{\xi_i}$ (t) of the air in box i will change to $\overline{\xi_i}$ (t+Δt) according to:

$$\overline{\xi_i}\,(t+\Delta t)=\sum_{j=1}^{N} c_{ij}(t,\,\Delta t)\overline{\xi_j}\,(t) \qquad (3.1,\,1)$$

Considering ξ to represent an N element column vector and **C** an N×N matrix, (3.1,1) represents a matrix multiplication. The N×N matrix **C**, called the transilient matrix (TM), consisting of elements c_{ij} (t, Δt), holds information regarding the mixing of air between various source-destination boxes within the model domain. Physically, the elements c_{ij} (t, Δt) represent the intensity of mixing between air in the various boxes. These c_{ij}'s and hence **C** are functions of the time step only so that at each particular time step, the same TM can be used to compute changes in the various state properties represented by $\overline{\xi_i}$. In the next time step, turbulent mixing will alter the c_{ij}'s and hence a new TM has to be conctructed to trace the changes in $\overline{\xi_i}$ in that interval of time.

The elements c_{ij} of the TM are subject to certain physical constraints required by the principles of conservation of mass and state. Mathematically, these imply

$$\sum_{j=1}^{N} c_{ij} = 1, \quad \sum_{i=1}^{N} c_{ij} = 1 \qquad (3.1, 2)$$

In addition, in order to satisfy the condition that turbulence should increase in randomness and entropy, we must have, $c_{ij} > 0 \ \forall$ i, j. Further, since the fraction of air within any grid box can never exceed unity, these two conditions together imply :

$$0 \le c_{ij} \le 1 \ \forall \text{ i, j} \qquad (3.1, 3)$$

The elements c_{ij} of the TM can be recognised as the unknown quantities associated with turbulence which must now be parameterized in terms of the mean flow variables at the grid points within the model domain. To make the parameterization more realistic, the continuous response of the ABL flow to external forcings and conditions at the earth surface, should be accounted for and incorporated. The ABL flow responds to these external and dynamical forcings in a manner analogous, to Le Chetalier's principle in Chemistry : Any external or dynamical forcing at the earths surface (such as insolation, frictional drag, wind shear etc.) causes destabilization of the mean flow within the ABL and generation of turbulence. Turbulent mixing then tends to restabilize the flow to a new equilibrium state. Mathematically, this concept can be written as (Stull, (c)):

$$\begin{aligned} \overline{\xi_i}^*(t+\Delta t) &= \overline{\xi_i}(t)+\Delta t \bullet \text{(net source at height z)} \\ \overline{\xi_i}^*(t+\Delta t) &= \sum_{j=1}^{N} c_{ij}(t+\Delta t)\, \overline{\xi_j}^*(t+\Delta t) \end{aligned} \qquad (3.1, 4)$$

with, $c_{ij}(t, \Delta t)$ = function of $(u_i, u_j, v_i, v_j, \theta_i, \ldots\ldots)$

The types of responsive parameterization scheme for constructing the c_{ij}'s are based on:

(i) the concept of turbulent adjustment (Stull, (b), (c)) using a non-local analogy to the bulk Richardson number, and

(ii) the concept of a mixing potential (Stull and Driedonks, 1987) using a non-local analogy to the Turbulence Kinetic Energy (TKE) budget equation .

Turbulent Adjustment Parameterization

The non-local bulk Richardson number between pairs of source destination boxes is computed from :

$$R_{ij} = \frac{g\left(\Delta_{ij}\,\theta_v\right)\left(\Delta_{ij}\,z\right)}{\left(\Delta_{ij}\,u\right)^2 \left(\Delta_{ij}\,v\right)^2} \qquad (3.1, 5)$$

where the symbol $\Delta_{ij}\,\overline{X} = \overline{X}_i - \overline{X}_j$ represents the non-local difference between values of $\overline{X}$ at levels i Δz and j Δz.

Turbulence is assumed to be initiated only when $R_{ij} < R_c$, R_c being the critical value for onset of turbulence. Turbulence is assumed to continue and generate mixing until R_{ij} reaches another critical value R_T and the flow becomes non-turbulent when $R_{ij} > R_T$. The potential for mixing is measured by :

$$Y_{ij} = W_{ij}\left[1-\left(R_{ij}/R_T\right)\right],\ i \neq j$$
$$W_{ij} = \frac{U_o\,\Delta t}{\Delta z\,|\,i-j\,|} \qquad (3.1,\ 6)$$

where, W_{ij} is a weighting factor, U_o is a velocity scale and $0 \leq Y_{ij}$, $W_{ij} \leq 1$. Then the c_{ij}'s are computed from:

$$c_{ij}\ (t, \Delta t) = Y_{ij} / N_d \qquad (3.1,\ 7)$$

where N_d is the number of gridpoints within the turbulent subdomain .

For the cases in which $R_{ij} > R_c$, $Y_{ij} = 0\ i \neq j$ (3.1, 8)

The diagonal elements, computed using (3.1, 2) are then :

$$Y_{ij} = 1 - \sum_{j=1}^{N} c_{ij}\ (t, \Delta t) \qquad (3.1,\ 9)$$

Turbulence Kinetic Energy (TKE) Parameterization

The TKE is a measure of the intensity of turbulence and is directly related to the transport of heat, moisture and momentum within the ABL. It is natural therefore, to use the TKE budget equation particularly in the form useful for vertical transport :

$$\frac{\partial \bar{e}}{\partial t} = \frac{g}{\theta_v}\left(\overline{w'\theta_v'}\right) - \overline{u'w'}\frac{\partial u}{\partial z} - \overline{v'w'}\frac{\partial v}{\partial z} - \frac{\partial}{\partial z}\left(\overline{w'e}\right) - \frac{1}{\rho}\frac{\partial}{\partial z}\left(\overline{w'p'}\right) - \varepsilon \qquad (3.1,\ 10)$$

Here $\bar{e} = \frac{1}{2}\left(\overline{u'^2} + \overline{v'^2} + \overline{w'^2}\right)$ is the TKE per unit mass. All primed quantities represent the turbulent components and unprimed ones their mean values. Overbars indicate averages. Thus, u,v,w, θ_v denote the velocity components and the virtual potential temperature. $\bar{\rho}$ is the mean density of air, p the pressure and ε is the dissipation of the TKE.

The non-local analogy of the TKE budget equation (Stull and Driedonks, 1987; Stull, 1988,1992) is obtained from (3.1, 10) after neglecting the turbulent transport and pressure correlation terms (terms 4 and 5) and integrating over t and normalizing the result by $\bar{e}$ The result is :

$$Y_{ij} = \frac{\Delta t.\ T_0}{\left(\Delta_{ij}\, z\right)^2}\left[\left(\Delta_{ij}\, u\right)^2 + \left(\Delta_{ij}\, v\right)^2 - g\left(\Delta_{ij}\, \overline{\theta_v}\right)\frac{\Delta_{ij}\, z}{\theta_v\, R_c}\right] - \frac{D_y\, \Delta t}{T_0} \qquad (3.1,\ 11)$$

Where as usual, the symbol $\Delta_{ij}\, X$ denotes a non-local difference in X . The last term represents the TKE dissipation. The characteristic time scale To = 1000s, the dissipation factor $D_y = 1$ and $R_c = 0.21$ is the critical Richardson number (Stull and Driendonks, 1987). The first two terms represent the mechanical or shear production of TKE while the third term represents the buoyant production or consumption term. The quantity Y_{ij}, termed the mixing potential, represents the contribution of the instability of the flow to the potential for mixing.

Initially, values of Y_{ij}, for $i \neq j$ are computed using observed values of u,v, θ_v in (3.1, 11). These values are then modified so that the row and column elements increase monotonically from all sides towards the main diagonal. Physically this means that the potential for mixing, as expected, should be high for closely spaced boxes than those further away. The diagonal elements Y_{ii} physically represent the amount of internal, sub-grid scale mixing within box i and is computed from :

$$Y_{ii} = \max\left(Y_{i,j-1},\ Y_{i,j+1}\right) + Y_{ref}$$

where $Y_{ref} = 1000$ is the parameter representing the mixing potential for these unresolved scales of mixing.

The elements of the TM are then computed from :

$$c_{ij}\,(t, \Delta t) = \frac{Y_{ij}}{\| Y \|},\ i \neq j$$

$$c_{ij}\,(t, \Delta t) = 1 - \sum_{j=1}^{N} c_{ij}\ \ (t, \Delta t)\ j \neq i \qquad (3.1,\ 12)$$

$$\text{where, } \| Y \| = \max_{i} \left[\sum_{j=1}^{N} Y_{ij} \right]$$

is the maximum row norm of the matrix of Y_{ij}'s.

Very often the concept of exchange hypothesis is invoked to yield a symmetric TM. This hypothesis rises from the physical consideration that for any fraction of air moving from grid box j into grid box i during the time Δt , an equal fraction of air must move from box i to box j. Mathematically, this implies :

$$c_{ij}\,(t, \Delta t) = c_{ji}(t, \Delta t) \qquad (3.1,\ 13)$$

The resulting TM, C (t, Δt) is a doubly stochastic matrix. In addition, due to the physical constraints (3.1, 2) (3.1, 3), the numerical computation using this TM is absolutely numerically stable for all time steps and grid spacing [Stull (1986, 1988)]. The only recommended numerical constraint is that all eigenvalues of the TM must be positive.

Finally, we come to the various non-local turbulence statistics that can be computed at each time step, once the elements of the TM have been constructed using any of the above two responsive parameterization schemes.

The non-local flux F_k (t, Δt), across the level k that is, at height z = k Δ z is computed from (Stull and Driedonks, 1987) :

$$F_k(t, \Delta t) = F_{k-1}(t, \Delta t) + \frac{\Delta z}{\Delta t} \sum_{j=1}^{N} c_{ij}\ (t, \Delta t)\left[\bar{\xi}_k(t) - \bar{\xi}_j(t)\right] \qquad (3.1,\ 14)$$

with F_k (t, Δt) = 0 at k = 0 (i.e, no advection like turbulent transport across the earth surface) and also, F_k (t, Δt) = 0 at k = N (i.e, in a non-turbulent zone above the ABL).

The transport spectral component $F_{k/m}$ (t, Δt) gives a measure of the contribution of eddies of size m Δ z to the total flux across the level k (z = k Δ z) (Stull, 1988, 1992).

Thus:

$$F_{k/m}(t, \Delta t) = \frac{\Delta z}{\Delta t} \sum_{i=1}^{k}\ \sum_{j=k+1}^{N} \delta_{m|i-j|} \left[\, c_{ij}\,(t, \Delta t)\ \bar{\xi}_i(t) - c_{ji}\,(t, \Delta t)\ \bar{\xi}_j(t) \right] \qquad (3.1,\ 15)$$

where $\delta_{m|i-j|}$ represents the Kronecker delta fuction. In contrast to computing state spectra using Fast Fourier Transform, which gives information about the mixing of fluid between pairs of gridpoints based on the variances of temperature, velocity or other state variables, non-local transport spectral components are based on fluxes and provide information regarding the contribution of the various sized eddies to the overall mixing process.

The transport spectrum, the sum of all such spectral components is given by :

$$F_k(t, \Delta t) = \sum_{m=1}^{N-1} F_{k/m}(t, \Delta t) \qquad (3.1,\ 16)$$

and is equal to the net transport that is the total flux across the level z = k Δ z.

Information regarding the mixing process and the contribution of different eddies to this is obtained from the process spectrum defined as :

$$P_{k/m}(t, \Delta t) = \sum_{i=1}^{k} \sum_{j=k+1}^{N} \delta_{m,|i-j|} \left[c_{ij}(t, \Delta t) + c_{ji}(t, \Delta t)\right] \ ; \ P_k(t, \Delta t) = \sum_{m=1}^{N-1} P_{k/m}(t, \Delta t) \qquad (3.1,\ 17)$$

The process spectral components $P_{k/m}(t, \Delta t)$ provides information about the contribution of various eddy sizes to the total mixing intensity.

The average mixing length, which is a measure of the average distance across which turbulence moves and mixes the air contained in eddies, is computed from :

$$l_k = \Delta z \sum_{i=1}^{N} 0.5 \left[c_{ik}(t, \Delta t) + c_{ki}(t, \Delta t)\right] \qquad (3.1,\ 18)$$

The relative importance of the various eddies to the overall mixing length are computed using the eddy sizes weighted by their respective process spectral components (amplitudes) :

$$L_k = \frac{\Delta z \sum_{m=i}^{N} m P_{k/m}(t, \Delta t)}{\sum_{m=i}^{N} P_{k/m}(t, \Delta t)} \qquad (3.1,\ 19)$$

This L_k is a weighted wavelength similar to the mixing length l_k at height z = k Δ z.

An idea about the one-dimensional anisotropy of the turbulent eddies of various sizes can be obtained by partitioning the mixing length l_k into upward and downward transport from the source box j (z = j Δ z) and upward and downward transport to the destination box i (z = j Δ z) denoted by $l_j\uparrow$, $l_j\downarrow$ and $l_i\uparrow$, $l_i\downarrow$ respectively :

$$l_j \uparrow (t, \Delta t) = \frac{\Delta z \sum_{i=j}^{N} c_{ij}(t, \Delta t)\, |i-j|}{\sum_{i=j}^{N} c_{ij}(t, \Delta t)} \qquad (3.1,\ 20)$$

$$l_j \downarrow (t, \Delta t) = \frac{\Delta z \sum_{i=1}^{j} c_{ij}(t, \Delta t)\, |i-j|}{\sum_{i=1}^{j} c_{ij}(t, \Delta t)} \qquad (3.1,\ 21)$$

$$l_j \uparrow (t, \Delta t) = \frac{\Delta z \sum_{j=1}^{i} c_{ij}(t, \Delta t)\,|i-j|}{\sum_{j=1}^{i} c_{ij}(t, \Delta t)} \qquad (3.1, 22)$$

$$l_j \downarrow (t, \Delta t) = \frac{\Delta z \sum_{j=1}^{N} c_{ij}(t, \Delta t)\,|i-j|}{\sum_{j=1}^{N} c_{ij}(t, \Delta t)} \qquad (3.1, 23)$$

For one-dimensional anisotropy, all the four components described above are distinct. Another indicator of the one-dimensional anisotropy of the turbulent eddies is the asymmetry of the TM elements with respect to its main diagonal.

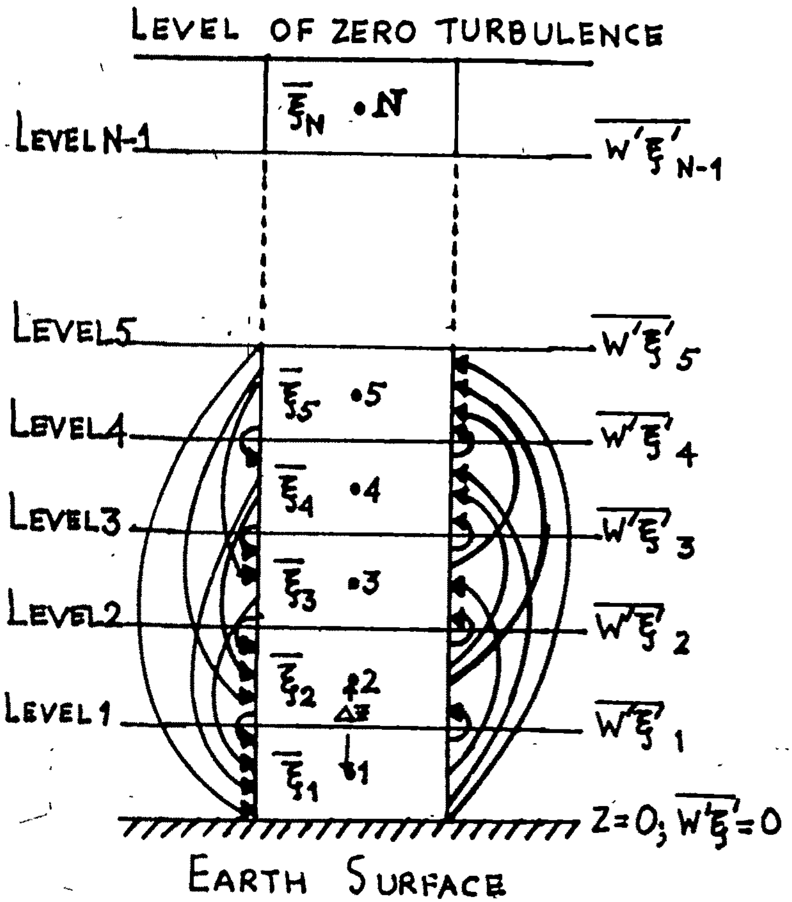

Figure 3.1 : Schematic showing transilient mixing (after Stull, 1992)

3.2 The Second Order Local Closure Model

Detailed descriptions of second order local closure equations being available (Wyngaard, 1984; Stull, 1988), we describe below, a brief outline of the one-dimensional model developed, based primarily on that due to Donaldson (1973).

Under assumptions of horizontal homogeneity and no subsidence in a dry atmosphere, the prognostic equations for the mean flow within the ABL are :

$$\frac{\partial u}{\partial t} = f\left(v - v_g\right) - \frac{\partial}{\partial z}\left(\overline{u'w'}\right) \tag{3.2, 1}$$

$$\frac{\partial v}{\partial t} = -f\left(u - u_g\right) - \frac{\partial}{\partial z}\left(\overline{v'w'}\right) \tag{3.2, 2}$$

$$\frac{\partial \theta}{\partial t} = \frac{\partial}{\partial z}\left(\overline{w'\theta'}\right) \tag{3.2, 3}$$

In addition to these prognostic equations for the second moments are also included alongwith the TKE equation :

$$\frac{\partial \bar{e}}{\partial t} = \overline{u'w'}\frac{\partial u}{\partial z} - \overline{v'w'}\frac{\partial v}{\partial z} + \frac{g}{\theta}\overline{w'\theta'} - \frac{\partial}{\partial z}\left(\overline{w'e}\right) - \left[\frac{1}{\rho}\frac{\partial}{\partial z}\left(\overline{w'p'}\right)\right] - \varepsilon \tag{3.2, 4}$$

$$\frac{\partial}{\partial t}\left(\overline{u'w'}\right) = \overline{w'^2}\frac{\partial u}{\partial z} + \frac{g}{\theta}\overline{u'\theta'} - \frac{\partial}{\partial z}\left(\overline{u'w'^2}\right) - \frac{1}{\rho}\left[\overline{u'\frac{\partial p'}{\partial z}} + \overline{w'\frac{\partial p'}{\partial x}}\right] \tag{3.2, 5}$$

$$\frac{\partial}{\partial t}\left(\overline{v'w'}\right) = \overline{w'^2}\frac{\partial v}{\partial z} + \frac{g}{\theta}\overline{v'\theta'} - \frac{\partial}{\partial z}\left(\overline{v'w'^2}\right) - \frac{1}{\rho}\left[\overline{v'\frac{\partial p'}{\partial z}} + \overline{w'\frac{\partial p'}{\partial x}}\right] \tag{3.2, 6}$$

$$\frac{\partial}{\partial t}\left(\overline{w'^2}\right) = -\frac{2}{\rho}\left[\overline{w'\frac{\partial p'}{\partial z}}\right] + \frac{2g}{\theta}\,\overline{w'\theta'} \tag{3.2, 7}$$

$$\frac{\partial}{\partial t}\left(\overline{w'\theta'}\right) = \overline{w'^2}\frac{\partial \theta}{\partial z} - \frac{\partial}{\partial z}\overline{w'^2\theta'} + \frac{g}{\theta}\overline{\theta'^2} - \frac{1}{\rho}\left[\theta'\frac{\partial p'}{\partial z}\right] \tag{3.2, 8}$$

$$\frac{\partial}{\partial t}\left(\overline{\theta'^2}\right) = 2\overline{w'\theta'}\frac{\partial \theta}{\partial z} - \frac{\partial}{\partial z}\left(\overline{w'\theta'^2}\right) - \chi \tag{3.2, 9}$$

As usual, primes denote fluctuating parts of the mean wind componments u,v,w, the potential temperature θ and the pressure, p. $\overline{\rho}$ is the mean density of air and g, the acceleration due to gravity.

The terms within the square bracket are the pressure covariances and describe the redistribution of the variances by the pressure perturbations and are often associated with buoyancy or gravity waves (Stull, 1988). The term $\frac{\partial}{\partial t}\overline{w'e}$, the turbulent transport term, describes the redestribution of TKE by eddies. ε denotes viscous dissipation of TKE, while χ denotes the molecular dissipation.

G166056

The system of equations (3.4) – (3.9) are then closed by specifying the third order moment terms as follows :

The molecular dissipation term χ in (3.2, 9)and the viscous dissipation ε in (3.2,4) are approximated as (Yamada and Mellor, 1975):

$$\chi=\frac{\bar{e}^{1/2}\,\overline{\theta'^2}}{\Lambda_4} \tag{3.2, 10}$$

$$\varepsilon=\frac{e^{3/2}}{\Lambda_1} \tag{3.2, 11}$$

The pressure covariance terms in the various equations are approximated, on the basis of, following Mellor and Yamada (1982) as :

$$-\frac{1}{\rho}\left(\overline{u'\frac{\partial p'}{\partial z}}+\overline{w'\frac{\partial p'}{\partial x}}\right)=\frac{\bar{e}^{1/2}}{\Lambda_2}\left(\overline{u'w'}\right) \tag{3.2, 12}$$

$$-\frac{1}{\rho}\left(\overline{v'\frac{\partial p'}{\partial z}}+\overline{w'\frac{\partial p'}{\partial y}}\right)=\frac{\bar{e}^{1/2}}{\Lambda_2}\left(\overline{v'w'}\right) \tag{3.2, 13}$$

$$-\frac{2}{\rho}\left(\overline{w'\frac{\partial p'}{\partial z}}\right)=\frac{\bar{e}^{1/2}}{\Lambda_2}\left(\overline{w'^2-\frac{2}{3}\bar{e}}\right) \tag{3.2, 14}$$

$$-\frac{1}{\rho}\left(\overline{\theta'\frac{\partial p'}{\partial z}}\right)=\frac{\bar{e}^{1/2}}{\Lambda_3}\overline{w'\theta'} \tag{3.2, 15}$$

$$\left(\overline{w'e}+\frac{\overline{w'p'}}{\bar{\rho}}\right)=\Lambda_e\,\bar{e}^{1/2}\frac{\partial\bar{e}}{\partial z} \tag{3.2, 16}$$

where the empirical length scales $\Lambda_e, \Lambda_1, \Lambda_2, \Lambda_3, \Lambda_4$ are expresed in terms of a characteristic turbulence length scale Λ, by (Mellor and Yamada, 1982, Wichmann and Schaller, 1986):

$$\Lambda_e = 0.2\ \Lambda,\quad \Lambda_1 = 5.75\ \Lambda,\quad \Lambda_2 = 2.08\ \Lambda,\quad \Lambda_3 = 2.14\ \Lambda \quad \text{and} \quad \Lambda_4 = 7.44\ \Lambda. \tag{3.2, 17}$$

Under weakly stable or neutral thermal stratifications of the ABL, turbulence is not very strong and hence, the triple correlation terms $\overline{u'w'^2}$, $\overline{v'w'^2}$ in equations (3.2, 6) and (3.2, 7) can be neglected. Since for stable boundary layers, $\overline{w'\theta'^2}$ in (3.2, 9) is negligiable in the surface layer and hence, throughout the ABL (Hogstorm, 1990), this term also been neglected. The assumption of a quasi-steady state, in which the characteristic scale of time changes is much greater than 20s, is usually satisfied (Wyngaard, 1984) in the ABL. Terms such as $\overline{u'\theta'}$, $\overline{v'\theta'}$ and $\overline{u'v'}$ have also been neglected.

Thus, using the closure approximations (3.2, 10) – (3.2, 17) and the above simplifications, the set of prognostic equations (3.2, 4) – (3.2, 9) reduce to the following set of diagnostic equations :

$$\overline{u'w'}\frac{\partial u}{\partial z}+\overline{v'w'}\,\frac{\partial v}{\partial z}-\frac{g}{\theta}\overline{w'\theta'}+\frac{\partial}{\partial z}\left(\Lambda_e\,\bar{e}^{\,3/2}\frac{\partial \bar{e}}{\partial z}\right)+\frac{\bar{e}^{\,3/2}}{\Lambda_1}=0 \qquad (3.2,\ 18)$$

$$\overline{w'^2}\frac{\partial u}{\partial z}+\frac{\bar{e}^{\,1/2}}{\Lambda_2}\overline{u'w'}=0 \qquad (3.2,\ 19)$$

$$\overline{w'^2}\frac{\partial v}{\partial z}+\frac{\bar{e}^{\,1/2}}{\Lambda_2}\overline{v'w'}=0 \qquad (3.2,\ 20)$$

$$\frac{2g}{\theta}\overline{w'\theta'}+\frac{\bar{e}^{\,1/2}}{\Lambda_3}\left(\overline{w'^2}-\frac{2}{3}\right)=0 \qquad (3.2,\ 21)$$

$$\overline{w'^2}\frac{\partial \theta}{\partial z}-\frac{g}{\theta}\overline{\theta'^2}+\frac{\bar{e}^{\,1/2}}{\Lambda_3}\overline{w'\theta'}=0 \qquad (3.2,\ 22)$$

$$2\overline{w'\theta'}\frac{\partial \theta}{\partial z}+\frac{\bar{e}^{\,1/2}}{\Lambda_4}\overline{\theta'^2}=0 \qquad (3.2,\ 23)$$

The system of coupled, first order ordinary differential equations is solved numerically to obtain $\overline{u'w'}$, $\overline{v'w'}$, $\overline{w'\theta'}$, $\overline{w'^2}$, $\overline{\theta'^2}$ and $\bar{e}$. The fluxes can then be used in the prognostic equations (3.2, 1) – (3.2, 3) to obtain the temporal evolution of u, v and θ within the ABL.

3.3 The Linear Wave Model

Earlier investigations on IGW's have been carried out by several outhors (Gossard and Moninger, 1976; Gossard and Hook, 1978; King et al., 1987; Rees, 1987; Mobbs and Darby, 1990; Lindzen, 1990 etc.). Further account of other investigations can be found in Andrews et al. (1987).

Following standard procedure (Andrews et al., 1987), we begin with the primitive equations linearized about a basic state. The equations of motion, continuity and conservation of energy then become :

$$\rho\frac{Du}{Dt}=-\frac{\partial p}{\partial x} \qquad (3.3,\ 1)$$

$$\rho\frac{Dv}{Dt}=-\frac{\partial p}{\partial y} \qquad (3.3,\ 2)$$

$$\rho\frac{Dw}{Dt}=-\frac{\partial p}{\partial z}-g\rho \qquad (3.3,\ 3)$$

$$\frac{D\rho}{Dt}+\rho\left(\frac{\partial u}{\partial x}+\frac{\partial v}{\partial y}+\frac{\partial w}{\partial z}\right)=0 \qquad (3.3,\ 4)$$

where,

$$\frac{D}{Dt}\equiv\frac{\partial}{\partial t}+u\frac{\partial}{\partial x}+v\frac{\partial}{\partial y}+w\frac{\partial}{\partial z}$$

Imposing the Boussinesq assumptions, (3.3,4) can be written as :

$$\frac{D\rho}{Dt}=0;\quad \frac{\partial u}{\partial x}+\frac{\partial v}{\partial y}+\frac{\partial w}{\partial z}=0 \qquad (3.3,\ 5)$$

Since we are investigating a mesoscale phenomenon where the frequency of the disturbance is large compared to the local inertial frequency, the effect of the earth's rotation and hence the Coriolis terms have been neglected in (3.3, 1) and (3.3, 2).

The symbols used in (3.3, 1) – (3.3, 5) are as usual : u,v,w denote the velocity components in the zonal, meridional and vertical directions respectively; ρ is the density of air at height z; p is the pressure and u,v,w,ρ,p are all functions of the space variables x,y,z and time t; g is the acceleration due to gravity.

The variables are expanded into basic and perturbed components :

$$\begin{aligned} u(x,y,z,t) &= U_0(z) + U'(x,y,z,t) \\ v(x,y,z,t) &= V_0(z) + V'(x,y,z,t) \\ w(x,y,z,t) &= W'(x,y,z,t) \\ \rho(x,y,z,t) &= \rho_0(z) + \rho'(x,y,z,t) \\ p(x,y,z,t) &= P_0(z) + P'(x,y,z,t) \end{aligned} \qquad (3.3,\ 6)$$

It is to be remarked in passing that, both zonal and meridional velocities are important for Nor'westers, with the storm coming from the northwest and travelling in an northwest to southeasterly direction. Hence, we have retained here, both the unperturbed velocities for u and v in (3.3, 6).

On the other hand, the unperturbed vertical velocity is neglected in view of the fact that it is negligibly small under a stable thermal stratification which occurs dominantly in our present study.

We next construct the linearized equations and adopt the following transformation for the perturbed variables :

$$[\,U',\ V',\ W',\ 1/P'\,] = (\rho_s/\rho_0)^{½}\ [\,U,\ V,\ W,\ 1/P\,] \qquad (3.3,\ 7)$$

In (3.3, 7), ρ_s is the unperturbed density of air at the surface.

The resulting partial differential equations are linear in U, V, W, and P. We seek solutions in the form :

$$\begin{aligned} [\,U,\ V,\ P\,] &= [\,U(z),\ V(z),\ P(z)\,]\ \sin(kx + ly - \sigma t) \\ W &= W(z)\ \cos(kx + ly - \sigma t) \end{aligned} \qquad (3.3,\ 8)$$

Elimination of U (z), V (z) and P(z) leads to the following ordinary differential equation in W(z) :

$$\frac{d^2}{dz^2} W(z) + \alpha(z)\, W(z) = 0 \qquad (3.3,\ 9)$$

where,

$$\begin{aligned} \alpha(z) &= -m^2 + \frac{1}{\omega}\left[k\frac{d^2U_0}{dz^2} + l\frac{d^2V_0}{dz^2} \right] + \left(\frac{Nm}{\omega}\right)^2 \\ \omega(z) &= k\,(c - U_0 - V_0 l/k) \\ m^2 &= l^2 + k^2\ ;\ c = \sigma/k \\ N^2 &= -\frac{g}{\rho_s}\frac{d\rho}{dz} = \frac{g}{\theta_v}\frac{d\theta_v}{dz} \end{aligned} \qquad (3.3,\ 10)$$

The expression for α (z) given above contains some additional terms (curvature terms) in addition to the usual ones occurring in the well-known Scorer's parameter. Thus α(z) is a modification of this parameter and shall be referred to as the modified Scorer's parameter.

In (3.3, 10), l, k, are the zonal and meridional wavenumbers; σ, the angular frequency of the wave; c, its phase speed, N the Brunt-Väisälä frequency; θ_v the virtual potential temperature at height z ; ω (z), the intrinsic frequency. The solution for (3.3, 9) is sought for in a multuilayered model. At the earth surface z = 0 we set W = 0. At the interfaces between the various layers, the kinematic condition is $W_L = W_U$ while the dynamic condition is $P_L = P_U$ where subscripts L and U refer to lower and upper layers. In addition, at the interfaces, W and dW/dZ are assumed to be continuous.

In order to solve (3.3, 9), N^2 (z), ω (z) and α(z) (the modified Scorer's parameter), are computed at several grid points along the vertical at which observed values of the meteorological parameters are available from radiosonde data. After computing α(z), the atmosphere is divided into several layers according to whether the α(z) profile is concave or convex within the layer. In all such layers, three grid points are selected, one each at the bottom and top of the layer and the third, in between these points at which α(z) attains either a minimum or maximum value, that is, $\frac{d\alpha}{dz} = 0$ at this point. Using these three values of α(z), we try to fit them to the functional form :

$$\alpha(z) = -\left(\tfrac{1}{4}\mu_i^{\,2}\right) + E_i^{\,2}\left[1 + D_{1i}\exp(\mu_i z) + D_{2i}\exp(-\mu_i z)\right]^{-2} \tag{3.3, 11}$$

which is a convenient form for depicting the concavity and convexity of the α(z) profile. Thus, for each layer i, we have an estimate of μ_1, E_1, D_{11}, and D_{21} respectively.

With each layer i, the solutions of (3.3, 9) are then obtained as :

$$\omega(z) = \begin{cases} D_i\left[C_{1i}\sin\Theta + C_{21}\cos\Theta\right], & \text{for } k_i^2 > 0 \\ D_i\left[C_{1i}\sinh\Theta + C_{21}\cosh\Theta\right], & \text{for } k_i^2 < 0 \end{cases} \tag{3.3, 12}$$

where,

$$D_i = \left[\text{abs}\left\{1 + D_{11}\exp(\mu_1 z) + D_{21}\exp(-\mu_1 z)\right\}\right]^{1/2} \tag{3.3, 13}$$

and

$$k_i^2 = E_i^2 + \mu_1(4D_{1i}D_{2i} - 1) \tag{3.3, 14}$$

The expressions for Θ used in (3.3, 12) are;

$$\Theta = \begin{cases} \dfrac{2\left(k_{ri} + k_{ji}\right)}{\mu_i(4D_{1i}D_{2i} - 1)^{1/2}}\left[\tan^{-1}(\Phi_i) - \tan^{-1}(\Phi_{0i})\right], & 4D_{1i}D_{2i} - 1 > 0 \\ \dfrac{k_{ri} + k_{ji}}{\mu_i(1 - 4D_{11}D_{2i})^{1/2}}\left[\ln(A_i) - \ln(A_{01})\right], & 4D_{11}D_{2i} - 1 < 0 \end{cases} \tag{3.3, 15}$$

where,

$$k_{r1} = \sqrt{k_i^2}\ ;\ k_{ji} = 0, \quad \text{if } k_i^2 > 0 \tag{3.3, 16}$$

and
$$k_{ri} = 0\ ;\ k_{ji} = \sqrt{-k_i^2}\ ,\quad \text{if}\ \ k_i^2 < 0 \tag{3.3, 16}$$

Further,
$$\Phi_i = \frac{\left[1+2\,D_{1i}\exp(\mu_i z)\right]}{\left[4\,D_{1i}\,D_{2i}-1\right]^{1/2}} \tag{3.3, 17}$$

$$A_i = \left[1+2\,D_{1i}\exp(\mu_i z)-(1-4\,D_{1i}\,D_{2i})^{1/2}\right]\times\left[1+2\,D_{1i}\exp(\mu_i z)+(1-4\,D_{1i}\,D_{2i})^{1/2}\right]^{-1}$$

The expressions for Φ_{0i} and A_{0i} can be obtained from the corresponding expressions for Φ_i and A_i by replacing z by z_{0i}, where z_{0i} is the height of the lower boundary of the i th layer.

The solutions (3.3, 12) will be completely determined if the values of the constants C_{1i}, C_{2i} for each layer i is known. For this, we being with the lowest layer i = 1 and use the lower boundary condition on z = 0. This enables us to determine C_{21} in terms of C_{11}. For other layers, C_{1i} and C_{2i} are determined from the continuity conditions for W(z) and $\frac{dW}{dz}$ at the interface. Thus all the C_{1i}'s and C_{2i}'s are evaluated in terms of C_{11}. To determine C_{11}, observations of wave amplitude at the surface are required. Since such observations were unavailable for the present study, we proceed with the normalized wave amplitudes C_{1i}/C_{11} and C_{2i}/C_{11} for each layer.

Chapter 4

Pre–Monsoon Scenarios : Model Results

The pre-monsoon scenario over the north Indian plains is dominated by thunderstorm activity as a result of the gradual transition of atmospheric characteristics from a state of extreme dryness (during April and May) to a state of very high humidity and precipitation with the advance of the monsoon in June. Observations indicate that this pre-monsoon thunderstorm activity displays some interannual variability and in many years, lead to the commencement of the monsoon rains without a well defined transition period (Das, 1986).

Locally known as Nor'westers, these pre-monsoon thunderstorms are mesoscale systems with typical horizontal and vertical scales of 20 kms and are usually initiated in the Chotanagpur Plateau region extending approximately over 22°–23°N, 83°–85°E, and having an elevation of 600–1000m above sea level (see, Figure 4.1). This acts as a localised, elevated, heat source and is the seat of intense convection during April–May (Koteswaram and Chakraborty, 1950), evident by the development of convective clouds over the slopes of the plateau. Characteristic features of these storms, which have a preferred tendency to propagate in a northwest to southeast direction, have been documented by the IMD (1944).

Desai (1950), Newton (1951), Rai Sircar (1954) and others sought to explain the physical mechanisms responsible for Nor'wester development. According to them, the prevailing configuration of two different types of airmasses namely, a 1-2 km deep moist southerly inflow from the adjoining Bay of Bengal capped by a deep layer of cold, dry westerly or northwesterly flow nearly upto the 200 mb level where the westerly jet is located during April–May, gives rise to latent instability conditions, particularly over Gangetic West Bengal (see Figures 4.1 and 4.2). The mechanism for releasing the energy of latent instability was attributed to low level conditions such as insolation; cold air outflow from a parent thunderstorm; cold katabatic flows from the Himalayas in the north etc. Ramaswamy and Bose (1953a,b ; 1954) and Ramaswamy (1956), through extensive analysis of surface and upper air data, drew attention to the dynamics of the middle and upper tropospheric westerlies, suggesting that, upper level divergence and compensating lower level convergence together with vorticity advection with the advancing trough in the westerlies, over the region of storm occurrence, was crucial to the development of Nor'westers rather than insolation and other low level conditions. Ramaswamy (1956) indentified wavy patterns in the 700-500 mb and 500-300 mb partial thickness lines over the storm region.

Koteswaram and Srinivasan (1958), in an attempt to clarify the roles of upper and lower tropospheric conditions in Nor'wester development concluded that the superposition of an upper level divergence, associated with a jet-stream, or a jet stream trough or, a trough over an anticyclonic vortex, on a lower level convergence associated with a low or trough with southerly flows in the ABL, was essential for Nor'wester development. Insolation and orography are additional features that aid storm development.

The conclusions reached in the abovementioned investigations imply that, the genesis of the pre-monsoon Nor'westers in the Chotanagpur Plateau region is strongly influenced by intense convection and orography; its development is favoured by a coupling between upper level divergence superposed on a lower level convergence with high moisture content in the ABL, and that its dynamics is controlled by these strong wind shear zones in the upper and lower troposphere.

The main motivation behind the present investigations of the pre-monsoon Nor'westers, was the diagnosis and identification of the physical mechanisms, that may exist in the prestorm boundary layer and the lower troposphere that lead to the storm development.

For the case studies, two contrasting situations were chosen: one in which occurrences of Nor'westers were not recorded over Calcutta (although it could have occurred in other parts of northeast India) which we have called a non-Norwester day and another, in which a Nor'wester occurred over Calcutta. Two such days were 10 May, 1988 (non-Nor'wester) and 22 May 1988 (Norwester). The data for these two days were radiosonde observations over Calcutta (22.34°N, 88.24°E), Ranchi (23.23°N, 87.20°E) and Bhubaneswar (20.15°N, 85.52°E) (all located well within the Nor'wester regime, see Figure 4.1) taken by the IMD during a Special Observation Period (10 may– 25 May, 1988) during the Nor'wester season. The data consisted of four times daily (00, 0515, 1215 and 1800 GMT) observations of wind speed and direction, dry and wet-bulb temperatures at the standard pressure levels upwards from 1000mb at 50 mb intervals.

The Nor'wester over Calcutta on 22 May 1988 occurred at 1408 GMT. It was accompanied by a squall with wind speeds reaching 72 kmph which lasted for about 7 minutes till 1415 GMT. It was preceded by precipitation which continued till nearly 1730 GMT.

For providing the basic input to the T3 model described in Section 3.1, the observed data were used to generate 50m interval data consisting of the virtual potential temperature θ_v u and v which were then initialized by the method outlined in chapter 2. The fluxes of heat and zonal and meridional momentum were computed by the T3 model for both days over Calcutta, Ranchi and Bhubaneswar. The intercomparison of the flux profiles for the non–Nor'wester and Nor'wester days reveal several interesting features which has been discussed in Section 4.1.

The possibility of the existence of an IGW mode on the Nor'wester day suggests itself from this study. To explore this further, a numerical experiment was performed for the same day with the linear wave model described in Section 3.3. The aim of this experiment was to explore the possibility of IGW modes being supported in the troposphere due to a disturbance having the typical spatial dimensions observed in Nor'westers and propagating horizontally with different phase speeds. The results have been discussed in Section 4.2. The interesting feature that emerges is that, IGW modes are indeed supported on 22 May and all these modes, generated in shear layers around 15 km, propagate downward with the transport of energy and momentum to the ABL intensifying with increasing phase speeds of the disturbance.

Using the same linear wave model, we next make a detailed study of the IGW mode characteristics over the three stations and compare them for the non-Nor'wester and Nor'wester days. The model outputs and the role of the associated diagnostics in aiding storm development or non-development have been discussed in Section 4.3. These investigations not only provide a theoretical basis for the study of mechanisms leading to Nor'wester development but reinforces also in a significant way, the fact that the concept of IGW modes is capable of providing some idea, although qualitative for the present, about the processes leading to the final occurrence of the storm.

Finally, an attempt at numerically simulating the pre-storm structure of the lower troposphere over Calcutta for 22 May, has been described in Section 4.4. Once again, the T3 model has been used for the purpose and the evolution of the virtual potential temperature and wind fields documented, from nearly 7 hours prior to the storm to 2 hours before its occurrence. Interesting features of heating/cooling patterns and injection of easterly or westerly momentum at the ABL top, above it and at the surface are the outcome of this investigation.

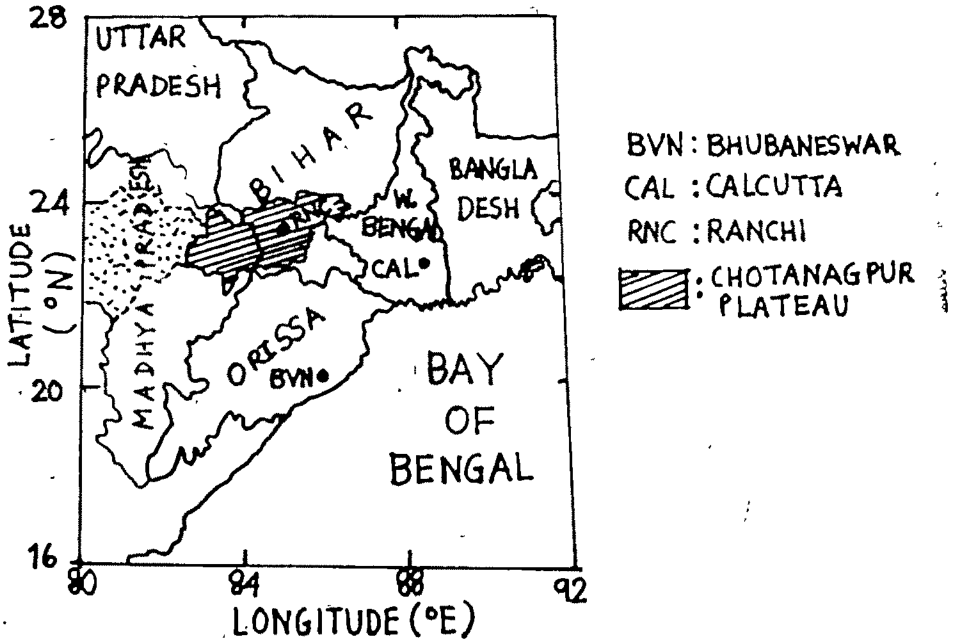

Figure 4.1 : Schematic showing location of the Nor'wester prone region. BVN–Bhubaneswar, CAL–Calcutta, RNC–Ranchi. Hatched area represents the Chotanagpur Plateau.

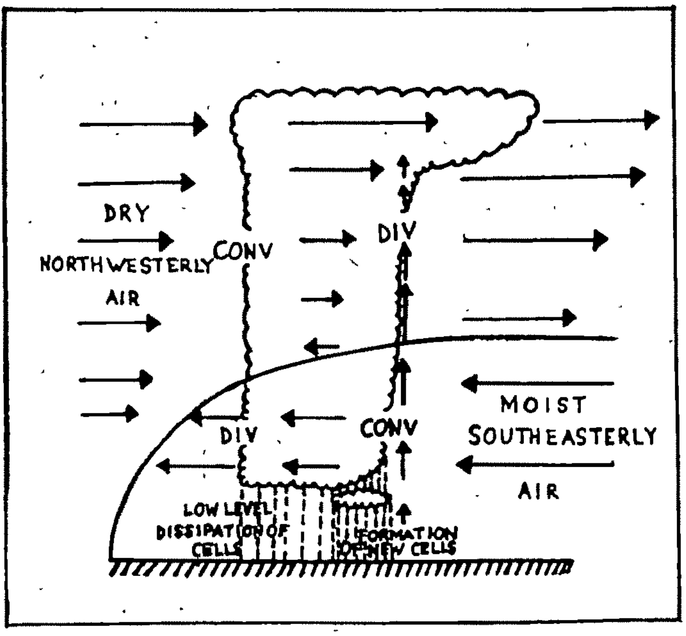

Figure 4.2 : Schematic showing the vertical structure of a Nor'wester (after Newton, 1951).

4.1. Intercomparison of ABL Fluxes During the Pre-Monsoon Period

The following discussion is based on the analysis of the T3 model outputs of turbulent fluxes of buoyancy $\overline{w\,\theta'_v}$ (K ms^{-1}), zonal momentum $\overline{u'w'}$ (m^2 s^{-2}) and meridional momentum $\overline{v'w'}$ (m^2 s^{-2}) over Calcutta, Ranchi and Bhuvaneshwar at 1100 LST (0530 GMT) on 10 May 1988, a non-Nor'wester day and at 1100 LST (0530 GMT) and 1745 LST (1215 GMT) over Calcutta on 22 May 1988, the Nor'wester day. In this investigation, the turbulence adjustment type of responsive parameterization (equations (3.1,5)–(3.1,9), was used for constructing the elements of the transilient matrix.

Inputs to the T3 model included initialized values of $\theta_{v,}$ u, v at 50m intervals, generated from the radiosonde data using the method outlined in Chapter 2, at 0515 GMT at the above three stations on 10 May and at 0515 GMT and 1200 GMT at Calcutta on 22 May. The T3 model was run for a 15 minute time step to compute the fluxes associated with the observed sounding.

(a) Case Study for 10 May 1988 : The Non–Nor'wester Day

The initialized profiles of $\theta_{v,}$ u, v at 0530 GMT have already been shown in Figures (2.1 – 2.3). Figure 4.3. (a,b,c) - 4.5 (a, b, c) contain the vertical variations of buoyancy, zonal momentum and meridional momentum fluxes at Calcutta, Ranchi and Bhubaneswar respectively. As seen from the θ_v and buovancy flux profiles, the ABL has an unstable structure at all the three places. The usual features, such as a shallow, constant flux layer adjacent to the surface (approximately 10% of the ABL height), a well defined mixed layer capped by a stable layer of free atmospheric air can be clearly discerned from the profiles. The heights of the ABL at the three stations, corresponding to the level of most negative heat flux are observed to be at 450 m above surface at Calcutta, 800 m above surface at Ranchi and 200 m above surface at Bhubaneswar.

Characteristics of the ABL features found for the 1100 LST simulations have been tabulated below.

TABLE 1 : ABL characteristics for 0530 GMT for Calcutta, Ranchi, Bhubaneswar

	CALCUTTA	RANCHI	BHUBANESWAR
Stability	Unstable throughout	Unstable throughout	Unstable in the lower levels
ABL height above surface (m)	450	800	200
Friction Velocity u* (ms^{-1})	.268	.413	.531
Free convection scaling velocity w* (ms^{-1})	1.424	1.917	.97
Surface Layer Texperature Scale (°K)	-0.129	-0.610	-0.278
Max. Values of:			
a) Buoyancy flux (K ms^{-1})	0.216	0.252	0.147
b) Zonal Mom. Flux (m^2 s^{-2})	0.135	0.166	0.213
c) Merid. Mom. Flux (m^2 s^{-2})	0.238	0.089	0.184

*LST stands for Local Standard Time,

CALCUTTA CENTRAL LIBRARY

These values are indicative of the fact that the ABL over Ranchi is the most convective followed by that over Calcutta. Bhubaneswar probably has a cloud cover which is reflected in the low height of ABL. In addition, the effect of the sea breeze is more pronounced at this coastal station.

At all these stations the lower level wind was easterly, changing to westerly over Ranchi in the upper portion of ABL. Variation of wind direction at different levels can be discerned from the accompanying figures.

In the 1215 GMT simulations (figures not provided), the ABL had become stable in the lower parts over all three stations. This is as expected, considering the fact that a few hours prior to sunset, the surface starts cooling and the development of the nocturnal stable boundary layer starts.

We thus note that on 10 May, the ABL characteristics over all the 3 stations do not show any unusual behaviour.

(b) Case Study for 22 May 1988 : The Nor'wester Day

Since the Nor'wester passed directly over Calcutta on this day we have focussed our attention on the ABL characteristics over Calcutta. Figure 2.4 shows the initialized vertical profiles of $\theta_{v,}$ u, v at 0515 GMT on this day. It is interesting to note that at mid-morning the ABL over Calcutta was stably stratified and this stratification extended right upto the 2 km level.

Figures 4.6 (a,b,c) represent the profiles of buoyancy and momentum fluxes, as obtained from the T3 model. Some details of ABL characteristics are given in Table 2:

TABLE 2 : ABL Characteristics for Calcutta for 0530 GMT and 1215 GMT on 22 May, 1988

	0530 GMT	1215 GMT
Stability	Stable	Unstable
ABL height (m) (above surface)	275	900
Friction velocity u* (ms^{-1})	0.854	0.664
Free convection Scaling velocity w*(ms^{-1})	0.795	0.689
Surface Layer Temperature Scale (°K)	-0.066	-0.017
Surface values of fluxes		
a) Buoyancy (K ms^{-1})	0.057	0.011
b) Zonal momentum ($m^2 s^{-2}$)	0.647	0.343
c) Meridional momentum ($m^2 s^{-2}$)	0.335	0.277

It is to be noted that during this period, the wind in the lower part of the ABL was north westerly, at 0530 GMT

A comparison of Figures 4.6 and 4.3. brings out an obviously distinguishing feature between the 0530 GMT flux profiles over Calcutta between the non-Norwester and the Norwester days. The wave like undulations observed in these profiles on 22 May were completely absent in the corresponding 10 May profiles.

As observed from the initialized profiles of θ_v, u,v at 1200 GMT (Fig. 2.5), the ABL has become unstable in contrast to the corresponding profiles for the 10 May case. Also the wind direction has now become south easterly, that is coming from the Bay of Bengal and a 1-1.5 km deep layer of moist sea breeze circulation exists in the ABL. The wave-like undulations in the flux profiles, obtained from the **T3** model (Figures 4.7 a,b,c), show considerable amplifications, especially in the lower levels .Since this wave like feature of the flux profiles is observed to be present persistently on 22 May, from almost 9 hours prior to the storm till about 2 hours prior to the storm, it would not be unlikely to assume that this wave mode provides the necessary trigger, in addition to convection and moisture, for storm intensification.

The main points emerging out of the two case studies can be briefly summed up as follows :

— Comparison of ABL characteristics on a non-Nor'wester and a Nor'wester day reveals some distinguishing features, with respect to thermal stratification and turbulent flux profiles.

— On the non-Nor'wester day 10 May 1988, the ABL over Calcutta was unstably stratified at 0530 GMT whereas, on the Nor'wester day, 22 May, a stable stratification existed throughout the lowest 2 kms of the troposphere at this time.

— On 10 May, northeasterly flow prevailed in the ABL over Calcutta at 0530 GMT. On 22 May, the mid-morning flow was northwesterly in the lowest 3 km but at 1215 GMT, a 1 to 1.5 km moist south easterly flow was observed in the ABL.

— The friction velocity at Calcutta on the Nor'wester day at 0530 GMT and 1215 GMT was higher than that observed on the non-Nor'wester day

— Profiles of the vertical components of turbulent fluxes $\overline{w'\theta_v'}$, $\overline{u'w'}$ and $\overline{v'w'}$ have wave like undulations at 0530 GMT over Calcutta on the Nor'wester day, a feature completely absent in the corresponding profiles on the non-Nor'wester day. These wave like undulations amplified further at 1215 GMT, which was 2 hours prior to the storm.

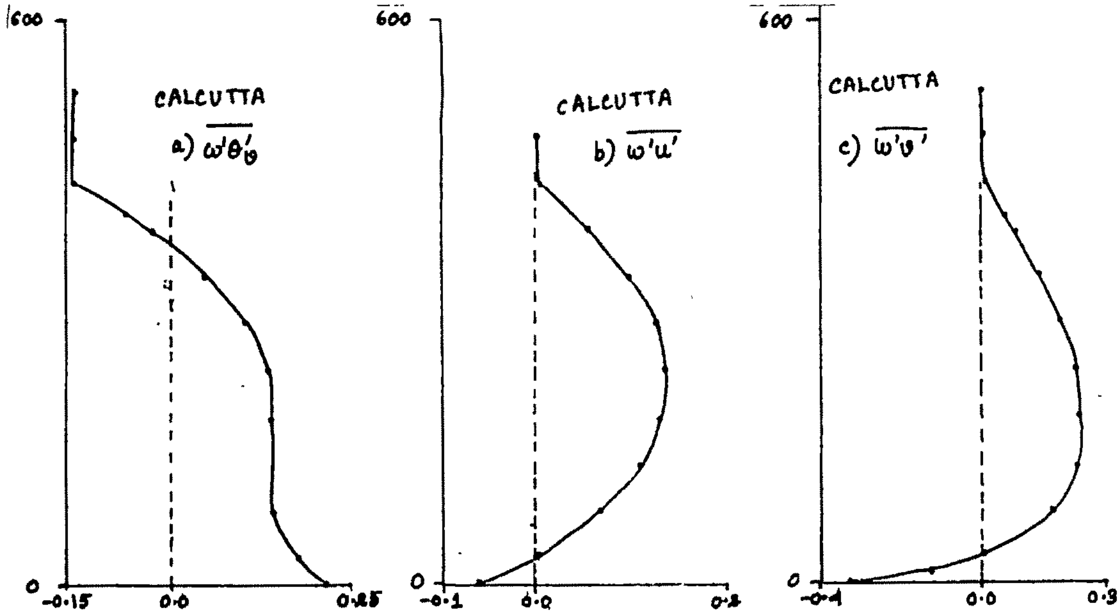

Figure 4.3 : Transilient model outputs. Vertical profiles of turbulent fluxes over Calcutta 0530 GMT, 10 May, 1988. (a) buyancy flux (K. ms^{-1}) (b) Zonal momentum flux (m^{2}s^{-2}) and (c) meridional momentum flux (m^{2}s^{-2}).

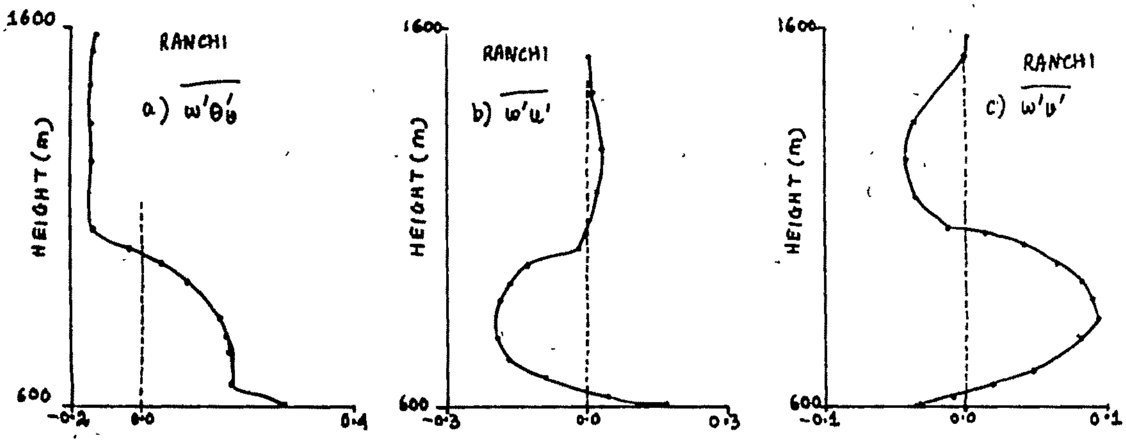

Figure 4.4 : Same as in Fig. 4.4, for Ranchi, 0530 GMT, 10 May 1988.

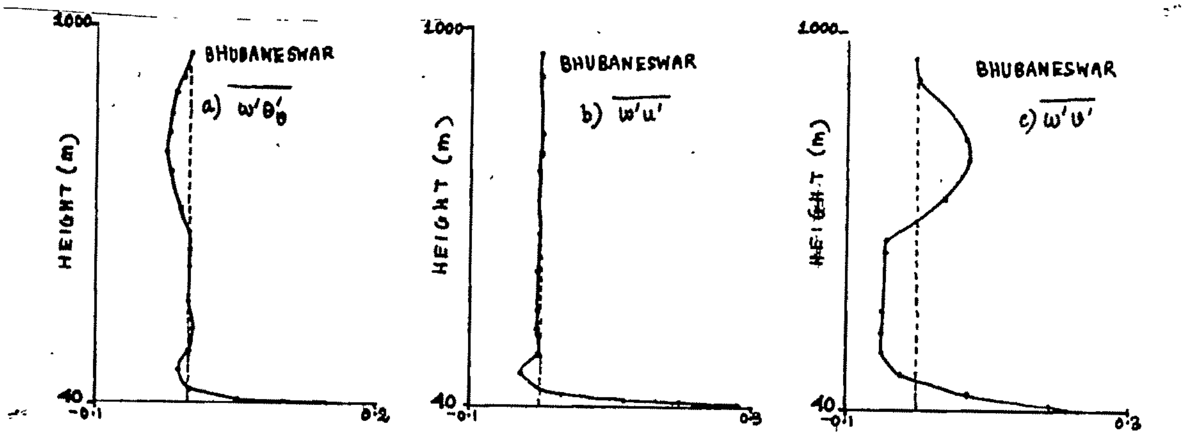

Figure 4.5 : Same as in Fig 4.4, for Bhubaneswar, 0530 GMT, 10 May 1988.

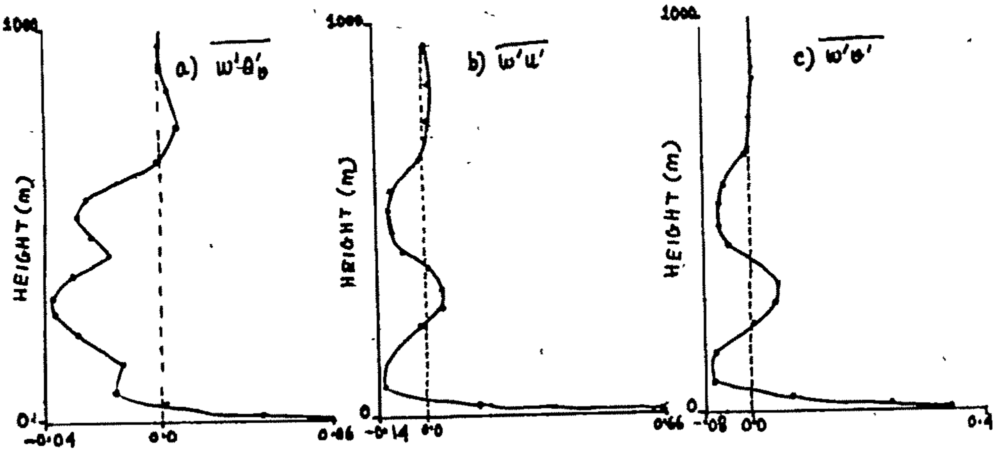

Figure 4.6 : Modelled vertical profiles of turbulent fluxes over Calcutta 0530 GMT, 22 May 1988. (a) buyancy flux (°K. ms^{-1}) (b) zonal momentum flux (m^2s^{-2}) and (c) meridional momentum flux (m^2s^{-2}).

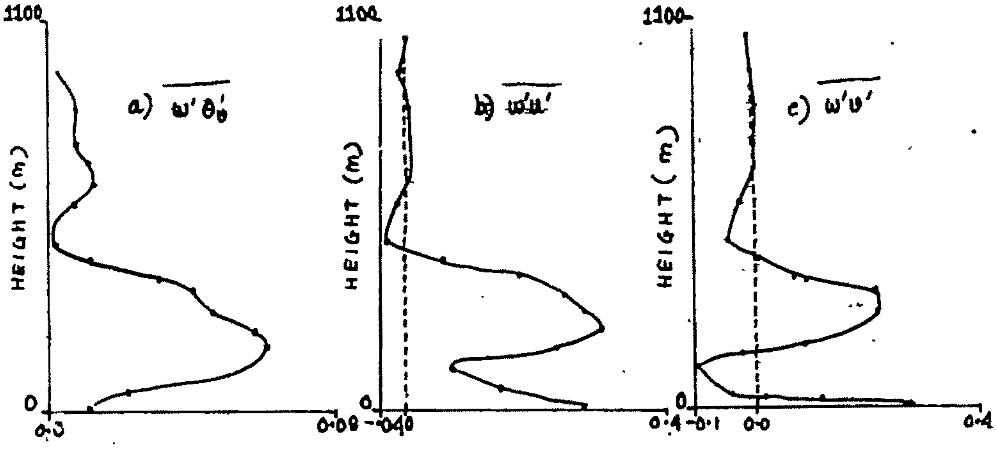

Figure 4.7 : Same as in Fig 4.6, for Calcutta, 1200 GMT, 22 May 1988.

4.2 Internal Gravity Waves in the Pre-Monsoon Troposphere — Part I : The Effect of Phase Speed on Stability.*

The linear wave model, described in Section 3.3 has been used to examine the stability of an Internal Gravity Wave (IGW) mode generated by a horizontally propagating disturbance with respect to the variations in its phase speed under prescribed meteorological conditions. Specifically, we wish to investigate at what phase speeds of the disturbance, the IGW mode just becomes unstable in the lower troposphere. It is interesting to find that this occurs when the phase speed of the disturbance approaches that observed in pre-monsoon Nor'westers.

The dataset used for this study consists of radiosonde observations of wind, temperature and humidity at 00 GMT over Calcutta on 22 May 1988. The observed profiles of the zonal and meridional wind components u and v (in ms^{-1}) and potential temperature θ (in °K) have been shown in Figure 4.8. It may be recalled that on this day a Nor'wester occurred over Calcutta, 14 hours later. The phase speed of the storm, computed by subtracting the mean wind speed from the reported speed of propagation, was found to be around 10 ms^{-1}.

To carry out this investigation, simulation experiments were carried out with a horizontally propagating disturbance having a fixed spatial scale of 20 km (the characteristic scale of Nor'westers) and phase speeds sequentially varying to 2.5 ms^{-1}, 5.55 ms^{-1}, 8.33 ms^{-1} and 8.9 ms^{-1}. These phase speeds correspond to time periods ranging from just over 2 hours to 30 minutes and are the observed time period of the surface presure wave recorded by the barograph at the surface observatory at the Centre for Atmospheric Sciences, University of Calcutta. The time period of just over 2 hours is representative of storm free conditions which was found to decrease to 30 minutes with the approach of the storm.

Figure 4.9 shows the vertical variation of the normalized perturbed vertical velocity, $W^*=W/C_{11}$ obtained for the first experiment in which the phase speed of the disturbance was kept at 2.5 ms^{-1}. It is found that k_i^2 (equation 3.3,4) in this case, is negative within the 5–15 km levels, which is thus a layer of dynamical instability. Inspection of Figure 4.11 reveals that this is a region of strong wind shear. This shear driven instability generates an IGW mode at the 15km level which propagates vertically (see Figure 4.9). Our interest is in the downward propagating branch of the wave, particularly in the levels below 5km. Within the lowest 5km of the troposphere, k_i^2 is positive. The IGW mode carries down sufficient energy so that below 5km, it is supported as a wave with a vertical wavelength of about 4.5km. The existence of a zone of strong wave induced convergence between 5–15 km. and a weak divergence below 5km can be inferred. This indicates the initiation of a downdraft around 15km reaching down to the surface.

The profile of W^* obtained on increasing the phase speed of the disturbance to 5.55 ms^{-1} is shown in Figure 4.10. The IGW mode in this case, has been generated around the 16.5km level with considerable amplification between the 4–13km. The wave amplitude is very small below 4km. The strong wave induced divergence within 13–16.5km and a convergence zone below 13km initiates an updraft from the surface level in this case.

---

* Contents of this section has been published in Proc. Indian Natn. Sci. Acad., 1994, Ser A., 60, pp 171-179.

In the next experiment, the phase speed of the disturbance is increased to 8.33 ms^{-1}. Once again, we find from the profile of W* given in figure 4.11, that the IGW mode has been generated at 15km with the dominant portion of the wave energy confined between 13–18km. Interestingly, the 7–12km layer is another region of dynamic instability in which the wave amplitude has another maximum around 11km. Thus, this layer has the potential for exciting another IGW mode. It may also be possible that, the IGW mode genreated at 15km amplifies within this layer during its downward propagation, by extracting energy from the mean flow in this layer. Below 7km, this mode is supported as an IGW with a vertical wavelength around 6km, with an amplitude considerably higher than that observed in the two earlier cases. A zone of strong wave induced divergence can be inferred between 7–11km with a relatively weaker convergent zone below, upto 2.5 kms.

In the final experiment, the phase speed of the disturbance was taken to be 8.9 ms^{-1}, which is close to the observed phase speed of the Nor'wester on that day. The IGW mode was once more found to have been generated at 15km, due to the shear generated instability of these layers. In this case, the wave amplitude was found to be so large above 10km, that in order to depict clearly, the variations at the lower levels, the profile of W* upto the 10km level has been shown in Figure 4.12. We find that between 7.5–10km, a strong zone of wave induced convergence overlies the zone of divergence between 3–7.5km. A weak convergence zone below 1km is also seen, capped by a zone of stronger divergence between 1–2.5km. A zone of strong convergence between 2.5–3km and a strong downdraft from around 10 km can be inferred in this case.

The main findings from this investigation can be summed up briefly as follows:

— The strong wind shear driven instability observed near the 15km level over Calcutta at 00 GMT on 22 May 1988, a Nor'wester day, is resposible for generating vertically propagating IGW modes.

— The amplitude of the downward propagating part of the IGW mode increases as the horizontal phase speed of the mode approaches that of the storm, implying a corresponding increase in the energy content of the mode.

— As the phase speed of the IGW mode approaches that of the storm, the increasing instability of the lower layers of the troposphere causes further amplification of the downward propagating mode through extraction of energy from the mean flow in these layers. Consequently, the transport of energy to these layers increases which is evident from the gradual amplification of the mode seen in Figures 4.9–4.12.

— The downward propagating IGW mode transports momentum downwards by organising zones of convergence and divergence, instrumental in initiating up-and-down drafts.

— A gradual increase in the strength of the downdraft from the 15km level is observed, as the phase speed of the mode approaches that of the storm.

The above conclusions suggest that downward propagating IGW modes generated in the upper layers of wind shear driven instability may perhaps be considered to be possible mechanisms aiding the development of Nor'westers.

In this context, it can be stated that, observational evidence of propagating, organised meso-scale cloudbands following a period of severe thunderstorm activity over Southwestern United States were attributed to the excitation of IGW modes by the storm (Erickson and Whitney, 1973; Ley and Peltier, 1981). Aircraft observations of IGW modes, acting as mechanisms for exchange of energy and momentum between the upper and lower atmospheres during the Convective Wave Project (1984,85), at the National Centre for Atmospheric Research, Boulder, Colorado led Clarke et al (1986) to develope a theoretical framework. Several investigators (Matsumoto et al., 1967 a,b; Matsumoto and Akiyama, 1969; Matsumoto and Ninomiya, 1969; Bosart and Cussen, 1973; Uccellini, 1975; Houze, 1976 a,b) have suggested that, travelling mesoscale disturbances produce IGW's which are responsible for initiation and intensification of precipitation and triggering of severe convective storms.

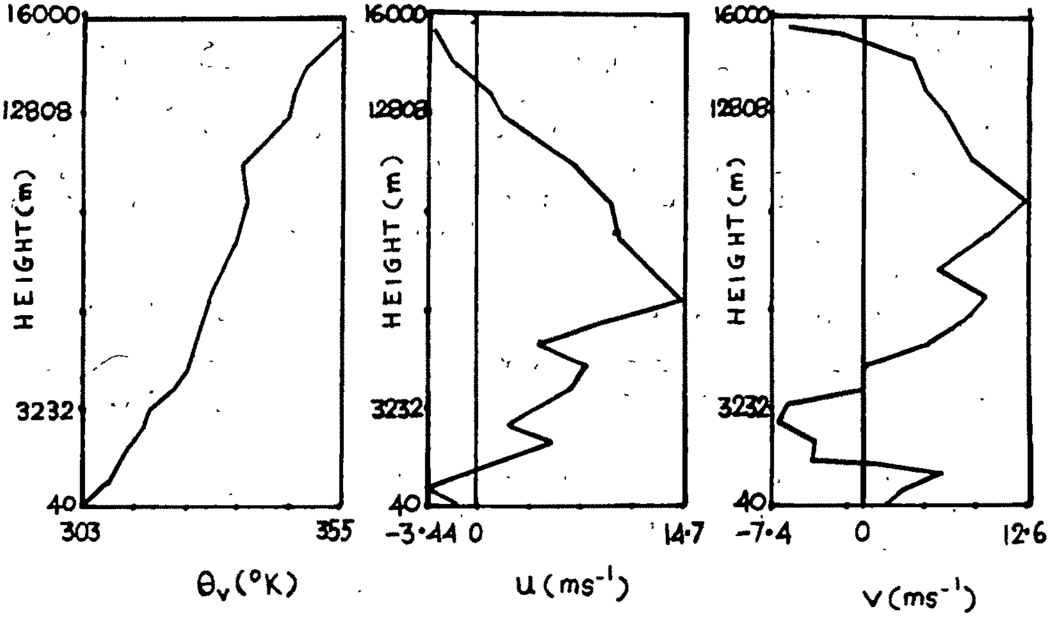

Figure 4.8 : Observed profiles of (a) potential temperature θ (°K), (b) Zonal wind u (ms^{-1}) and (c) meridional wind v(ms^{-1}) over Calcutta, 00 GMT, 22 May 1988.

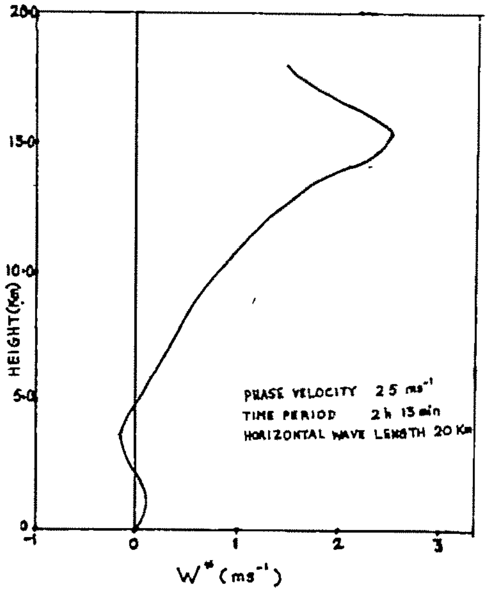

Figure 4.9 : Variation of normalized perturbed vertical velocity W* with height over Calcutta, 00 GMT, 22 May 1988. Phase speed of disturbance c = 2.5 ms^{-1}.

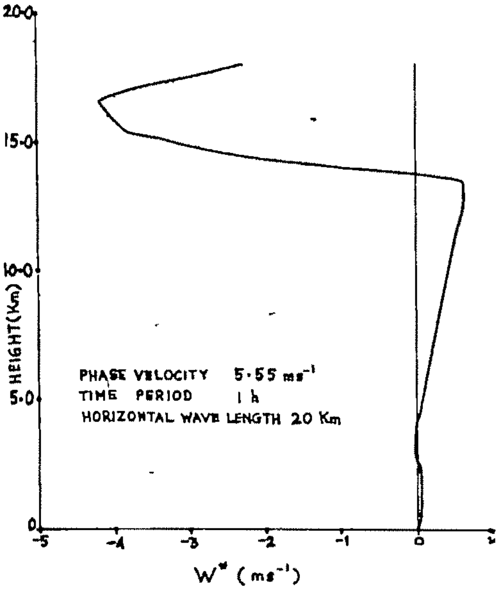

Figure 4.10 : Same as in Fig 4.12, for c = 5.55 ms^{-1}.

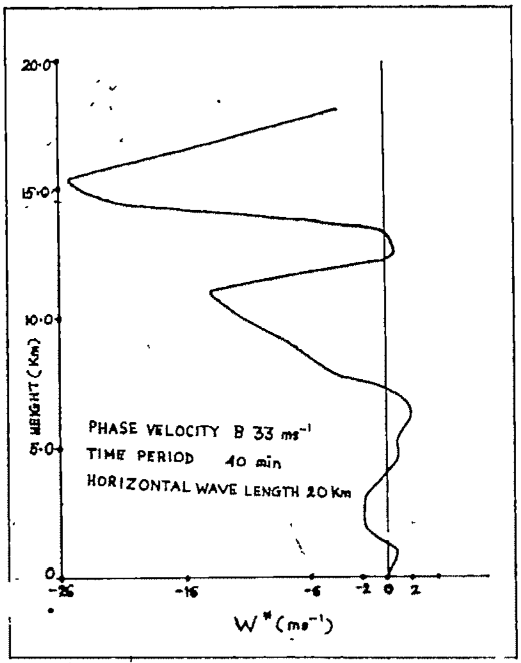

Figure 4.11 : Same as in Fig 4.12, for c = 8.33 ms^{-1}.

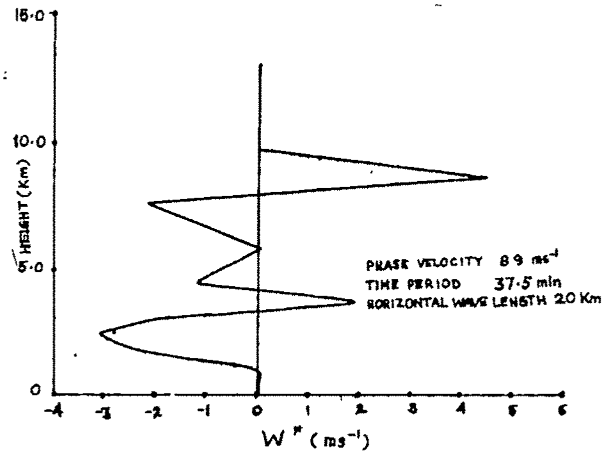

Figure 4.12 : Same as in Fig 4.12, for c = 8.9 ms^{-1}.

4-3. Internal Gravity Waves in the Pre-Monsoon Troposphere Part-II : Their Role in Storm Development.

Emboldened by the findings of the previous section, namely, that IGW modes can be a possible mechanism for triggering Nor'wester development, we have attempted to investigate how the transport of energy and momentum by IGW modes affect the process of storm development. We use again, the linear wave model described in Section 3.3 and study the behaviour and properties of the IGW modes under the meteorological conditions observed on the non-Nor'wester day over Calcutta, 10 May, 1988 and on 22 May 1988, on which Calcutta experienced a Nor'wester in the evening.

Following the procedure mentioned in 4.2, we examine the stability of IGW modes generated by a small amplitude, horizontally propagating disturbance with spatial dimension of 20 kms, as observed in a Nor'wester and a phase speed of 10 ms^{-1}, in a northwest–southeast direction.

The prescribed meteorlogical conditions are those indicated by the radiosonde observations of wind, temperature and humidity over Calcutta and Ranchi at 0515 GMT and 1200 GMT. Extension of the analyses to Ranchi has been made because of its location well within the storm genesis region of the Chotangpur Plateau. The choice of the mid-morning soundings was motivated by the fact that Nor'wester development usually begins around local noon. The late afternoon soundings were the closest available observations of the storm's occurance over Calcutta.

In the following sections, detailed description of the observed structure of the lower troposphere over Calcutta and Ranchi has been given, together with discussion and analyses of the model outputs of N^2, the squared Brunt-Vaisala frequency, $\alpha(z)$, the modified Scorer's parameter, W*, the normalized perturbed vertical velocity and $D^* = -\frac{dW^*}{dz} / C_{11}$, the normalized wave induced divergence.

Following these, we have discussed the implications that our findings have for aiding storm development, comparing closely the distinctive characteristies of the IGW modes generated under the two contrasting meteorological conditions observed between the non-Norwester and Nor'werster days, as well as those, from 9 hours prior (0515 GMT soundings) to 2 hours prior (1200 GMT soundings) to the storm. Qualitative validation of the model results could be achieved by comparison with available hourly radarscope data from the IMD for 22 May 1988.

(a) Description of Observed Data and Analyses of the 0515 GMT Model Outputs for the Non-Nor'wester day, 10 May, 1988.

Case-1, Ranchi : The observed profiles of the virtual potential temperature θ_v, wind components u,v and specific humidity q are shown in Figures 4.13 (a,b,c and d) respectively. The lowest 400 m are unstably stratified $\frac{\partial \theta_v}{\partial z} < 0$, overlying which is a deep, well mixed, nearly adiabatic or weakly stable layer extending from 1.14–4.5 km asl. Above this lies a strongly stable layer extending upto 5.5 km asl*. This θ_v profile is typical of a mid-morning, convective lower troposphere. The entire lower tropospheric flow from surface to 5.5 km asl is northwesterly with a strong, deep, wind shear zone between 2–4km asl. The specific himidity q decreases sharply in the lowest 400 m above which q decreases slowly with height upto nearly 4.5 km asl and again decreases sharply above this. This indicates that convection in the lower layers is suppressed above 400m and the incursion of the dry northwesterly air is drying up the lower layers.

---

*asl stands for above surface level.

The profiles of $N^2(z)$, $\alpha(z)$, $W^*(z)$ and $D^*(z)$ are illustrated in Figures 4.16 (e,f,g and h) respectively. The effect of convection is reflected in the $N^2(z)$ profile, which is negative upto nearly 1.5 km asl, above which, it is weakly positive upto nearly 4km asl and strongly positive upto 5 km asl. As observed from Figure 4.13 (f), $\alpha(z)$, in the lower layers, assumes near zero values upto nearly 2.5 km asl. Between 2.5–4 km asl, the $\alpha(z)$ profile acquires a wedge–like shape with $\alpha(z)$ attaining its maximum value around 3.25 km asl. Above 4 km asl, $\alpha(z)$ is positive and increases slowly upto 5.5 km asl. The wedge shape in this profile corresponds to the strong wind shear zone.

The $W^*(z)$ profile, Figure 4.13g, shows that an IGW mode has been generated, with considerable amplification below 2 km asl. Recalling that below this level, the effects of convection, rather than that of wind shear dominates, one can infer that this IGW mode has been generated due to convective processes at the lower levels. Corresponding to the wedge shaped zone in the $\alpha(z)$ profile (which is also the zone of strong wind shear), the wave mode becomes stable and remains so upto nearly 5.5 km asl. The wave amplitude also decreases in this zone.

As seen from Figure 4.13 h, a region of wave induced convergence existes from surface upto nearly 5 km asl with divergence above this.

Case–2, Calcutta : The observed θ_v profile (Figure 4.14a), shows unstably stratified layers in the lowest 500 m and in another zone between 2.5–3.75 km asl. Stably stratified layers exist between 0.5–2.0 km asl and again above 4.5 km asl. Zones of adiabatic lapse rates are located between 2–2.5 km asl and 3.75–4.4 km asl. The lower tropospheric flow is northeasterly throughout (Figures 4.14 b,c), with moderate northeasterly shear below 500m and strong shear above 3 km asl. Within the lowest 400m, the specific humidity q (Figure 4.14d) decreases, then increases upto nearly 1.5 km asl decreasing sharply again upto 5km asl and then remaining nearly constant upto 6 kms asl.

Figures 4.14e and f, depiciting the vertical variations of $N^2(z)$ and $\alpha(z)$ are nearly similar in shape, at least within the lowest 2.5 km asl where wind shear is moderate and convective effects are dominant.

The profile of $W^*(z)$, shown in Figure 4.14 g, represents an IGW mode which is evanescent above the 3.5 km level. From Figure 4.14 h, we find that the low level convergence increases upto 3.5 km and then decreases rapidly to attain values near to zero above this level.

(b) Description of Observed Data and Analyses of the 0515 GMT Model Outputs for the Nor wester Day, 22 May, 1988.

Case–3, Ranchi : The θ_v profile (Figure 4.15a) for Ranchi, on this day indicates that,except for an adiabatic layer between 2.22 –3.3 km asl, the lower atmosphere from the surface upto 6 km asl is stably stratified. The lower tropospheric flow (Figure 4.15b and c), is dominantly northwesterly, with the exception of a thin layer between 1.4–1.5 km asl and a deeper layer above 4.5 km asl, where the flow is from the southwest. Strong northwesterly shear zones exist below 1 km asl and above 1.5 km asl. Southwesterly wind shear exists between 4.5–6 km asl. The specific humidity q (Figure 4.15d), decreases slowly from surface upto 2.5 km asl and rapidly above it upto 6 km asl.

The $N^2(z)$ profile, Figure 4.15e, shows that $N^2(z)$ is positive throughout the lowest 6 km asl being studied, reaching very small values within the adiabatic zone between 2.22–3.8 km asl and increasing rapidly above this. The $\alpha(z)$ profile, Figure 4.15f, also shows positive values throughout. Thus conditions are favourable for supporting a stable IGW mode. The familiar wedge–shaped zone containing a maximum value of $\alpha(z)$ around 5 km asl is, in this case, located approximately between 4.4–6 km asl, that is, higher than that observed at the same time on the non-Nor'wester day. Another smaller wedge shaped zone can also be discerned at lower levels, between 1.5–2.5 km asl. The location of these two zones correspond to the zones of high wind shear and indicates the dominance of wind shear over convective processes.

The variation of $W^*(z)$ with height, has been illustrated in Figure 4.15g. From this one finds the existence of a well defined, stable, IGW mode, with vertical wavelength around 5.5 km. The amplitude of the wave mode increases with height. Noting again, the existence of stronger wind shears above 4 km asl which shows also an increasing trend with height, it can be inferred that the wave mode is generated at some dynamically unstable shear layer of low Richardson number located above 5 km asl. It can also be inferred that this wave mode is transporting energy from the upper to the lower levels.

Figure 4.15 h, shows a zone of strong convergence between 2-4.5 km asl, with a maximum near 2.3 km asl and a stronger maximum around 3.8 km asl. Zones of divergence exist below 2 km asl and above 4.5 km asl, with the upper divergence being relatively stronger.

Case–4, Calcutta : The θ_v profile, Figure 4,16a, indicates that the lower troposphere between surface to 2 km asl and above 2.5 km asl, has a stable stratification. In between, from 2–2.5 km asl exists an unstably stratified layer. The mean flow throughout the 3.1 km asl studied, is northwesterly (Figures 4.16b and c), with strong northerly shear between 1–2 km asl and strong westerly shear above 2 km asl. The specific humidity (Figure 4.16d), is constant within the lowest 400 m and then decreasing sharply upto 2.5 km asl, assumes its minimum value at this level and begins to increase very slowly above this.

$N^2(z)$, seen from Figure 4.16e, is weakly positive and almost constant in the lowest 1.5 km asl, increases sharply to attain its maximum positive value around 2 km asl, decreases rapidly to its maximum negative value around 2.5 kms asl and increases above this again. Thus, below 1.5 km asl, buoyant effects are suppressed, which is compatible with the stable stratification of this layer. The $\alpha(z)$ profile, illustrated in Figure 4.16f, is positive throughout the lowest 3.1 km. Wind shear effects dominate above 2.5 kms asl. Thus, once again, we find conditions favourable for supporting a stable IGW mode.

That this actually happens can be inferred from the profile of $W^*(z)$, shown in Figure 4.16g. The amplitude of the wave mode increases with height. The growth rate of the amplitude, though small, is found to have a layerwise increasing trend, from 2.9×10^{-6} in the lowest 1 km to 5.8×10^{-6} above this level. In comparison, the growth rate of amplitude of the IGW mode observed at the same time on 10 May 1988 for the corresponding levels was about 10^3 times larger. For the present case, noting again that the upper level wind shear increases with height, it can be inferred that the wave mode has been generated within a dynamically unstable shear layer situated above the region of analysis and that the wave propagates downwards.

Figure 4.16 h, shows that the lowest 3.1 km being studied, is a zone of convergence, with a decreasing trend discernible above 2.5 km asl. In keeping with the stable character of the generated IGW mode, it can be inferred that an upper level divergent zone will also exist above 3.1 km asl.

(c) Description of Observed Data and Analysis of the 1200 GMT Model Outputs for the Nor'wester Day, 22 May, 1988.

Case–5, Ranchi : For the present case, as seen from the θ_v profile in Figure 4.17a, the lowest 300 m and the deeper layer between 2 - 3.7 km asl over Ranchi, has an unstable stratification. Stably stratified layers exist between 1-2 km asl and again, above 3.7 km asl. Figures 4.17 b and c, indicate that the observed mean flow throughout the lowest 6 kms of the troposphere is northwesterly. Strong northwesterly shear exists above 2.5 km asl, with the northerly shear decreasing rapidly within 5-6 km asl. The specific humidity (Figure 4.17d), decreases in the lowest 300 m, remains almost constant between 1 - 2.2 km asl, and decreases rapidly between 2 - 3.7 km asl then more slowly above this level. Once again, the incursion of a cold, dry north-westerly air mass between 2 - 3.7 km asl can be inferred.

As observed from Figure 4.17e, $N^2(z)$ is negative in the lowest 200 m and again between 1.7 - 3.5 km asl. Elsewhere, $N^2(z)$ remains positive. $\alpha(z)$, as seen from Figure 4.17f, is nearly zero between surface to 1.5 km asl. Above this level, it is negative upto nearly 3.5kms and elsewhere, strongly positive. A partly formed wedge like shape in the $\alpha(z)$ profile can be discerned above 5 km asl, corresponding to the zone of strong northwesterly shear.

From Figure 4.17g, showing the vertical variation of $W^*(z)$, we find again that, a stable IGW mode has been supported with considerable amplification above 1 km asl, over that found at corresponding levels during the 0515 GMT analysis. As can be seen, the wave mode, generated above 6 km asl, is propagating downwards with the maximum amount of wave energy being confined within 1.5 - 5.9 km asl.

Figure 4.17 h, indicates that below 3 km asl exists a zone of divergence which intensifies considerably above 2.5 km asl. Overlying this, above 5 km asl, is a zone of very strong convergence.

Case–6, Calcutta : The lowest 500 m of the atmosphere over Calcutta for the present case, is unstably stratified, as seen from the observed θ_v profile in Figure 4.18a. Above this level, stable stratification exists upto nearly 6 km asl. From Figure 4.18b and c, we observe that the flow is southeasterly from surface upto 1 km asl, northeasterly between 1 - 1.5 km asl and northwesterly above this, upto nearly 5 km asl. Above this, the mean flow is southwesterly. Strong northeasterly shear exists between 1 - 1.8 km, above which the northerly shear becomes moderate but the westerly wind shear strengthens upto 2.5 km. Northerly shear intensifies above this, upto nearly 5 km. Above 5 kms, southwesterly shear begains to increase. The specific humidity, as seen from Figure 4.18d, increases slightly in the lowest 500m. This can be attributed to the incursion of moisture carried in by the southeasterly flow from the Bay of Bengal. Above this level, upto 1.8 km asl and again, between 2.4 - 3.0 km asl, the specific humidity decreases sharply. Above 3 kms, the decrease is considerably slower.

$N^2(z)$ Figure 4.18e, is found to be positive throughout, except in the lowest 500m, which as already mentioned, is an unstably stratified layer. In Figure 4.18f, we find the familiar wedge shaped pattern in the $\alpha(z)$ profile that was also observed earlier at Ranchi (Cases 1 and 3) which is located between 4 - 5.5 km asl, with a maximum positive value around 5 kms. Below 4 kms, $\alpha(z)$ assumes very low positive values ($\sim O(10^{-7})$). The wedge shaped pattern corresponds to the zone of strong wind, shear shown in Figures 4.18 b and c. Thus, in this case also, we find that conditions favourable for supporting a stable IGW mode exists.

Examination of the W*(z) profile, Figure 4.21g, shows a stable IGW mode with considerable amplification (in comparison to the 0515 GMT mode) at all levels. The fact that the amplification increases with height and so does the wind shear enables us to infer that this wave mode has also been generated in some dynamically unstable zone at upper levels due to wind shear and that the wave mode propagates downwards, thus transporting energy from the upper to the lower levels.

From Figure 4.18 h, we find that the low level convergence, in comparison to the 0515 GMT analyses, has intensified and is now one order of magnitude higher and occupies the layer from surface to nearly 4.5 km asl, with a maximum around 3.6 km asl. Strong divergence exists within 4.5 - 5 km asl, overlying which is another layer of stronger convergence between 5-6 km asl.

Discussion of the Results : Implications for Storm Development

The case studies presented in the foregoing section, enable us to identify some distinctive characteristics of the IGW modes generated on the non-Nor'wester day (10 May, 1988) and the Nor'wester day (22 May, 1988). Furthermore, the previous analysis also helps us to trace the role played by the IGW modes generated on 22 May, 1988 in the development of the storm occurring over Calcutta, later on.

On 10 May, 1988, at both Ranchi and Calcutta, the IGW modes were generated at lower levels, primarily due to convection. Both these modes propagated upwards, transferring lower level energy to the upper levels. However, the mode at Calcutta was trapped below 4 km asl. At Ranchi, the IGW mode induces the development of convergence/divergence zones so that a low level updraft with a core around 1.5 km asl results. At Calcutta, the low level updraft rises upto 3.5 km asl (above which the mode becomes evanescent) and then rapidly mixes with the surrounding air, producing very little vertical motion between this level and that at 4 km asl.

On the Nor'wester day, 22 May 1988, all the IGW modes at Ranchi and Calcutta were stable and downward propagating modes, generated at dynamically unstable shear layers located above the region of analysis. It may be recalled from section 4.2, that for the 00 GMT analysis for this day, IGW modes had been generated in dynamically unstable layers around 15 kms due to windshear. Thus, the mechanisms generating the IGW modes on the non-Nor'wester and the Nor'wester days are quite different.

We now focus our attention on the vertical convergence/divergence induced by the IGW modes. For convenience, we have provided a schematic in Figure 4.19, where the vertical motions associated with these have been shown for Ranchi and Calcutta 9 hours and 2 hours prior to the storm.

At Ranchi, 9 hours prior to the storm strong updraft and downdraft ensues from around the 3.8 km or 650 mb level, (R 9, in Figure 4.19) with the downdraft occupying the lower levels. As mentioned earlier, the 2-4.5 km layer is also a zone of rapid decrease of specific humidity and a zone of adiabatic lapse rate, suggesting the incursion of a cold, dry northwesterly air mass at this level. All these facts suggest the possibility of two processes being simultaneously operative within this zone: cumulonimbus formation is well under way around 2 km asl, and the large scale northwesterly momentum from the incoming air mass is being transported to both upper and lower levels. The low level downdraft is bringing down colder air and possibly precipitation from the mid-level cloud. The updraft is a zone of condensation, with the released latent heat imparting the increasing trend observed in the θ_v profile Figure 4.15a. The schematic R9, is very similar to the schematic of a precipitating mesoscale convective system described in Houze (1989). Thus, 9 hours prior to the storm, the stable IGW, mode at Ranchi has already organised convection so that cumulonimbus activity has begun and further, there is a scope for the Cb cell to propagate along the northwesterly-southeasterly direction, that is along the direction of the mid-level flow.

On the other hand, 9 hours prior to the storm, the stable IGW mode at Calcutta has been able to induce only a weak updraft from the lower levels (C9 in Figure 4.19). That condensation has ensued and has led to the release of latent heat, conspicuously above 2.5 km asl, is evident from the decrease in the specific humidity and corresponding increase in θ_v at and above this level (see Figures 4.16a and d). It may be recalled that in the layer above 1 km asl, the growth rate of the IGW mode is considerably higher. This is in accord with the findings of Chimonas et al. (1980), namely, that the latent heat released during condensation reinforces the IGW mode which in turn augments the condensation process and leads to organised convection (and hence Cb development), at a later stage. Thus, this IGW mode at Calcutta displays the tendency for organising convection later on.

Before we move on to discuss the features 2 hours prior to the storm, it will be useful to consider Figure 4.20, which is a composite of hourly radarscope observations taken at Calcutta between 1140 GMT to 1540 GMT. One finds at 1140 GMT, the formation of three major Cb cells, with the dominant cell already 7 kms tall and positioned approximately 120 kms northwest of Calcutta. It is also seen that of the two other cells, one is positioned near the dominant cell while the other is further northwest of it.

The schematic, Figure 4.19, also provides us with some glimpses of the qualitative behaviour of the mesoscale disturbances induced by the IGW. To do this, we analyse the vertical tilt of the trough line. We begin with R9, in which a westward tilt, increasing with height at all levels is seen. One also finds two levels of non-divergence, at 850 mb (1.47 km asl.) and at 584.5 mb (4.6 km asl), which are levels of maximum mesoscale vertical motion. One can attribute this westward tilt to the velocity of the large scale westerly flow, being greater than the propagation speed of the disturbance, particularly above 2 km asl. The large amount of tilt above 650 mb (in the updraft zone) is responsible for generation of a large amount of potential energy (PE) in the disturbance which converts itself to kinetic energy (KE) as soon as there is an equalization of these two speeds. It may be noted that at fairly low levels there are zones where PE is created, but this does not count much because of continuing dissipation due to boundary layer processes.

On the other hand, if we look to C9, we find a weak westward tilt upto 650 mb, the level of non-divergence. It is also an updraft zone, with little but not as yet effective PE available for storm development. The upper divergence is not yet organised at these levels.

In R2, there occurs below 700 mb, a very weak eastward tilt is the trough line, while above 650 mb, a strong westward tilt and a good amount of eastward tilt between 700-650 mbs. In terms of energy, the lower level is characterized by a conversion of PE to KE and is in a stable state, as evidenced by the faster propagation (than mean flow) of the disturbance at the 700-650 mb level. The upper level is still holding its PE.

At Calcutta, vide C2, there is a considerable westward tilt above 600 mb and this exceeds its counterpart at R2. The PE is thus very large and has increased with time. Below 700 mb, the eastward tilt is very weak but suddenly increases between 750-600 mbs. One can thus take the conversion of energy to be on, but not to a large extent and this may increase with time if the non-diverence level comes down. C2 also brings out two non-divergence levels.

An interesting point to be mentioned is that the level at 4.7 km asl is always a level of non-divergence for both Ranchi and Calcutta at all times. This quasi-stable nature can be possibly explained in terms of a wider consideration of energetics of the relatively higher levels.

Let us now recall the situation at Ranchi at 1200 GMT, that is, two hours prior to the storm at Calcutta. The fact that the wave amplitude below 1 km asl has decreased in comparison to that observed in the lower layers at 0515 GMT can be interpreted as the restabilization of these lower layers. Thus restabilization process may be due to either of the two causes :

(a) the parent storm, after genesis and development, has moved away from Ranchi and the atomsphere is returning to an equilibrium state, or,

(b) the parent strom has moved away from Ranchi and the atmosphere having attained an equilibrium state within the 7 hours (0515 GMT–1200 GMT), is again becoming destabilized.

The fact that the wave energy is confined to higher layers, between 1.5–5.9 km asl suggest that the stabilization process begins at the lowest levels.

Below 1 km asl, the divergence associated with the wave is lesser in magnitude in comparison to the corresponding divergence observed at 0515 GMT. Above this level, divergence intensifies and becomes strongest between 4.5–5 kms. Thus the associated out flow at these levels is considerably greater than that at the lower levels.

This induces a weak vertical motion at the lower levels. The overlying convergence above 5 km asl, increases with height and is stronger than the upper level divergence. This results in a downward motion from these levels upto the level of maxmum outflow. Moreover, the downward motion is comparitively stronger, that is, there is a subsidence of the northesterly air mass into outflow region.

Going back to the pre-storm scenario at Calcutta, the amplification of the downward propagating IGW mode can be attributed to the intensification and the gradual lowering with time of the dynamically unstable shear layer aloft in which the wave mode was generated. The intensification of the shear layers aloft occurs due to the advection of the northwesterly air forming the outflow of the Cb cells northwest of Calcutta, formed earlier (See, Figure 4.20). The low level intensification of this IGW mode causes these layers to become more unstable dynamically and thus enhance the transport of energy into these layers. The intensification of this IGW mode leads to the augmentation of organised convection in the lower trosphere. The vertical convergence / divergence zones due to this mode results in a stronger low level updraft (in comparison with that obseved 9 hours prior the storm) and also lead to the formation of a strong downdraft zone from above 6 kms asl which was not discernible in the 0515 GMT analyses. The formation of the strong downdraft should be taken to mean that subsidence of northwesterly air has begun over Calcutta. Arguing further, one may say that the intensification of the low level updraft accelerates the horizontal inflow of low level northwesterly air apparently coming from the neighbouring Cb down draft region. Thus, subsidence and horizontal acceleration result in a slanted descent of the northwesterly air masses towards the lower levels over Calcutta.

The foregoing remarks stem essentially from possible interpretations, with a view to developing a conceptual framework, for storm development taking an IGW mode as the basic premise. The model outputs and findings thereof, obviously form a basis for this conceptual construct. That this theoretical layout is capable of providing insight into the development of phenomena in the fairly close vicinity of the time of occurrence of the storm may be visualised as follows : In particular, let us seek how the IGW, whose role two hours prior to the storm has been investigated above, evolves after this, till the occurrence of the storm.

For this, let us go back to figure 4.20. We find that at 1240 GMT, the dominant Cb cell has grown to 8kms and has moved closer towards Calcutta, now being located about 75 kms to its northwest, with the two other cells very close to it. With the approach of the strom, at 1340 GMT a well defined squall line, with five major Cb cells can be discerned, lying 60 kms northwest of Calcutta, with the dominant cell now 9 kms high. We note also that at 1340 GMT, a Cb Cell has formed directly over Calcutta.

It is clear that with time, between 1200 GMT and 1340 GMT, cumulonimbus activity over Calcutta and areas in its northwest, has increased considerably. This ought to enhance the various up and down-draft regions and intensify them further. Arguably, this can be organised by the existing IGW mode which itself must also amplify with time. Close to the time of occurrence of the storm, we ought to expect a strong downdraft from aloft to cover the entire lower troposphere over Calcutta. With the amplification of the wave mode with time, this can only be possible with the strengthening of the upper level subsidence and lowering of the divergent zone towards the surface. However, in view of the large increase of mean kinetic energy with the approach of the storm, it is expected that instead of the wave amplification continuing unabated, the wave breaking phenomena would occur just prior to the storm occurrence.

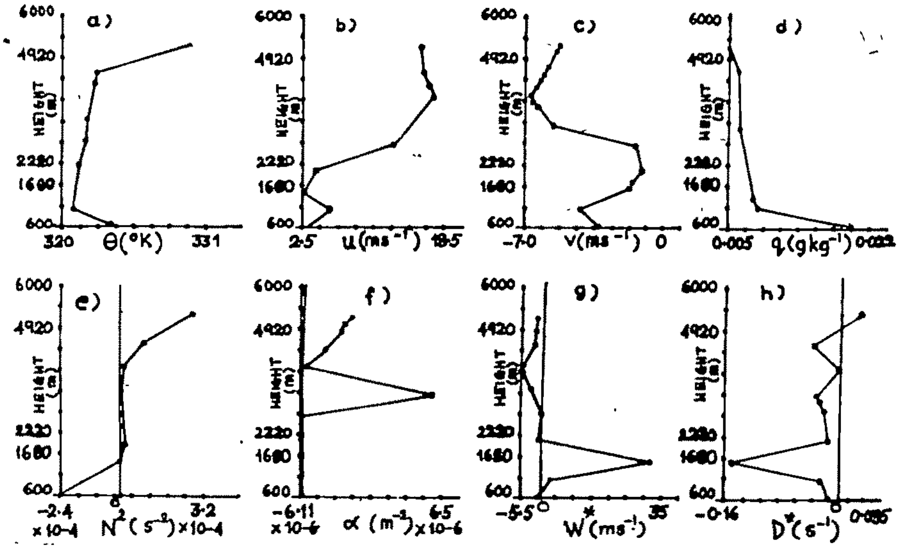

Figure 4.13 : Results of the linear stability analysis for Ranchi, 0515 GMT, 10 may 1988. Vertical profiles of (a) observed virtual potential temperature, θ_v (°K), (b) observed zonal wind u (ms^{-1}), (c) observed meridional wind (ms^{-1}), (d) observed specific humidity q (gms kg^{-1}), (e) squared Brunt Väisälä frequency N^2 (s^{-2}), (f) modified Scorer's parameter, α (z), (g) normalized perturb vertical velocity W* and (h) normalized wave induced convergence D*.

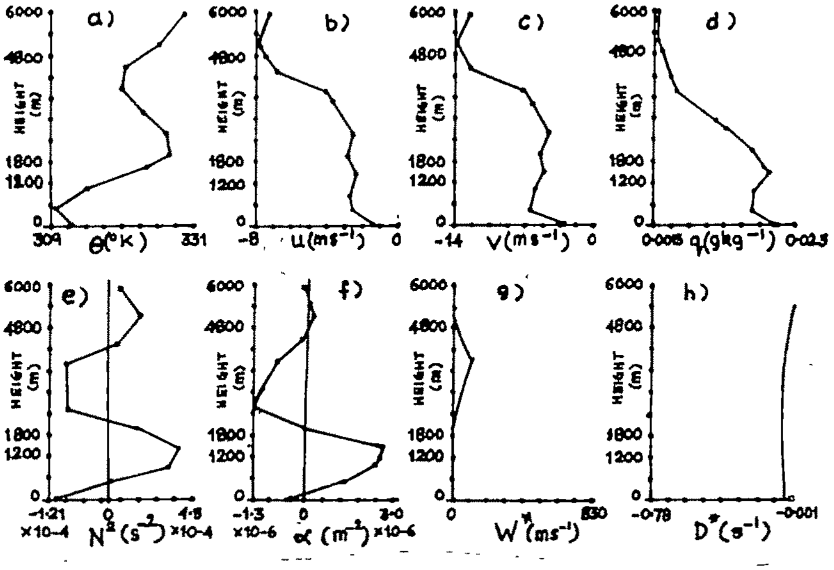

Figure 4.14 : Same as in Fig 4.13, for Calcutta, 0515 GMT, 10 May 1988.

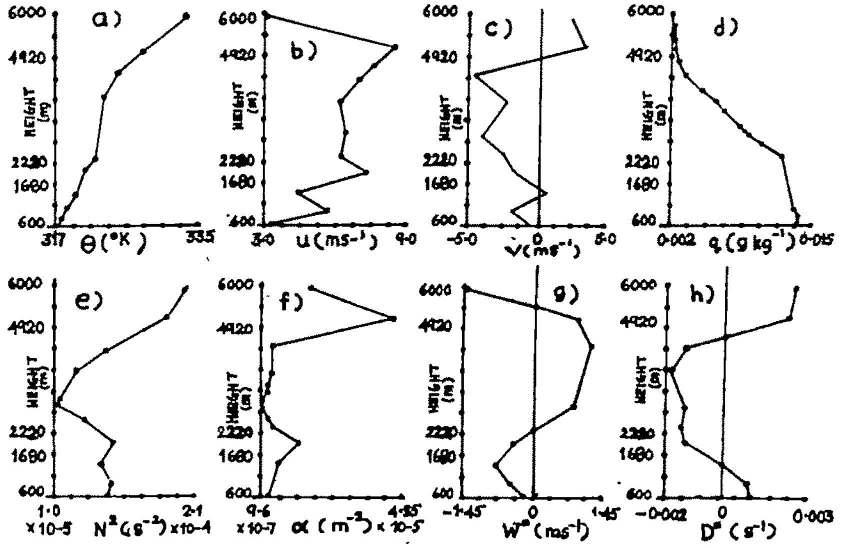

Figure 4.15 : Same as in Fig 4.13, for Ranchi, 0515 GMT, 22 May 1988.

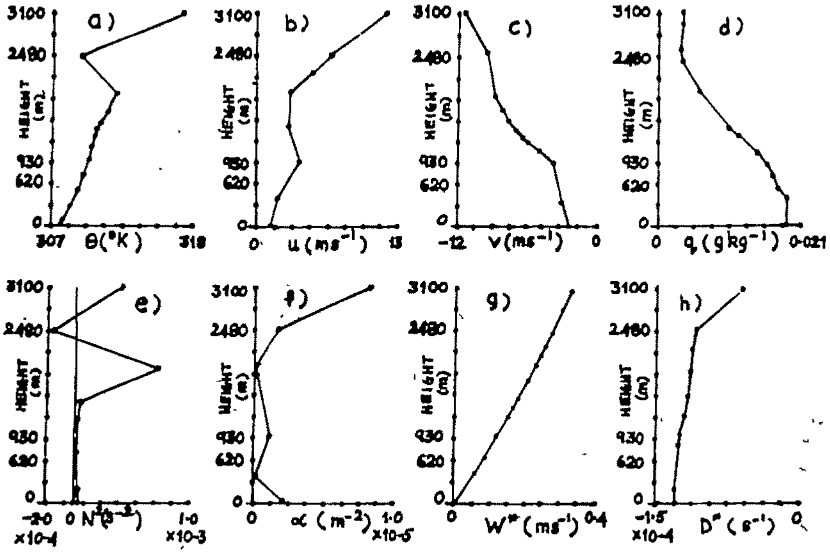

Figure 4.16 : Same as in Fig 4.13, for Calcutta, 0515 GMT, 22 May 1988.

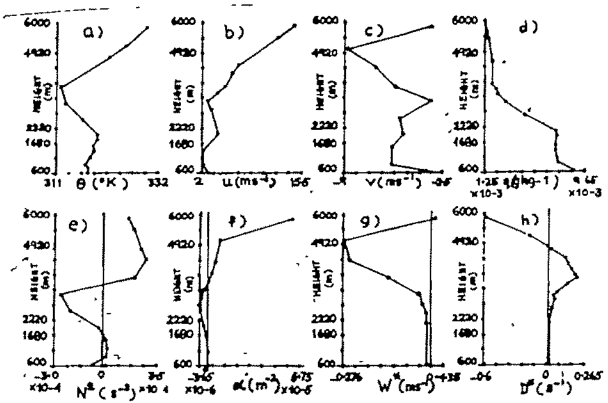

Figure 4.17 : Same as in Fig 4.13, for Ranchi, 1200 GMT, 22 May 1988.

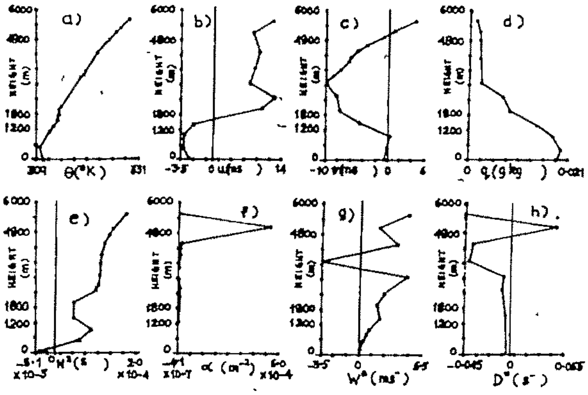

Figure 4.18 : Same as in Fig 4.13, tor Calcutta, 1200 GMT, 22 May 1988.

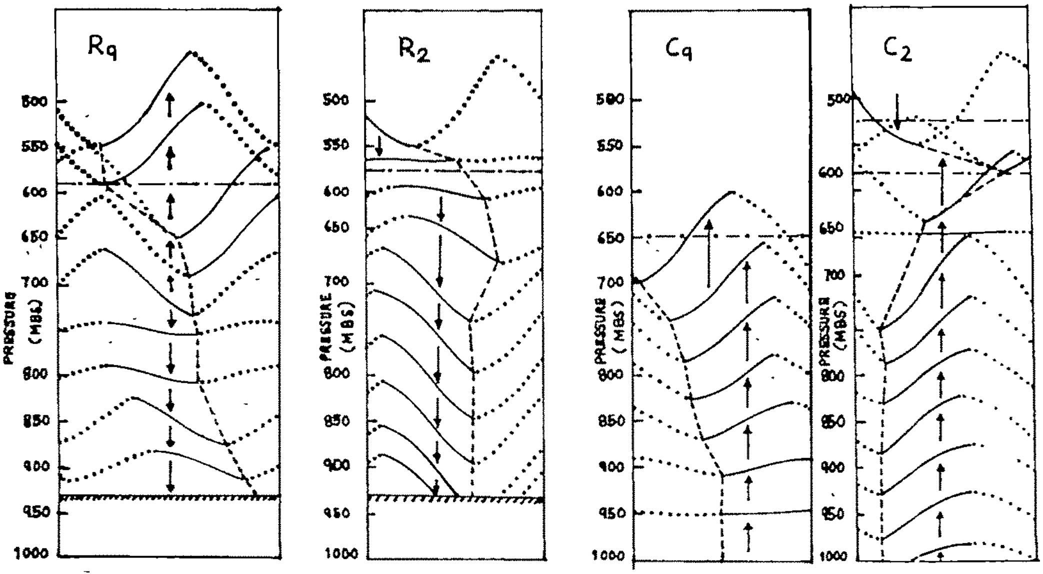

Figure 4.19 : Schematic showing the pre-storm conditions at Ranchi (R) and Calcutta (C) due to IGW activity. Subscripts 9 and 2 correspond to 0515 GMT and 1200 GMT conditions respectively. Dashed lines show the trough line and dash-dot line the levels of non-divergence.

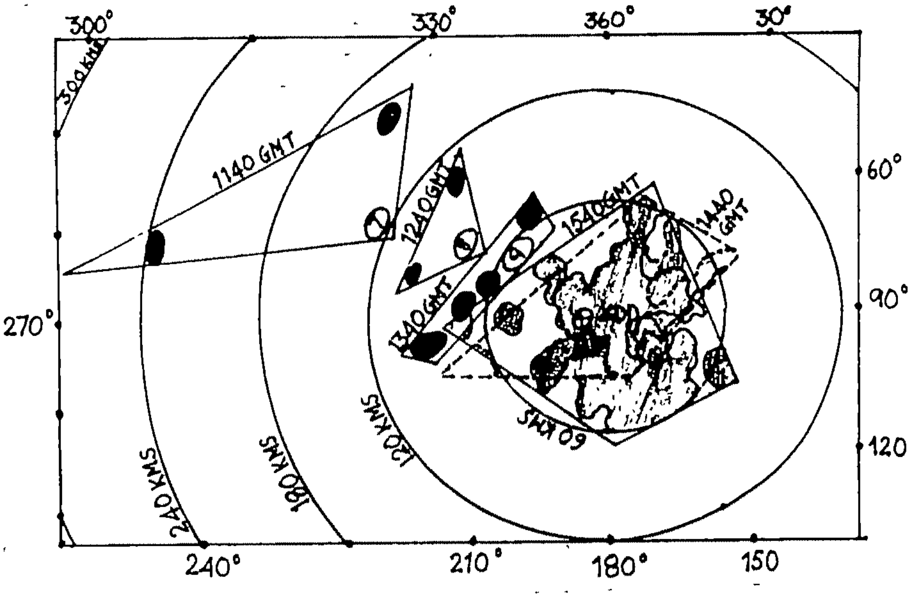

Figure 4.20 : Composite of hourly radarscope observations over Calcutta from 1140 GMT to 1540 GMT on 22 May 1988. DD : Dum Dum and ALP : Alipore, the two Meteorological observatories at Calcutta. The Radar is located at DD. Open circles indicate the dominant Cb cells and the numbers within, their height in kilometers. ⊗ Marks the Cb cell over Calcutta at 1340 GMT.

4.4 Numerical Simulation of the Lower Tropspheric Stucture During A Nor'wester

The successful numerical simulation of the observed characteristics of the atmosphere, such as wind, temperature and humidity profiles and thier fluxes, is essential for gaining insight into the possible physical processes that lead to the genesis, development and occurrence of meteorological disturbances.

A fairly good amount of investigations (see for example, Bengtsson and Lighthill, 1982; Pielke, 1984; ECMWF, 1985; Houze, 1989; Lilly, 1990 etc.) attempting to simulate particular classes of meteorological disturbances and their associated circulation patterns on all significant meteorological scales exist at present. Considerable attention has been given to the simulation of mesoscale disturbances such as Thunderstorms (Klemp and Wilhelmson, 1978a,b; Schlesinger, 1978, 1980; Anthes et al., 1982; Weismann and Klemp, 1982); Cumulonimbus and Squall Lines (Moncrieff and Green, 1972; Miller and Pearce, 1974; Betts et al., 1976; Moncrieff and Miller, 1976; Thorpe et al., 1982) and Tornadoes (Bengtsson and Lighthill 1982). All such studies, involving extratropical and tropical cases, have stressed the crucial role played by surface forcings and the influence of the ABL on the free atmospheric flow which must necessarily be incorporated to provide a realistic simulation.

Investigations of Nor'westers, with respect to the physical mechanisms leading to their development have been mentioned at the beginning of this chapter. Of partidular relevance to the present study, are the findings of Koteswaram and Srinivasan (1958), which identifies the conditions in the upper and lower tropospheres that favour Nor'wester development. These conditions, namely, the superposition of an upper level divergence associated with a westerly jet on a lower level convergence associated with southerly flows in the ABL. In the light of later studies (for example, Moncrieff, 1985), these imply the injection of upper level westerly momentum which decreases the easterly flow and injection of easterly momentum into the middle and lower tropospheric levels due to subsidence. The thermodynamic and dynamic changes associated with convection during the development of a tropical squall line were investigated earlier by Miller and Moncrieff (1978) using a three dimensional model for studying deep convection.

In the following sections we have described the numerical simulation of the vertical structure of the lowest 3 kms of the troposphere over Calcutta on 22 May 1988, prior to the Nor'wester on that day.

Our motivation for the simulation experiments described below was to investigate whether prescribed thermodynamic and dynamic changes, for example, such as those reported in Miller and Moncrieff (1978), could produce a pre-storm lower tropospheric structure conducive to strom development under the conditions prevailing over Calcutta.

With the above motivation, we have used the T3 model (Section 3.1), with initial inputs of virtual potential temperature θ_v, zonal and meridional wind conponents u and v, generated at 50 m intervals and initialized as described in Chapter 2 from the 0515 GMT radiosonde observations over Calcutta on 22 May 1988. It may be recalled that these observations represent the vertical structure of the atmosphere over Calcutta about 9 hours prior to the storm. Prescribing hourly changes of θ_v,u and v, the T3 model was integrated with 15 minute time steps upto 1200 GMT, which is 2 hours prior to the storm. To facilitate comparison with the model results, the 1200 GMT radiosonde observations were also subjected to the procedure described in Chapter 2. The mixing potential approach, described in section 3.1 (equations (3.1, 11) — (3.1, 12), has been used to compute the elements of the transilient matrix in this case.

The agreement between the **T3** model results and the 1200 GMT initialized data, for three experiments in each of which different sets of thermodynamic and dynamic changes were prescribed, is found to be good in some cases and considerably different in others. Nevertheless, these experiments provide some insight into the physical processes responsible for producing the observed lower tropospheric structure 2 hours prior to the storm.

In keeping with the basic concept of the responsive approach to the parameterization of turbulent quantities, external forcings of heat and momentum fluxes has been prescribed at each time step at three specific model levels, namely, 6m (surface), 1.05 km asl (850 mb, assumed to be the ABL top) and 2.25 km asl (750 mb, free atomosphere) to cause destabilization of the flow within these layers. Ten minutes of transilient mixing then causes the flow to reach a new equlibrium state.

In order to asses the roles played by these forcings in bringing about the observed vertical structure of the lower (suface to 3 km asl) atmosphere at 1200 GMT, three separate numerical experiments, referred to as experiments A, B and C have been conducted in each of which three different sets of thermodynamic ($\Delta\,\theta_v$) and dynamic (Δu, Δv) changes have been prescribed at these specified levels at the beginning of each time step. The prescribed hourly changes have been listed in Tables 3, 4 and 5 respectively.

Discussion of the Result of the Simulation Experiments

In Figures 4.21 a, b and c, the profiles of θ_v, obtained from the experiments A, B and C respectively , at 0530 GMT, 0930 GMT (for A), 0830 GMT(for B and C) and 1200 GMT (for A, B, C) have been presented with the 1200 GMT observed profiles included for comparison. It can be seen that within the first 1.05 km asl, the 1200 GMT θ_v profile from experiment A show the closest agreement with the 1200 GMT observed profile while that from experiment B overestimates and that from experiment C underestimates them. Above 1.05 km asl, all the θ_v profiles underestimate the observed one, although the magnitude of the differences between 1.05 –1.8 km asl is much larger in Experiments A and B (See, Figures 4.21 a and c) than those from C . However, it may also be seen from Figure 4.21 a, that above 1.2 km asl, the closest agreement between the 1200 GMT observed profiles is reached at 0930 GMT that is at the 5th hour of the simulation.

In Figures 4.22 a, b, c, the profiles of the zonal wind at 0530 GMT and 1200 GMT, for all three exprimments, 0630 GMT (for A) and 0730 GMT (for B and C) have been shown alongwith the 1200 GMT observed profiles. None of the simulated 1200 GMT profiles agree completely with the observed ones. However, below 1.2 km asl, the closest agreement between simulated and observed 1200 GMT profiles come from Experiment C, although the observed transition of the low level easterly flow to a westerly flow above 1.2 km asl does not occur in this case. For experiment A, this transition occurs at 600m, much lower than the observed level. For experiment B, the transition of easterly to westerly flow occurs around 1.6 km asl but in this case, the magnitude of the simulated low level easterlies underestimates the observed ones below 300m asl and overstimates them between 300–1400m asl (see, fig. 4.22 b). Above this level, the simulated westerly wind has magnitudes much less than the observed one. Thus, out of the three the experiments, simulated zonal wind profile from experiment B is by far the closest in agreement to the observed one at 1200 GMT.

Figures 4.23 a, b and c depict the simulated meridional wind profiles from the three experiments at 0530 GMT and 1200 GMT (A, B, C), 0830 GMT (A), and 1030 GMT (B and C) alongwith the 1200 GMT observed profiles. The simulated v-profile in Experiment A indicates a northerly component throughout, while those from B and C are predominantly southerly and are overestimates of the 1200 GMT observed values. Only Experiment C produces a meridional wind profile that becomes northerly around 1.8 km asl (while the observed profile does so around 1.2 km asl) during the 6th hour of simulation. The 1200 GMT simulated profile of v from this experiment shows a tendency to become northerly at much higher levels.

Thus we find that the simulated θ_v profiles from Experiment A agree closely with the observed θ_v profiles within the first 1km of the atmosphere, that is within the ABL. Experiment C produces u and v profiles which are in fair agreement with the observed ones as far as the wind directions are concerned. Magnitudes of the wind speed are underestimates (for u) and over estimates (for v) in this case. The simulated θ_v profiles above 1 km asl for experiment B come closest to the observed ones.

We now look into the physical implications behind providing the prescribed thermodynamic and dynamic changes in these experiments. For example, a striking feature is Experiment A, which simulates most closely, the θ_v profile within the ABL. In order to reconcile the simulated θ_v profile above the ABL in this experiment with the observed profile, a relatively larger heating at 2.25 km is required, which leads to an overestimate of θ_v within the ABL. In physical terms, we may state that the upper levels provide a source of latent heat released due to condensation and cumulonimbus activity facilitating the existence of the larger heating at these levels. The θ_v thus produced at these levels could have been countered by inclusion of mechanisms for transporting the excess heat energy away from the lower levels. This implies the advection of a cold air mass, for example that coming from the outflow of an adjacent thunderstorm, thereby leaving the ABL tempratures relatively unaffected. The advective mechanism, if included, will also influence the wind speeds by injecting northwesterly momentum into the ABL which in turn will perhaps wipe out much of the underestimates in the magnitudes of the simulated wind speeds.

Finally, let us turn to the structure of the lower troposphere that emerges from these simulation experiments. Combining the results from experiments producing the closest θ_v, u and v profiles, we find that by 1200 GMT. ABL has become well mixed and a southeasterly sea breeze now occupies the ABL. Above the ABL top, temperatures increase upto 2.25km and a north westerly flow prevails at this level. Thus, conditions conducive to the occurrence of a Nor'wester have been simulated fairly well.

Table – 3 : Prescribed hourly thermodynamic changes $\Delta \theta_v$ (°k h-1)

Experiment	Height asl (m)	Prescribed Hourly Changes						
		1	2	3	4	5	6	7
A,B,C	6	0.5	1.0	0.5	0	-1.0	-1.0	-1.0
A,B,C	1050	-1.0	-0.5	-1.0	-0.5	-0.5	-0.5	-0.5
A,C	2250	1.0	1.0	1.0	1.0	1.0	1.0	1.0
B		1.0	1.0	1.0	1.0	2.0	1.5	1.0

Table – 4 : Prescribed hourly dynamic changes Δu (ms-1 h-1)

Experiment	Height asl (m)	Prescribed Hourly Changes						
		1	2	3	4	5	6	7
A,B,C	6	1.0	1.0	-1.0	-2.0	-2.0	-2.0	-1.5
A	1050	-1.0	-1.0	-2.0	-2.0	-1.0	1.0	1.0
B,C		-1.0	-1.0	-2.0	-2.0	-1.0	1.0	-1.0
A,B,C	2250	2.0	2.0	2.0	2.0	2.0	2.0	2.0

Table – 5 : Prescribed hourly changes Δv (ms-1 h-1)

Experiment	Height asl (m)	Prescribed Hourly Changes						
		1	2	3	4	5	6	7
A	6	-1.0	-1.0	-1.0	1.0	1.0	1.0	1.0
B,C		-1.0	-1.0	-1.0	1.0	1.0	2.0	1.5
A	1050	1.0	1.0	1.0	1.0	1.0	-1.0	-1.0
B,C		1.0	1.0	1.0	1.0	1.0	-1.0	1.0
A,C	2250	1.0	-1.0	-1.0	-1.0	-1.0	-1.0	-1.0
B		1.0	-1.0	-1.0	-1.0	2.0	1.0	1.0

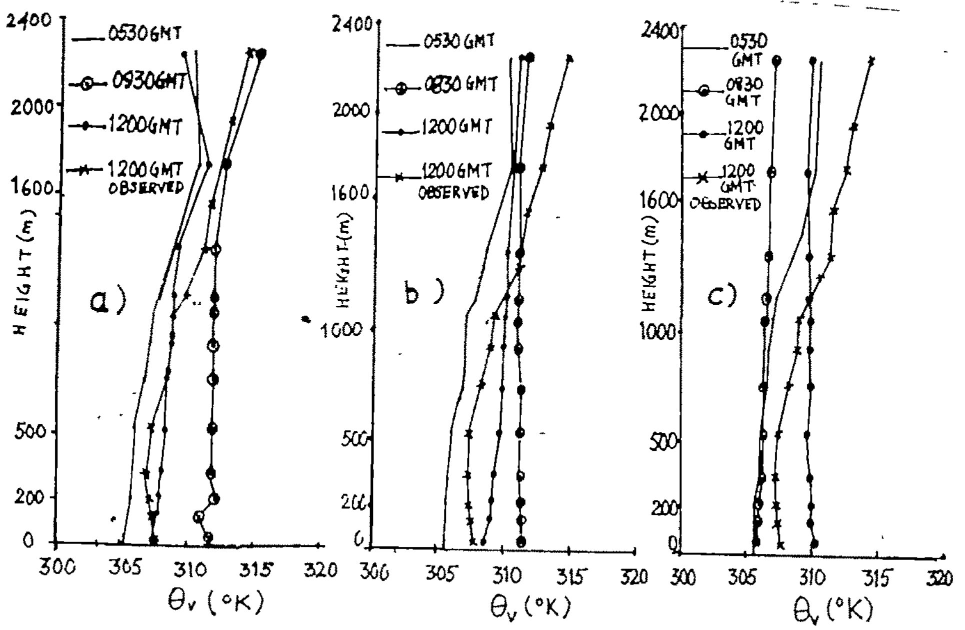

Figure 4.21 : Simulated vertical profile of virtual potential temperature θ_v (°K) for Calcutta, 22 May 1988. (a) Experiment A, 0530, 0930 and 1200 GM (b) Experiment B, 0530, 0830 and 1200 GMT (c) Experiment C, 0530, 0830 and 1200 GMT

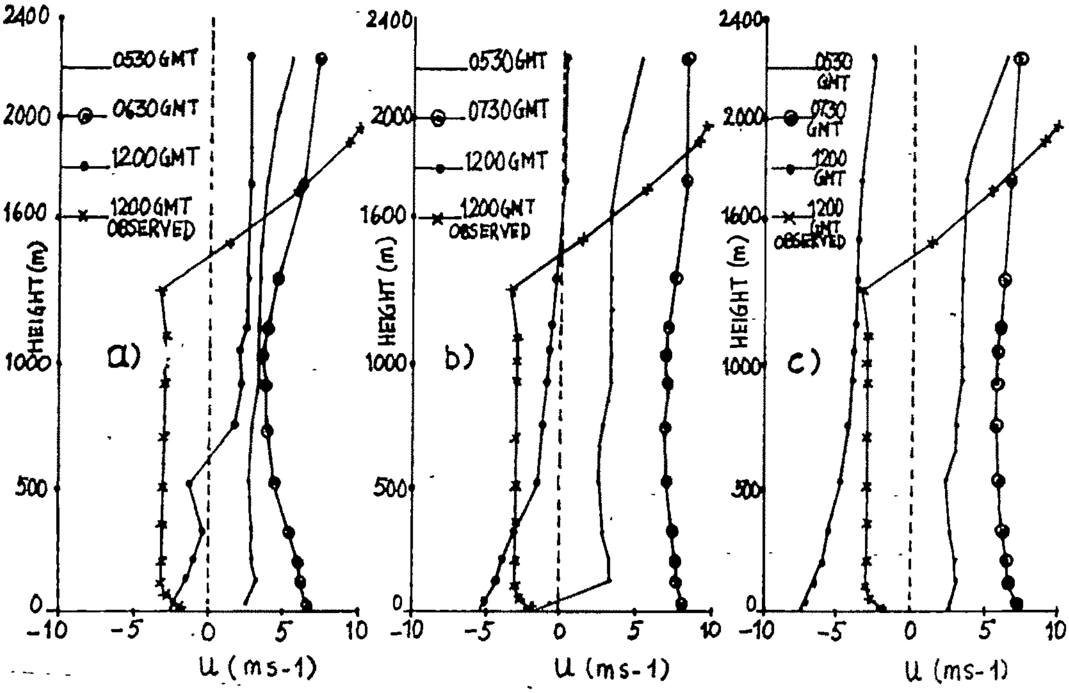

Figure 4.22 : Simulated vertical profiles of zonal wind velocity u (ms^{-1}) for Calcutta, 22 May 1988. (a) Experiment A, 0530, 0630 and 1200 GMT (b) Experiment B, 0530, 0730 and 1200 GMT (c) Experiment C, 0530, 0730 and 1200 GMT

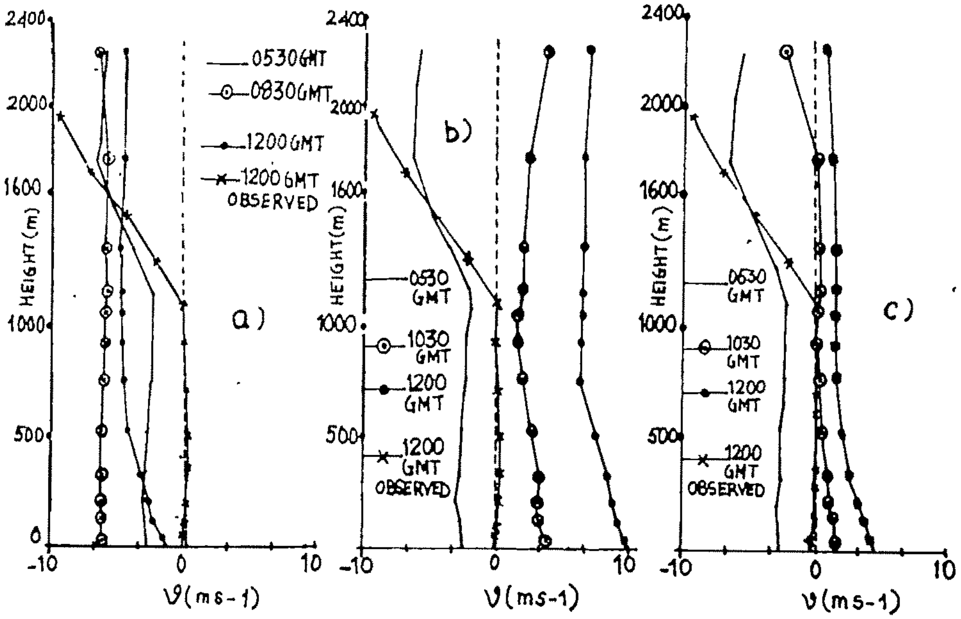

Figure 4.23 : Simulated vertical profiles of meridional wind velocity $v(ms^{-1})$ for Calcutta, 22 May 1988. (a) Experiment A, 0530, 0830 and 1200 GMT (b) Experiment B, 0530, 1030 and 1200 GMT (c) Experiment C, 0530, 1030 and 1200 GMT

Chapter 5

Monsoon Scenarios : Model Results*

1990 was representative of a good monsoon year with an early onset and a prolonged withdrawal phase, characterised by an exceptionally well distributed cumulative rainfall spatially and temporally, with the monsoon trough being active in its normal position (see Fig 1.1.), 50 % of the time. A brief summary of the synoptic conditions observed during the 1990 monsoon (Gupta, 1990) will not be out of the context here.

During the first week of June, the monsoon trough was observed to be in its formative stages with easterlies over northeast India. A low pressure system over north Bay of Bengal observed on 12 June, intensified into a depression and moving in a west-nothwesterly direction made a landfall in the early hours of 14 June at Contai near Kharagpur in West Bengal. With this depression, the monsoonal flow advanced into eastern Uttar Pradesh and the eastern sector of the trough was active (Mohanty et al., 1992). The monsoon trough was established in its position between 13-19 June. Following a shift in the trough position as a result of Western disturbances in northern India, a very deep trough formed during 1–12 July, during which the monsoon was active and substantial rainfall occurred over the entire trough region. After a non-convential break perion during 3–9 August, the monsoon trough assumed its normal position under the influence of another Bay depression on 15 August which again brought in an active monsoon spell.

This withdrawal phase of the monsoon, beginning in mid-August, was prolonged by the occurrence of this and another deep depression centred in north Bay of Bengal between 20–25 August, which brought in a marked change in the trough position to the south. A land depression, from the Arabian Sea side, formed between 3–7 September, bringing widespread rain over the entire monsoon trough region.

In the present chapter, we describe attempts to understand the turbulence structure of the monsoon trough boundary layer using the **T3** and the second order local closure models described in Sections 3.1 and 3.2. For both these models, we have used the tetheredsonde (kytoon) data for 17-21 June, 1990 from Kharagpur (22.3°N, 87.2°E), which is located in the deep moist convective zone of the eastern end of the trough (see Figure 1.1).

From the description of the synoptic conditions given above, we find that the period 17-21 June coincided with the early stages of the monsoon, with the monsoon trough established in its normal position. This period also corresponded to an undisturbed period with no rainfall at or around Kharagpur (Mohanty et al., 1992).

The tetheredsonde observations, consisting of pressure height, air and dew point temperature, wind speed and direction were taken at 00 GMT for 17-20 June. For 21 June, these observations were taken at 1130 GMT. The timings of these observations enable us to study the turbulence characteristics of the early morning ABL (17-20 June) and also the late afternoon ABL (21 June), during its transition from the daytime convective, to the stable, nocturnal, boundary layer.

The findings from these diagnostic studies, described in detail in Sections 5.1 and 5.2, reveal various interesting aspects of turbulent transports within the ABL. These include non-local turbulence statistics obtained from the **T3** model such as, kinematic fluxes of heat and momentum, the mixing length profiles, the contribution of eddies of different sizes to the turbulent fluxes at each level and the one-dimensional anisotropy of the turbulent eddies.

---

* Contents of this Chapter has been partly published in Proc. Indian Acad. Sci. (Earth Plant. Sci.), 1994 **104**,2.

The results from the second order local closure model reveals the strong correlation between the turbulence kinetic energy (TKE) and the vertical velocity variance maxima. It is interesting to find that from some of the cases studied, during which the ABL had a very weakly stable or nearly neutral thermal stratification in the lower levels, distinct zones existed, in which these maxima occurred. These zones have been interpreted as zones of patchy turbulence, a commonly observed feature in stable boundary layers.The behaviour of the pressure covariance terms in the TKE and turbulent flux equations, the vertical velocity variance equation and the dissipation terms is another interesting upshot of the study.

5.1 Understanding the turbulence structure of the monsoon trough boundary layer – Part I : Results from the T 3 model.

The basic inputs to the T3 model are the potential temperature θ (^{o}K) and wind components u and υ (ms^{-1}) computed from the tetheredsonde observations at 10m intervals. These have been used to compute the mixing potentials (equations 3.1, 11 — 3.1,12) and hence the elements of the transilient martrix. The intial profiles of θ, u , v over Kharagpur during 19 - 21 June have been shown in Figure 5.1. The vertical variations of the gradient Richardson numbers, computed from these, shown in Figure 5.2a, give an idea about the thermal stratifications within the ABL on these days. Thus we find that on 19 June, the lowest 15 m of the ABL is unstable, above which lies a stable layer with highly stable zones around 70 - 80m, 100 - 200m and 155 - 211m, with the ABL top around 200m. On 20 and 21 June, the ABL stratification was weaker, with the lowest 15m having a weakly unstable or near neutral stratification on 20 June and a weak stable stratification on 21 June. We further find that on 20 June, stable stratification existed above this level with the ABL top around 175m, while on 21 June the layers between 40 - 90m were highly stable with the ABL top around 125m.

In addition to these basic inputs, prescribed heat and momentum fluxes were provided at the lowest model level. These were estimated in the usual manner from the first two levels of observations, namely, 3m and 15m. After 10 minutes of transilient mixing, the model outputs consisting of vertical profilis of θ, u , v and fluxes $\overline{w'\theta'}, \overline{u'w'}, \overline{v'w'}$ have been displayed in Figures 5.3 – 5.5.

The Richardson number variation with height as computed from the model outputs have been shown in Figure 5.2b. This may be compared with Figure 5.2a to get an idea about how the turbulent zones have changed within these 10 minutes. The heat flux, as seen from Figures 5.3d, 5.4d and 5.5d are negative upto a considerable height for all three days. This implies subsidence and downward transport of heat which is as expected in stably stratified zones. The ABL tops on these days, have been estimated to be around z_i = 230m, 178m and 85.5m respectively. Thus for the early morning case studies, 19 - 20 June, the ABL has warmed up (as observed also from Figures 5.3a and 5.4a), and the tops have risen. As seen from Figure 5.5a, on 21 June, although the temperature has risen at the lowest level, temperature has decreased above this. This cooling of the upper layers has brought down the ABL top.

To gain some insight into the TKE, the contribution at different levels, of the various terms in the TKE budget equation, namely, $\overline{u'w'}\frac{\partial u}{\partial z}$, $\overline{v'w'}\frac{\partial v}{\partial z}$ and - (g / θ) $\overline{w'\theta'}$ has been plotted in Figures 5.6a-c, in which the vertical variation of the computed sum of the above three terms has also been shown. It is seen that on all the days, the mechanical shear production terms are dominating, particularly, the term $\overline{u'w'}\frac{\partial u}{\partial z}$, which is mostly a negative term. This suggests that TKE is being produced due to wind shear. The buoyant production term $(g / \theta)\ \overline{w'\theta'}$, representing the rate of working against buoyancy forces, is negative on all the three days, indicating that TKE production is being suppressed. The sum of these three terms represent the excess of TKE production over consumption. In this case, it should be noted that, we have not considered the turbulent transport and pressure correlation terms in the TKE budget equation. These terms are thought to have significant contributions , at least in the surface layer (Wyngaard and Cote, 1971). Thus, from Figure 5.6a, we find that on 19 June, there is a net production of TKE in the zones (shaded in the figure) between 50 - 90m, 110 - 130m and 150 - 200m. In between these layers, TKE is lost, but as seen from the figure, the gain exceeds the loss. The build up of TKE between 110 - 130m and above 160m is quite significant on this day. At the lowest levels, gain and loss almost balance each other.

On 20 June, as may be observed from Figure 5.6b, a large build up of TKE occurs below 60m, with significant gain between 40 - 60m. A considerable amount of TKE seems to be lost above 140m. On 21 June, as seen from Figure 5.6c, where we are dealing with a transition boundary layer, the TKE consumption always exceeds production, with significant losses below 60m. It may be noted that as defined in the non-local parameterization for turbulent fluxes [equation (3.1,11)], the potential for mixing is related to the excess of TKE production over consumption and dissipation. So, the shaded zones in Figures 5.6a and b, are zones of vigorous turbulent mixing. In contrast, on 21 June, (Figure 5.6c) the potential for mixing is quite low, particularly in the lower levels.

At this point, it would be useful to obtain some information regarding the turbulent eddies that are involved in the mixing process. We may recall that, the transport spectra and the mixing length are two very important parameters in this connection. The transport spectra gives an idea about the contribution of eddies of various sizes to the flux across any level. The mixing length at any level is a measure of the mean distances moved by the air parcels during the mixing process.

The contribution of the eddies ranging in sizes between 10 - 30m, 40 - 100m, 120 - 170m and 180 - 230m to the heat flux across different levels has been illustrated in Figures 5.7a and b, for 19 and 20 June respectively. In Figure 5.7c, the contribution to the heat flux by eddies ranging in sizes between 10 - 40m, 50 - 70m and 80 - 100m has been shown for 21 June. Recalling that the heat fluxes (Figures 5.3d, and 5.5d) are all negative at least upto the ABL top on all three days, we may conclude that all eddies being considered in Figure 5.7a - c, are transporting heat downwards.

The major contribution to the downward heat flux, throughout the ABL comes from the 120 - 230m eddies for 19 and 20 June. The largest contribution upto the level 1.1 z_i, on both days are from the 180 - 230m eddies. At this level, the contribution from the 120 - 170m eddies begin to dominate. The contribution of the 180 - 230m eddies remain nearly constant (but less than that from the 120 - 170m eddies), between 0.9 - 0.5 z_i on 19 June (Figure 5.7a). On 20 June, as Figure 5.7a indicates, the contribution of these eddies keep on increasing till 0.8 z_i, although this contribution is less than that of the 120 - 170m eddies at these levels. Below 0.5 z_i (0.8 z_i), on 19 June (20 June), the contribution to the heat flux by the 180 - 230m class of eddies become weaker but increases again below 0.4 z_i (0.5 z_i) where it once more exceeds the contribution from the 120 - 170m class.

The 120 - 170m eddies dominate between 0.9 z_i - 0.5 z_i (1.04 z_i - 0.72 z_i) on 19 June (20 June). The smaller eddies belonging to the 40 - 100m class contribute less significantly than the above two classes all throughout the ABL on 19 June. On 20 June however, the contribution of the 40 - 100m eddies follow a different pattern, showing increasing contributions at 1.4 z_i and again at 0.6 z_i. Figure 5.7c, for 21 June, reveals much the same pattern. However, on this day, the largest class of eddies, 80 - 100m, contribute significantly to the heat flux as low as 0.2 z_i The major contribution (between

0.7 z_i - 0.4 z_i) comes from the 50 - 70m eddies on this day. Below this, all the eddies are seen to contribute to the heat flux with the 10 - 40m eddies dominating below 0.25 z_i. Thus only on 21 June, within the transition boundary layer in the late afternoon, we find that the smallest class of eddies contribute largely in the downward heat transfer in the surface layer, whereas, in the early morning ABL's of 19 and 20 June, all eddy sizes considered, contribute in the surface layer.

We next consider the mixing length profiles for 19 - 20 June, illustrated in Figure 5.8. A zone of vigorous mixing exists in the lowest 50m of the ABL on both these days. This agrees with the earlier finding that the zone below 60m is a zone of TKE production and vigorous mixing (Figures 5.6a and b). Above this level, on 19 June, the vigour of mixing decreases around the 55m level, which again corresponds to the zone of TKE consumption shown in Figure 6a. The largest values of the mixing length occurs near the ABL tops on both the days. The mixing also appears to be more intense on 20 June than on 19 June. The mixing length profiles for 21 June, again display a different pattern. The amount of mixing is relatively more below 35m although far less than that found on 19, 20 June and increases again near the ABL top, after which it decreases steadily. In between, mixing is highly suppressed. This can perhaps be attributed to the TKE consumption exceeding production throughout the ABL on this day.

Finally, we have shown the one - dimensional anisotropy of turbulence in Figures 5.9a - c. We recall that on all three days, the lowest levels in the ABL had a very weak, or near neutral stratification with stable layers above this. The transilient matrix obtained in this situation was symmetric, in contrast to the matrices obtained in convective situations. Consequently, partitioning of the mixing length into upward and downward components for each source - destination boxes, resulted in $l_j\uparrow = l_i\downarrow$ and $l_j\downarrow = l_i\uparrow$. Nevertheless, since $l_j\uparrow$ is not equal to $l_j\downarrow$, the anisotropic structure of the turbulent eddies is highlighted.

Figures 5.9a and b reveal that for the early morning boundary layers on 19 and 20 June, the downward transport dominates the upward transport at all but the lowest levels. The maximum downward transport occurs from the level 0.9 z_i on 19 June, upward transport on that day being confined mostly below 0.4 z_i. On 20 June, downward transport is maximum from the 1.5 z_i level and the ABL top. Upward transport is quite strong for this day and exceeds the downward component below 0.23 z_i, and equals it around 0.23 - 0.27 z_i. As Figure 5.9c indicates, for the late afternoon transition boundary layer on 21 June, the upward transport dominates upto 0.73 z_i, above which downward transport dominates between the 1.6 z_i and ABL top.

In conclusion, we state that the case studies for 17 - 21 June, 1990 reveal certain interesting features from this diagnostic study on the turbulent transports within the monsoon trough boundary layer. The case studies for the early morning ABL's of 19 - 20 June indicate that distinct zones exist where TKE production exceeds consumption and thus supports turbulent activity. In contrast in the late afternoon, transition boundary layer (21 June), turbulence is suppressed due to TKE consumption exceeding production all throughout the ABL. TKE production on all these days is seen to occur dominantly through mechanical wind shear.

The contribution to the downward heat flux by several classes of eddies indicates that for 19 20 June, eddies ranging in sizes between 40 - 230m contribute dominantly upto and within the surface layer, while for 21 June, only the smallest eddies (10 - 40m) dominate within the surface layer. The early morning boundary layers of 19 - 20 June are characterised by downward turbulent transport dominating over upward transport while the reverse holds true for the late afternoon case of 21 June.

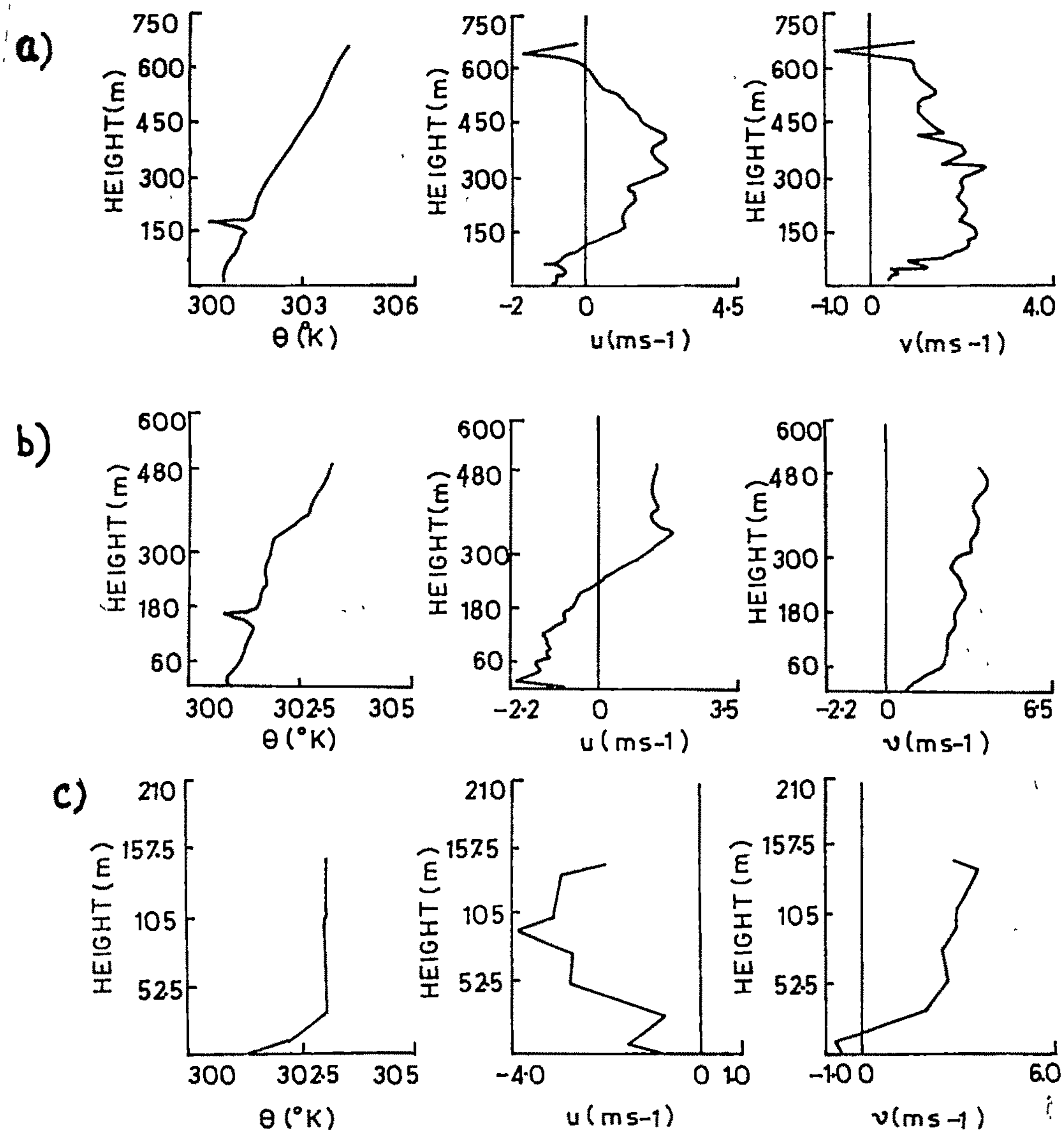

Figure 5.1 : Observed profiles of potential temperature θ (°K), zonal wind u (ms^{-1}) and meridional wind v (ms^{-1}) at Kharagpur a) 19 June 1990, 00GMT b) 20 June 1990, 00GMT and c) 21 June 1990, 1130 GMT.

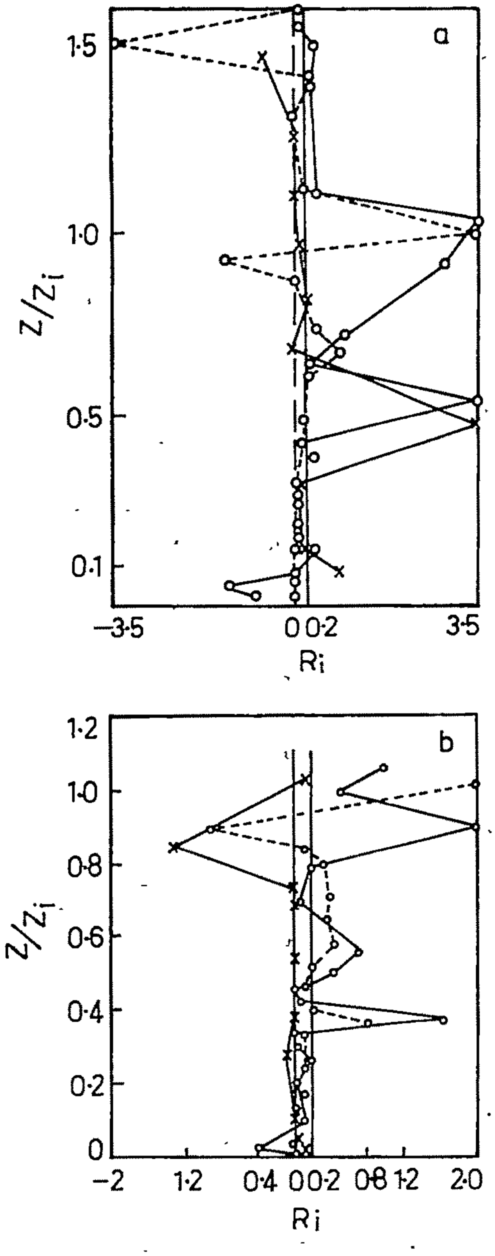

Figure 5.2 : Variation of Richardson number with height at Kharagpur computed from a) Observed profiles b) **T3** model outputs —⊙— 19 June 1990; – -⊙- – 20 June 1990; —×— 21 June 1990

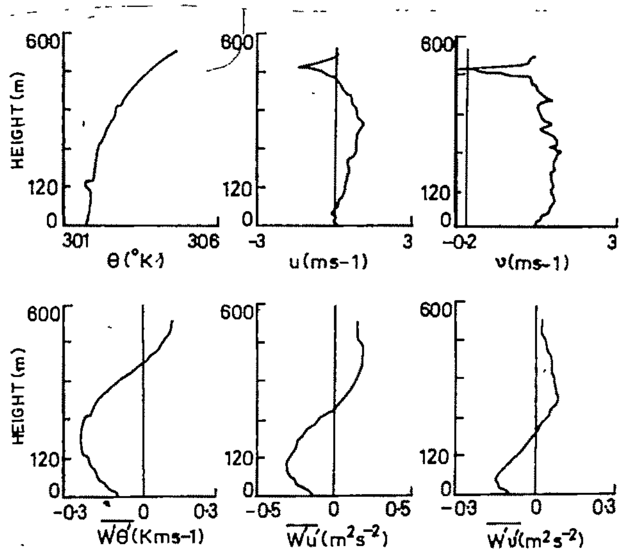

Figure 5.3 : T3 model outputs for Kharagpur 19 June 1990 a) Potential temperature b) zonal wind c) Meridional wind d) heat flux e) zonal momentum flux and f) Meridional momentum flux.

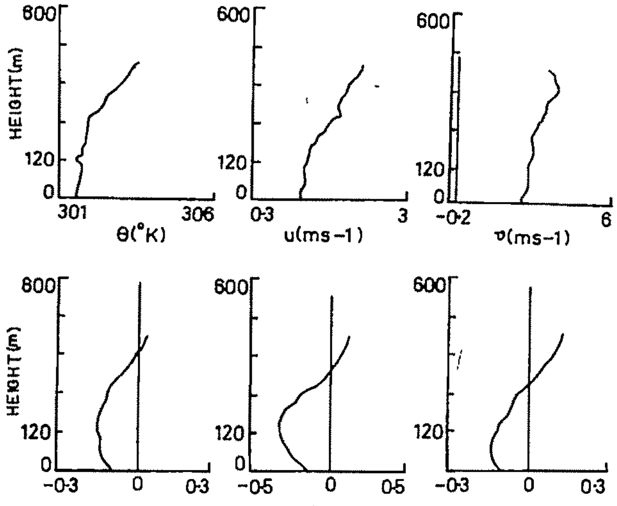

Figure 5.4 : Same as in Figure 5.3, but for Kharagpur, 20 June 1990.

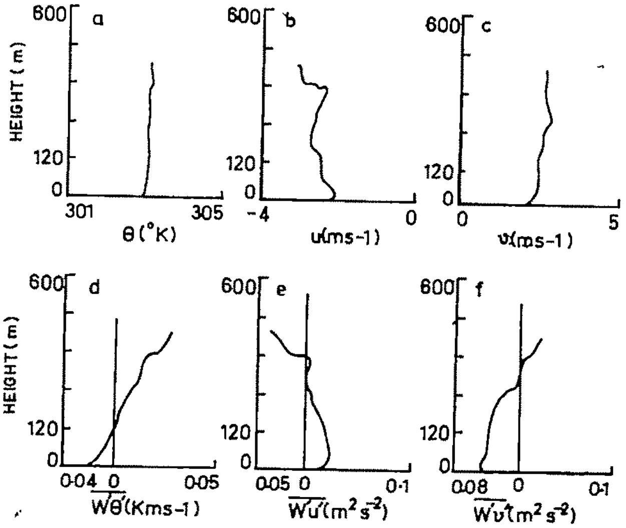

Figure 5.5 : Same as in Figure 5.3, but for Kharagpur, 21 June 1990

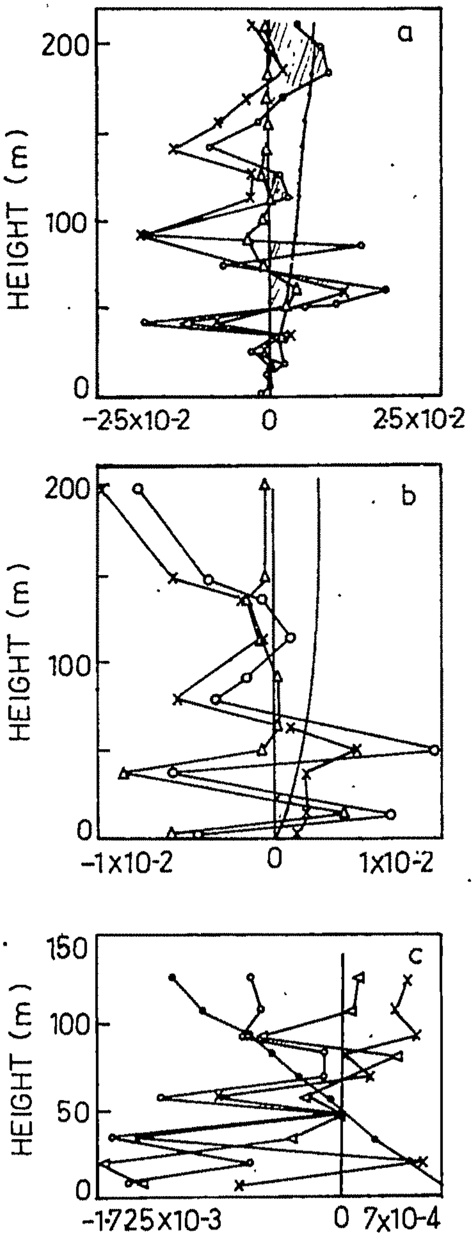

Figure 5.6 : Turbulence kinetic energy budgets for Kharagpur a) 19 June 1990 b) 20 June 1990 and c) 21 June 1990. ——●—— buoyant production; ——×—— mechanical shear production (zonal); ——△—— mechanical shear production (meridional) and ——⊙—— total of all terms.

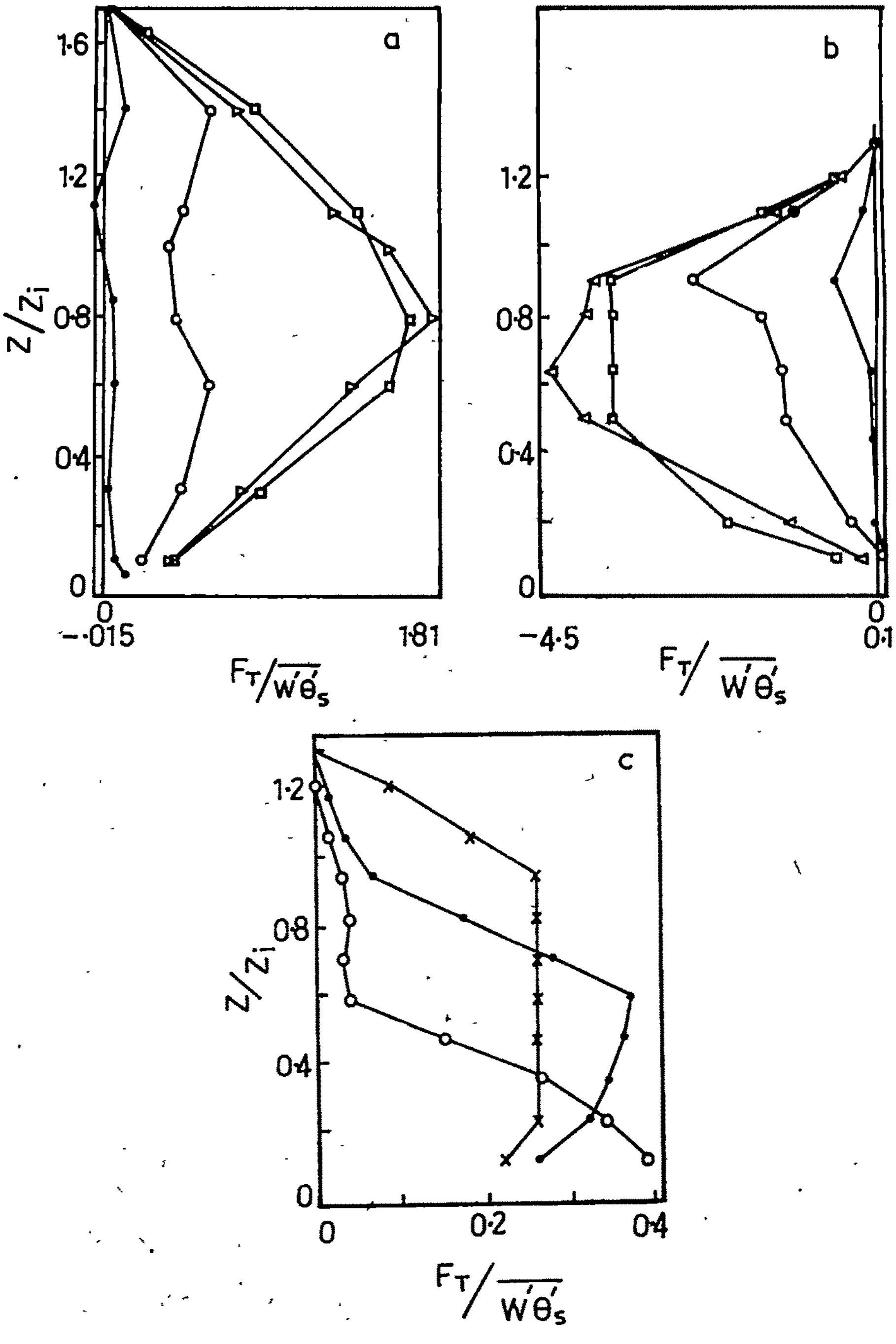

Figure 5.7 : Contribution to the heat flux across different levels by eddies of various sizes. a) 19 June 1990 b) 20 June 1990 and c) 21 June 1990. In a) and b) : ——●—— 10 – 30m; ——⊙—— 40 – 100m; ——△—— 120 – 170m and ——□—— 180 – 230m. In c) : ——⊙—— 10 – 40m; ——△—— 50 – 70m; ——×—— 80 – 100m.

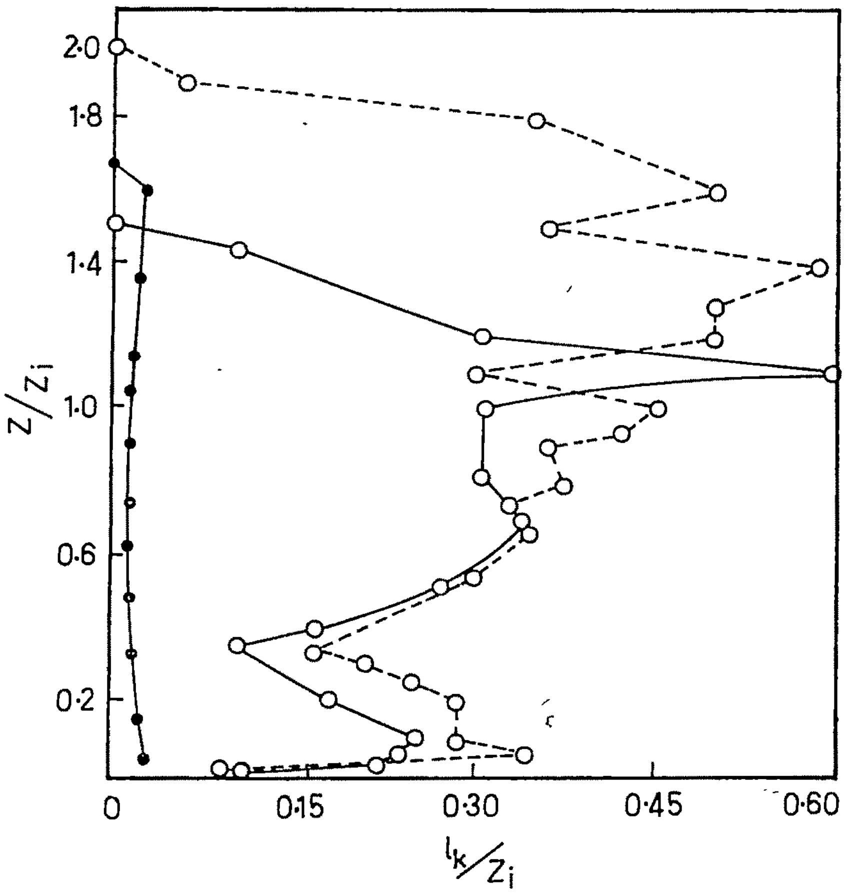

Figure 5.8 : Total mixing length profles for Kharagpur. —⊙— 19 June 1990; - -⊙- - 20 June 1990; —●— 21 June 1990.

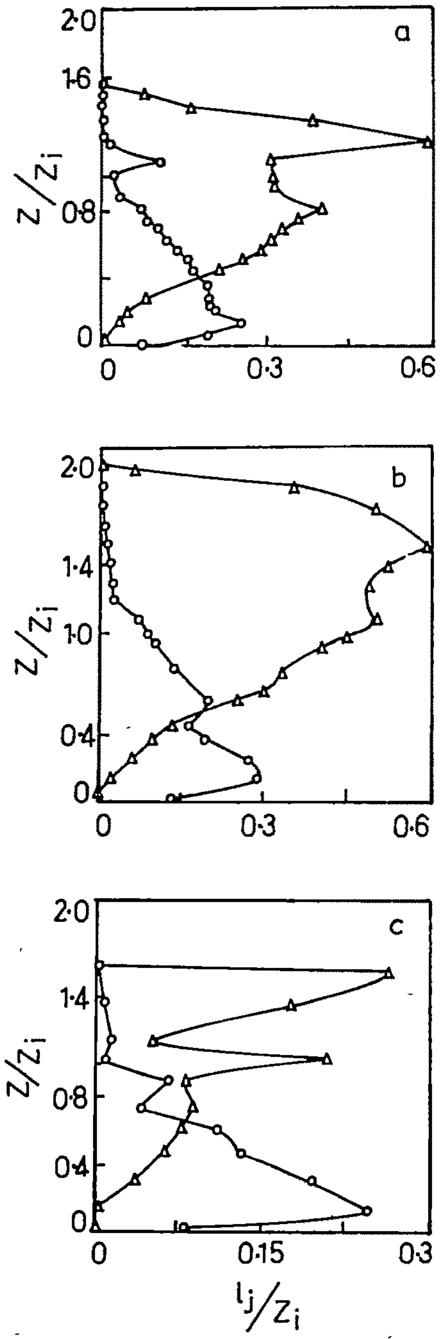

Figure 5.9 : One dimensional anisotropy of turbulent eddies at Kharagpur.a) 19 June 1990 b) 20 June 1990 and c) 21 June 1990. ——⊙—— lj↑ ——△—— lj↓.

5.2 : Understanding the turbulence structure of the monsoon trough boundary layer – Part II : The role of pressure covariance and dissipation

In order to get some idea about the roles of the pressure transport, turbulent transport and dissipation terms in the turbulent exchange processes within the ABL, the second order local closure model described in Section 3.2 has been used. In the first case, Case (a), we focus attention on a single a class of eddies represented by the characteristic constant length scale $\Lambda = 0.2$. In the second case, Case (b), the vertical variations of Λ corresponding to a prescribed heat and momentum flux profile has been examined.

The data used for the study were the same tetheredsonde observations over Kharagpur during 17 – 21 June 1990 described in section 5.1. The observed profiles of potential temperature θ and wind components u and v for 17th and 18th June have been shown in Figure 5.10 a and b. The observation were taken at 00 GMT. As seen from this figure, on both days, the ABL was stably stratified throughout. The top of the ABL's were estimated to be around 170m on 17 June and 125m on 18 June. The profiles of θ, u, v on 19 – 21 June (Figure 5.1 a - c) and the ABl stratifications on these days have already been discussed in Section 5.1.

Case (a) : Constant Turbulence Length Scale

The model outputs consisting of the turbulent fluxes $\overline{w'\theta'}$, $\overline{u'w'}$, $\overline{v'w'}$ for 17 – 19 June and 21 June have been shown in Figures 5.11 – 5.14, while the composite profiles of W'^2 and $\bar{e}$, the TKE, has been illustrated in Figures 5.15 and 5.16 respectively.

It is seen from Figures 5.11a and 5.14a, that due to the relatively stronger stable stratification of the ABL on both these days (see Figures 5.10a and 5.1a), the surface heat flux is negative on both 17 and 21 June, with the downward flux being stronger on 21 June that is, in the late afternoon case than in the early morning one. Figures 5.12a and 5.13a indicate an upward surface heat flux, in keeping with the near neutral stratification of the lower levels of the early morning ABL's on 18 - 19 June. On all these days, the upper levels of the ABL are stably stratified (see Figures 5.10a and 5.1a). Heat fluxes in these layers are found be negative or weakly positive. This implies the bringing down of warmer air from aloft.

Turbulence in the stably stratified ABL's on 17 - 19 and 21 June being highly suppressed, we can expect that the turbulent transfer is being carried out by smaller sized eddies. This implies that turbulent transport of TKE by these eddies will be smaller than the redistribution of the TKE by pressure perturbations (Wyngaard and Cote, 1971; Wyngaard, 1975).

Figure 5.15 and 5.16 show that close to the earth's surface, upto 0.2 z_i, the TKE as well as $\overline{w'^2}$ is quite high on 21st June. On the other days, higher values of TKE and $\overline{w'^2}$ occur near the middle of the ABL. It is interesting to note that throughout the ABL, a reasonable degree of correlation being particularly good on 17 June.

To gain further insight into this interesting feature, we have looked into the contribution at various level, of the pressure covariance terms in the turbulent flux, vertical velocity variance, and TKE budget equations. The vertical profiles of each of these terms and the profiles of the molecular and viscous dissipation terms have been plotted in Figure 5.17, for 17th June. On this day, the strong zonal wind shear at lower levels (see Fig. 5.10a) contributes dominantly to the generates TKE.

It is well known (Wyngaard, 1984 ; Stull, 1988) that the respective presure covariance terms in the mometum flux budget equations (3.3,19), (3.2,20) destroy the production of turbulence by the corresponding mean gradients. In this case, one may observe from Fig 5.17, That the presure covariance in the momentum equations is very high below $0.1z_i$, around 0.3-$0.4z_i$ and again around 0.6-$0.8z_i$ with the zonal contribution dominating over the meridional one. It can be inferred that these layers are zones of strong turbulence.

The presure covariance in the heat flux budget equation (equation 3.2,22) destroys the turbulence produced dominantly by the mean temperature gradient, particularly below $0.09z_i$. Thus, we find three distinct zones within the ABL where turblence has been produced dominantly by wind shear and destroyed by the pressure covariance.

We now examine the terms in the TKE and $\overline{w'^2}$ budget equations, equations (3.2,18) and (3.2,21) respectively.

It is found that the viscous dissipation of TKE is very high in the three zones mentioned above. The effect of the pressure covariance and turbulent transport terms is to redistribute the TKE to the $\overline{w'^2}$ component. This is suppored by the correlation existing in the TKE and * profiles of Fig 5.15 and 5.16.

Another interesting feature is the structural similarity between the pressure covariances in the heat flux and $\overline{w'^2}$ budget equations. A possible explanation lies in the fact that the rate of destriction of the turbulent production and buyonat production is nearly equal to the rate at which the TKE is being redistributed to the $\overline{w'^2}$ component particularly above the $0.3z_i$ level.

We thus find that in thie case study related to the monsoon trough boundary layer, clear evidences of distinct zones of turbulence exist indicating the presence of patchy turbulence. Another interesting conclusion can be drawn from the destruction of turbulence production by the pressure covariances in the turbulent flux equations. This pertains to the existence of internal gravity waves in the SBL which are generated in the strong shear layers within the ABL, propagate upwards extracting considerable amount of energy from the turbulent zones. This extraction of energy is facilitated by the pressure covariance terms.

In conclusion we may state that, during the onset phase of the monsoon, the generation of IGW in stably stratified ABL's and the transport of TKE out of the ABL by the pressure covariance terms via the vertically propagating IGW is a remarkable feature which may play a crucial role in initiating and orgaising condensation and cumulus convection.

Case (b) : The vertical variation of the turbulent length scale

The difficulty in specfying a vertical distribution of the characteristic length scale Λ of the most energetic turbulent eddies in the ABL has been realised by several investigators (Wyngaard, 1980). The accuracy of the parameterization schemes used in the second order closure models (see Section 3.2) depends crucially on Λ which is a multiple value parameter within the ABL. Specification of Λ through conservation equation are thawrted again by additional closure problems and the back of direct measurments. Most investigators therefore specify Λ distributions a priori (Wyngaard, 1984).

In the present case, we have attempted to obtain the variation of Λ with height in a simple manner. The grid point values of the turbulent fluxes obtained from the second order model are compared with corresponding values from the **T3** model. The grid point value of Λ for which the outputs from both models agree closely determines the distribution of Λ

for a prescribed flux profile. As is to be expected, grid point values and hence the Λ distributions will be different for the prescribed heat and momentum fluxes. In order to examine the Λ distribution for the case (A) in which surface stresses are dominant and the case (B) in which surface heat flux dominates, two numerical experiments were conducted with the second order model using the data for Kharagpur on 20 June.

In Experiment A, the prescribed surface fluxes were identical to those used in the T3 model, namely, a surface heat flux $\overline{w'\theta's}$ = – .004 K ms-1 and a momentum flux corresponding to a drag coefficient C_D = .0039. These are the values of the fluxes computed from the observations as described in Section 5.1 and produce the flux profiles illustrated in Figure 5.4 (d) – (f).

In Experiment B, the prescribed heat flux was $\overline{w'\theta's}$ = – .006 K ms-1 and a surface momentum fluxe corresponding to C_D = .0015.

The Λ distribution corresponding to the higher surface stresses (Experiment A) and the momentum flux profile from the T3 model has been shown in Figure 5.18. In this figure, the Λ distribution corresponding to the higher surface heat flux and corresponding to the heat flux profile from the T3 model (not shown) has also been plotted. A comparison with Figure 5.8 shows that a fair amount of agreement exists, particularly below 0.5 z_1 Figure 5.18 also indicates that the turbulent eddies are most active near 0.14 z_1 (Experiment A) and 0.23 z_1 (Experiment B). Another turbulent zone occurs a little higher, around 0.4 z_1 (Experiment A) and 0.63 z_1 (Experiment B). Λ decreases to a minimum at the ABL top but increases again, above it. It is interesting to note that the two Λ profiles come close to each other above 0.8 z_1, while at lower levels, their difference is significant.

It can thus be inferred that the large energy containing eddies transporting heat and momentum are active in the lower levels. Intermediate zones around 0.2 - 0.3 z_1 (Experiment A) and 0.3 z_1 (Experiment B) exist where the active eddies become smaller. Further, eddies transporting heat are larger and more active particularly around 0.5 z_i than those transporting momentum

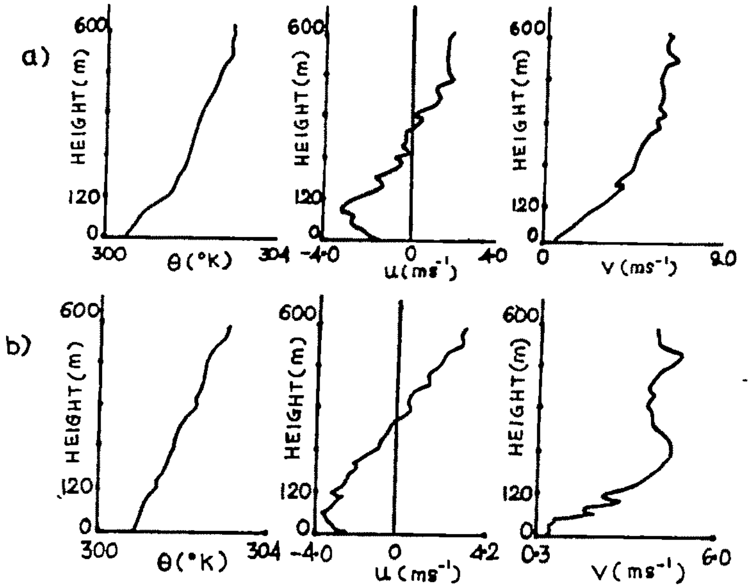

Figure 5.10 : Observed profiles of potential temperature θ(°K), zonal wind u (ms^{-1}) and meridional wind v (ms^{-1}) at kharagpur, 00 GMT on a) 17 June, 1990 and b) 18 June, 1990.

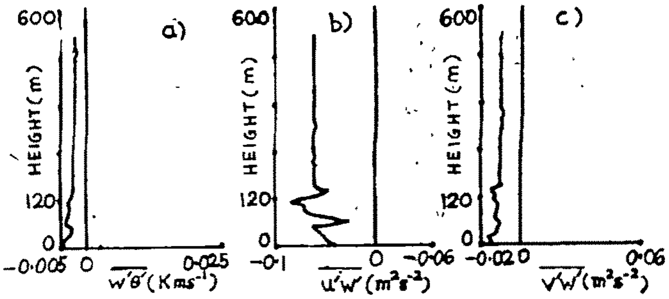

Figure 5.11 : Second order model outputs of a) buoyancy flux $\overline{w'\theta'}$ (K ms^{-1}), b) zonal momentum flux $\overline{u'w'}$ (m^{2}s^{-2}) and c) meridional momentum flux $\overline{v'w'}$ (m^{2}s^{-2}) for kharagpur, 00 GMT, 17 June 1990.

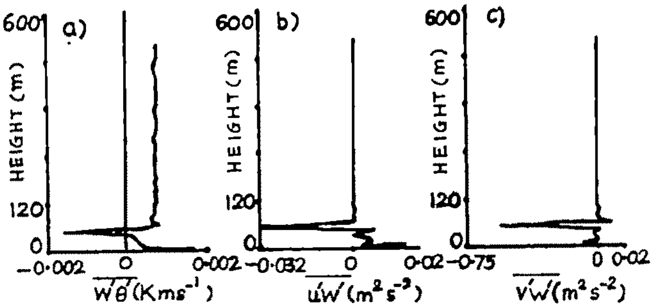

Figure 5.12 : Same, for Kharagpur, 00 GMT, 18 June 1990.

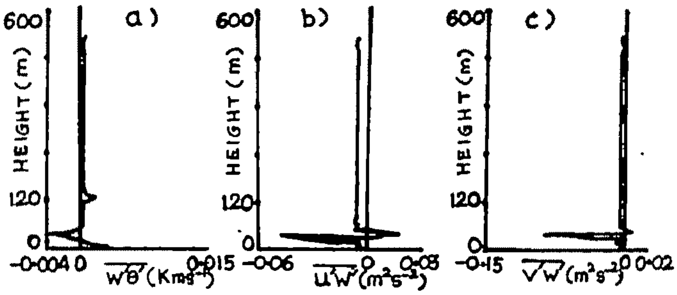

Figure 5.13 : Same, for Kharagpur, 00 GMT, 19 June 1990.

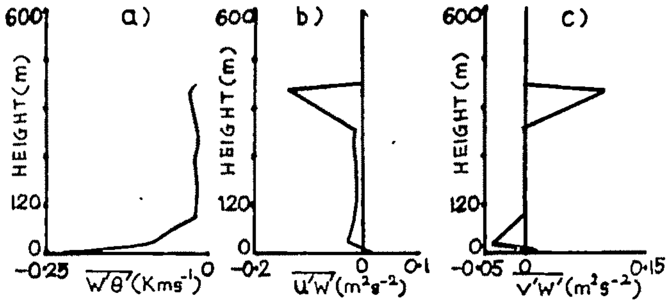

Figure 5.14 : Same, for Kharagpur, 1130 GMT, 21 June 1990.

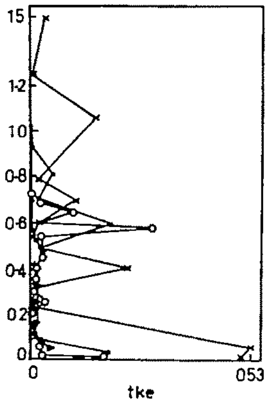

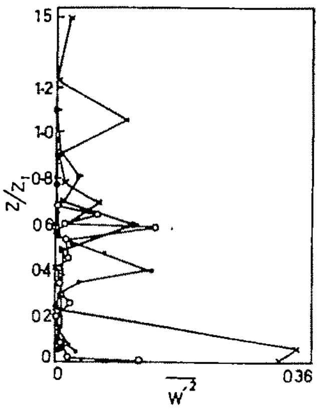

Figure 5.15

Figure 5.16

Figure 5.15 : Vertical profiles of the turbulence kinetic energy $\bar{e}$ for Kharagpur obtained from the second order model.
—⊙— 17 June, —●— 18 June, —▲— 19 June, —×— 21 June

Figure 5.16 : Vertical profiles of the turbulent vertical velocity variance $\overline{w'^2}$ for Kharagpur obtained from the second order model.
—⊙— 17 June, —●— 18 June, —▲— 19 June, —×— 21 June

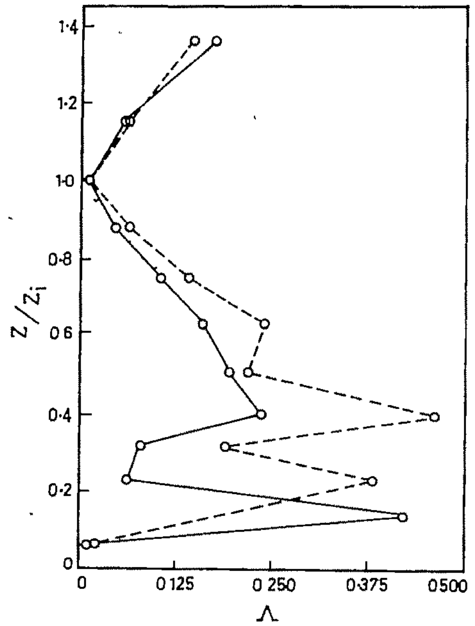

Figure 5.17 : Contribution of the pressure covariance at different levels to the —●— heat flux , —✕— zonal momentum flux , —▲— meridional momentum flux, – ⊙ – turbulence kinetic energy and —⊙— vertical velocity variance at Kharagpur, 00 GMT, 17 June 1990. Vertical profiles of —■— molecular and – ● – viscous dissipation Z_i = 170m

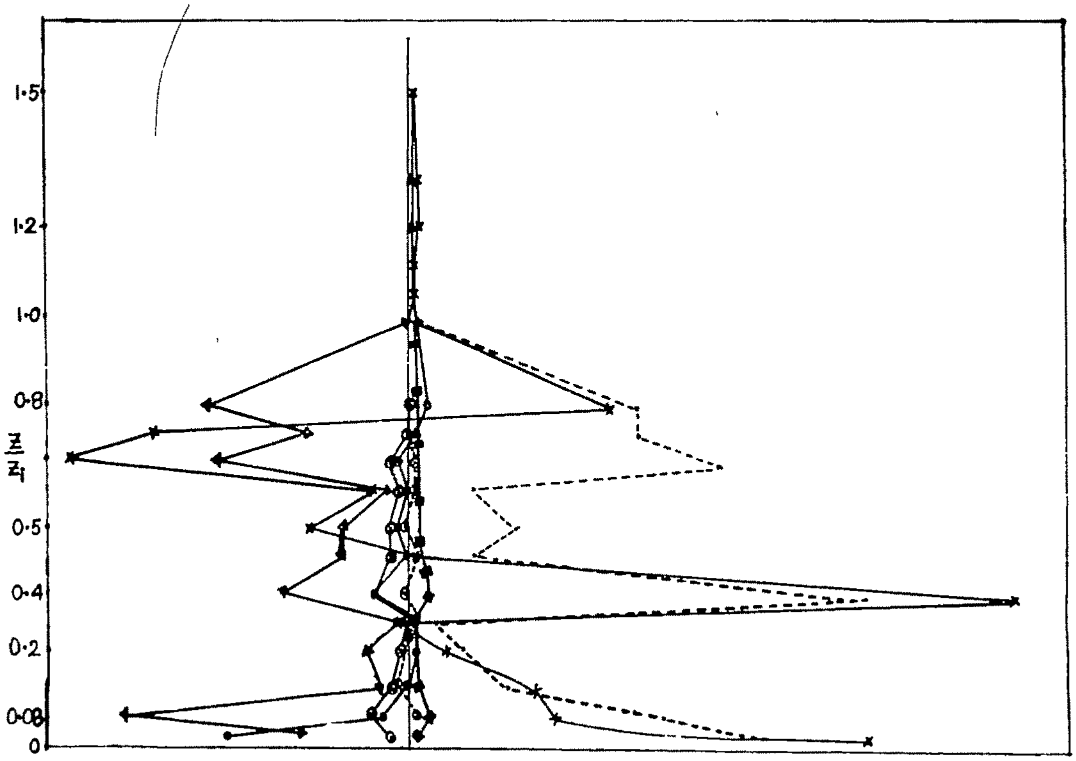

Figure 5.18 : Profiles of the characteristic length scale Λ, obtained from the second order model for 20 June 1990. —⊙— Experiment A; – ⊙ – Experiment B.

BIBLIOGRAPHY

1. Ackerman, S.A. and Cox, S.K.,1982 : The Saudi Arabian heat low: aerosol distribution and Thermodynamic structure. *J.Geophys. Res.*, 87, 8991–9002.
2. André, J.C. and Mahrt, L., 1982 : The nocturnal surface inversion and influence of clear – air radiative cooling. *J. Atmos.Sci.*, 39, 864–878
3. André, J.C., 1983 : Planetary boundary layer parameterization and turbulence closure. pp 651–669 in **Mesoscale Meteorology–Theories, Observations and Models.** D.K.Lilly and T.Gal Chen (eds.). D.Reidel Publishing Company, Dordrecht, Holland.
4. Andrews, D.G., Holton, J.R. and Leovey, C.B., 1987 : **Middle Atmosphere Dynamics.** Academic Press, Orlando, Florida. 489 pp.
5. Anthes, R.A., 1985 : Introduction to parameterization of physical processes in numerical models. pp 1–32 in : **Proc. Seminar on Physical Processes for Numerical Models of the Atmosphere.** ECMWF, Shinfield Park, Reading, U.K. 9–13 Sept.
6. Augstein, E., 1979 : The atmospheric boundary layer over the tropics, pp 73–79 in : **Meteorology Over the Tropical Oceans.** D.B.Shaw (ed.). Royal Meteorology Society, Bracknell, U.K.
7. Bates, J.R., 1977 : Parameterization of convective processes. pp 160–229 in : **The Parameterization of the Physical Processes in the Free Atmosphere.** ECMWF, Shinfield Park, Reading, U.K.
8. Betts, A.K., 1978 : Convention in the tropics. pp 105–132 in : Proceedings of the conferense on Metorology over the Tropical Oceans.
9. Betts, A.K., Grover, R.W. and Moncrieff, M.W., 1976 : Structure and motion of tropical squall lines over Venezuela. *Q.J.R. Meteorol. Soc.*, **102**, 395–404.
10. Bengtsson, L. and Lighthill, J. (eds.), 1982 : **Intensive Atmospheric Vortices.** Springer Verlag, Heidelburg. 327 pp.
11. Berkowicz, R., 1980 : On the spectral turbulent diffusivity theory for homogeneous turbulence. *J. Fluid Mech.*, **100**, 433–448.
12. Berkowicz, R., 1984 : Spectral Methods for atmospheric diffusion modelling. *Bound.–Layer Meteorol.*, **30**, 201 - 220.
13. Berkowicz, R. and Prahm, L. P., 1979 : Generalization of K - Theory for turbulent diffusion. Part I : Spectral turbulent diffusivity concept. *J. Appl. Meteorol.*, **18**, 266 - 272.
14. Berkowicz, R. and Prahm, L.P., 1984 : Spectral representation of the vertical structure of turbulence in the convective boundary layer. *Q.J.R. Meteorol Soc.*, **110**, 13–34.
15. Bhumralkar, C.M., 1975: A survey of parameterization techniques for the planetqry boundary layer in atmospheric circulation models. *Defence Advanced Research Project Agency R-1653 - ARPA Order No. 189 - 1.* 84 pp.
16. Blackadar, A. 1962 : The vertical distribution of wind and turbulent exchange in a neutral atmosphere. *J. Geophys. Res.*, **67**, 3095 - 3102.
17. Blackadar, A. K., 1979 : Modelling pollutant transfer during daytime convection. pp 443 - 447 in **Preprints, 4th Symp. on Turbulence Diffusion and Air Pollution, Reno.** *American Meteorological Society.*

18. Blake, D.W., Krishnamurti, T.N., Low - Nam, S.V. and Fein, J.S., 1983 : Heat low over the Saudi Arabian desert during May 1979 (Summer MONEX). *Mon. Weather Rev.*, **111**, 1759 - 1775.

19. Bosart, L.F. and Caussen, J.P., 1973 : *Mon. Weather Rev.*, **101**, 146

20. Boudreau, B. P. and Imboden, D.M., 1987 : Mathematics of tracer micing in sediments : III. The theory of non local mixing within dediments. *Amer. J. Sci.*, **287**, 693 - 719.

21. Businger, J. A., 1984 : Equations and concepts. pp 1 - 36 in : **Atmospheric turbulence and air pollution modelling**. F.T.M. Nieuwstadt and H. Van Dop (eds.). D. Reidel Publishing Company, Dordrecht, Holland.

22. Charney, J.G., 1969 : A further note on large scale motions in the tropics. *J. Atmos. Sci.* **26**, 182 - 185.

23. Charney, J.G., 1973 : Planetary fluid dynamics. pp 97-352 in, **Dynamic Meteorlogy.** P. Morel (ed). D. Riedel Publishing Company. Dordrecht. Hloland.

24. Chatterjee, M., Sen, G.K. and Sinha, D.K., 1995 : Understanding the turbulent structure of the atmospheric boundary layer : A diagnostic approach. *Proc. Indian Acad. Sci.* (Earth Planet. Sci.) **104**, No.2. (in Press)

25. Chimonas, G., Einaqudi, F. and Lalas, D.P., 1980 : A wave theory for the onset and initial growth of condensation in the atmosphere. *J. Atmos. Sci.*, **37**, 822 - 845.

26. Chimonas, G. and Grant, J.G., 1984 : Shear excitation of gravity waves. Part I : Modes of a two scale atmosphere. *J. Atmos. Sci.*, **41**, 269 - 2277.

27. Chollet, J.P. and Lesieur, M., 1981 : Parameterization of small scales of three dimensional isotropic turbulence utilizing spectral closures. *J. Atmos. Sci.*, **38**, 2747 - 2757.

28. Clarke, T.L., Hauf, T. and Kuettner, J.P., 1986 : Convectively forced internal gravity waves : Results from two dimensional numerical experiments. *Q. J.R. Meteorol. Soc.* **112**, 899 - 925.

29. Das, P.K., 1986 : Monsoons. **Fifth IMO Lecture, WMO. No. 613**. World Meteorological Organization. Geneva. 155 pp.

30. Datta, R.K., Rao, A.V.R.K., Puri, R.S. and Lal, M., 1982 : Relation of equatorial trough and ITCZ during the onset of monsoon. pp 35 - 41 in, **Proc. Int. Conf. on Scientific Results of MONEX. Denpasar, Bali, Indonesia.** WMO, Genefva, Session 6.

31. Deardorff, J.W., 1966 : The countergradient heat flux in the lower atmosphere and in the laboratory. *J. Atmos. Sci.* **23**, 503 - 506.

32. Deardorff, J.W., 1972a : Numerical investigation of neutral and unstable planetary boundary layers. *J. Atmos. Sci.*, **29**, 91 - 115

33. Deardorff, J.W., 1972 b : Theoretical expression for the countergradient vertical heat flux. *J. Geophys. Res.*, **77**, 5900 - 5904.

34. Deardroff, J. W., 1974 a : Three dimensional numerical study of the height and mean structure of a heated planetary boundary layer. *Bound.– Layer Meteorol.*, **7**, 81 - 106.

35. Deardroff, J.W., 1974b : Three dimensional numerical study of turbulence in an entraining mixed layer. *Bound.– Layer Meteorol.*, 7, 199 - 226.

36. Desai, B. N., 1950 : Mechanism of Nor'westers of Bengal. *Ind. J. Met. Geophys.*, **1**, 74 - 76.

37. Department of Science and Technology, Government of India, 1990 : **MONTBLEX Designs and Operations Plan.** DST., New Delhi. 44 pp

38. Dixit, C.M. and Jones, D.R., 1965 : A kinematic and dynamical study of active and weak monsoon conditions over India during June and July 1964. **Report of the International Meteorological Centre, Bombay.** 26 pp.

39. Donaldson, C. duP., 1973 : Construction of a dynamic model of the production of atmospheric turbulence and dispersal of atmospheric pollutants. pp 313 - 392 in, **Workshop on Micrometeorology**. D.M. Haugen (ed.) American Meteorological Society, Boston.

40. Erickson, C.O. and Whitney, L.E., 1973 : Gravity wave following severe Thunderstorm - Picture of the month. *Mon. Weather Rev.*, **101**, 708 - 709.

41. Eringen, A.C., 1972 : On nonlocal fluid mechanics. *Int. J. Engng. Sci.*, **10**, 561 - 575.

42. Estoque, M. A., 1968 : Vertical mixing due to penetrative convection. *J. Atmos. Sci.*, **25**, 1046 -1051.

43. Estoque, M.A. and Bhumralkar, C.M., 1970 : A method of solving the planetary boundary layer equations. *Bound.– Layer Meteorol.*, **1**, 169 - 194.

44. European Centre for Medium Range Weather Foirecasts, 1985 : **Proceedings of Seminar on Physical Parameterization for Numerical Models of the Atmosphere. Vol. I.** September 9 - 13, ECMWF, Shinfiled Park, Reading, U.K. 332 pp.

45. Fiedler, B. H., 1984 : An integral closure model for the vertical turbulent flux of a scalar in a mixed layer. *J. Atmos. Sci.*, **41**, 674 - 680.

46. Fiedler, B. H. and Moeng, C.H., 1985 : A practical integral closure model for mean transport of a scalar in a convective boundary layer. *J. Atmos. Sci.*, **42**, 359 - 363.

47. Finnigan, J.J., Einaudi, F. and Fua, D., 1984 : The interaction between an internal gravity wave and turbulence in the stably stratified planetary boundary layer. *J. Atmos., Sci.*, **43**, 2048 - 2060.

48. Fortak, H.G., 1987 : Non-Markovian turbulent dispension in the atmosphere. **Preprints. 16th International Tech. Meeting on Air Pollution Modelling and its Applications.** 6 - 10 April, Lindau, F.R. Germany.

49. Garratt, J.R. and Brost, R.A., 1981 : Radiative cooling effects within and above the nocturnal boundary layer. *J. Atmos. Sci.*, **38**, 2730 - 2746.

50. Gossard, E.E. and Moninger, W.R., 1975 : The influence of a capping inversion on the dynamic and convective instability of a boundary layer model with shear. *J. Atmos. Sci.*, **32**, 2111 - 2123.

51. Gossard, E.E., and Hooke, W.H., 1975 : **Waves in the Atmosphere, Atmospheric Infrasound and Gravity Waves New York. 456 pp their Generation and Propagation** Elsvier Scientific Publication Co.,

52. Gupta, M.G., 1990 : **Report on MONTBLEX Operation Centre**. Department of Science & Technology. Technology Bhawan, New Delhi 110 016.

53. Hogstorm, U., 1990 : Analysis of turbulence structure in the surface layer with a modified similarity formulation for near neutral conditions. *J. Atmos. Sci.*, **47**, 1949 - 1972.

54. Hooke, W.H. and Jones, R.M., 1986 : Dissipative waves excited by gravity wave encounter with the stably stratified planetary boundary layer. *J. Atmos. Sci.*, **43**, 2048 -

2060.

55. Hossain, M.S. and Rodi, W., 1974 : Equations for turbulent buoyant flow and their modelling. *Sonder forschungslereich. 80* Austreitungsund Transport vorgange in Strommungen. **Ref. SFB 80/T/46. Universitat Karlsruhe.**
56. Hostetler, C.J. and Opitz, B.E., 1982 : Simulation of solute transport : A Markov model. **Report from pacific Northwest Lab**, P.O. Box 999, Richland, WA 99352, 14pp
57. Houze, R.A. Jr., Hobbs, P.V., Biswas, K.R. and Davis, W.M., 1976a : Mesoscale rainbands in extratropical cyclone. Mon. *Weather Rev.*, **104**, 868–878
58. Houze, R.A. Jr., Locatelli, J.D. and Hobbs, P.V., 1976b : Dynamics and cloud microphysics of the rainbands in an occluded frontal system. *J. Atmos. Sci.* **33**, 1921–1936.
59. Houze, R.A. Jr., 1989 :Observed steucture of mesoscale convective systems and implications for large scale heating. *J.R. Meteorol. Soc.*, **115**, 425–461.
60. Imboden, D.M., 1981 : Tracers and mixing in the aquatic envionment : A critical discussion of diffusion models and an introduction into concepts of non–Fickian transport. *Habilitation thesis. Swiss Federal Institute of Technology.* (ETH), Zurich. 137 pp.
61. India Meteorological Department, 1944 : **Nor'westers of Bengal.** *Technical Note No. 10.* PP
62. India Meteorological Department, 1960 : **Monsoons of the world.** Hind Union Press, New Delhi. 270 pp.
63. India Meteorological Department, 1970 : **Forecasting Manual Report (Four volumes).** The Deputy Director General of Observatories, Pune.
64. Inners, P.N. and Gregory, D., 1994 : Simulation of the Indian monsoon and tropical interseasonal variability by a general circulation model. *Climate Research Technical Note No.52.* Hadley centre. Metrological office, Bracknell, U.K. 25pp
65. Jenkins, A.D., 1985 : Simulations of turbulent dispersion using a simple random model of the flow field. *Appl. Math Modelling*, **9**, 239–245.
66. Keller, L.V. and Freidman, A.A. 1924 : Differentialgleichung für die turbulente Bewegung einer Kompressiblen Flüssigkeit. *Proc. 1st Intern. Congr. Appl. Mech.*, Delft, 395–405.
67. Keshvamurty, R.N. and Awade, S.T., 1974 : Dynamical abnormalities associated with drought in the Asiatic summer monsoons. pp 159–162 in, **Proceeding, Symposium on Tropical Meteorology, Nairobi.** *American Meteorological Society, Boston.*
68. King, J.C., Mobbs, S.D., Derby, M.S. and Rees, J.M., 1987 : Observation of an internal gravity waves in the lower tropophere at Halley, Antarctica. *Bound.–Layer Meteorol,* **39** 1–13.
69. Klemp, J.B. and Lilly, D.K., 1978: Numerical simulation of hydrostatic mountain waves. *J.Atmos. Sci.*, **35**, 1076-1096.
70. Klemp, J.B. and Wilhelmson, R.B., 1978b: Simulation of right and left moving storms produced through storm splitting. *J.Atmos. Sci.*, **35**, 1974-1986.
71. Koteswaram, P. and Chakraborty, K.C., 1950: Distribution of temperature lapse rate in the upper air over India during different months. *Ind. J.Met. Geophys.*, **1**, 167-170.
72. Koteswaram, P. and Srinivasan, V., 1959: Thunderstorms over gangetic West Bengal in the pre-monsoon season and the synoptic factors favourable for their formation. *Ind. J. Met. Geophys.*, **9**, 301-312.

73. Kraichnan, R.H., 1959 : The structure of isotropic turbulence at very high Reynolds numbers. *J. Fluid Mech.*, **5**, 497-543.

74. Kraichnan, R.H., 1976 : Eddy-viscosity in two and three dimensions. *J.Atmos.* Sci., 33, 1521-1536.

75. Kraus, H., Malcher, J. and Schaller, E., 1985: Nocturnal low-level jet during PUKK. Bound.– Layer Meteorol., 31, 187–195

76. Krishnamurti, T.N., 1984: **Review: Summer Monsoon Experiment (Preprint, Monthly Weather Review).** *FSU Report-No. 84.* Dept. of Meteorology Florida State University. Tallahassee, Florida 43pp.

77. Krishnamurti, T.N., Jayakumar, P.K., Sheng, J., Surgi, N. and Arun Kumar., 1984 : Divergent circulations on the 30-50 day time scale *J.Atoms. Sci.,*

78. Krishnamurti, T.N. and Kanamitsu, M., 1981: Northern summer planetary scale monsoons during the drought and normal rainfall months. pp. 19-43 in **Monsoon Dynamics**. Sir James Lighthill and R.P.Pearce (eds.). Cambridge University Press.

79. Krishnamurti, T.N. and Ramanthan, Y., 1982: Sensitivity of the monsoon onset to defferential heating. *J.Atmos. Sci.*, **39**, 1290-1306.

80. Krishnamurti, T.N. and Subrahmanyam, D., 1982: The 30 to 50 day mode at 850 mb during MONEX. *J.Atmos. Sci.*, **39**, 2088-2095.

81. Lalas, D.P. and Einaudi, F., 1976: On the characteristics of gravity waves generated by atmospheric shear layers. *J.Atmos. Sci.*, **33**, 1248-1259.

82. Lalas, D.P. and Einaudi, F., 1980: Tropospheric gravity waves: Thier detection by and influences on rawinsonde balloon data. *Q.J.R. Meteorol. Soc.*, **106**, 855-864.

83. Leslie, D.C., 1973: **Developments in the theory of turbulence.** Clarendon Press, 368pp.

84. Ley, B.E. and Peltier, W.R., 1981: Propagating mesoscale cloud bands. *J.Atmos. Sci.*, **38**, 1206-1219.

85. Lighthiss, J. and Pearce, R. P., (eds.), 1977: **Monsoon Dynamics.** Cambridge University Press, Cambridge. 735 pp

86. Lilly, D.K., 1990 : Numerical Prediction of Thunderstorms–has its time come ? *Q.J.R. Meteorol. Soc.*, **116**, 779-798.

87. Lindzen, R.S., 1990. **Dynamics in Atmospheric Physics.** Cambridge University Press. 310 pp

88. Mastrantonio, G., Einaudi, F., Fua, D. and Lalas, D.P., 1976 : Generation of gravity waves by jet streams in the atmosphere *J. Atmos. Sci.* **33**, 1730-1738.

89. Matsumoto, S. and Akiyama, T., 1969 : Some characteristic features of the heavy rainfalls observed over western Japan on July, 1967. Parts I & II . *J. Meteorol Soc. Japan.*, **47**, 255-278.

90. Matsumoto, S., Ninomiya, K, and Akiyama, T., 1967a : A synoptic and dynamic study of the three dimensional structure of mesoscale disturbances observed in the vicinity of a cold vortex centre. *J. Meteorol. Soc. Japan*, **45**, 64-81.

91. Matsumoto, S., Ninomiya, K. and Akiyama, T., 1967b : Cumulus activities in relation to the mesoscale convergence field. *J. Meteorol Soc. Japan*, **45**, 292-304.

92. Mc Bean, G.A. (ed.) 1979 : **The Planetary Boundary Layer.** *WMO Technical Note No.* **165**. 201 pp

93. Mc Bean, G.A. and Elliott, J.A., 1975 : The vertical transports of kinetic energy by turbulence and pressure in the boundary layer. *J. Atmos., Sci.*, **32**, 753-766.

94. Mellor, G.L. and Yamada, T., 1982 : Development of a turbulence closure model for geophysical fluid problems. *Rev. Geophys. Space. Phys.*, **20**, 851-875.

95. Miller, M.J. and Pearce, R.P., 1974 : A three dimensional primitive equation model of cumulonimbus convection *Q.J.R. Meteorol. Soc.*, **100**, 133-154.

96. Miller, M.J. and Moncrieff, M.W., 1978 : Models of deep convection and their large scale interaction. pp 48-72, in **Erratum to the Proceedings. Workshop on the Parameterization of cumulus convection. ECMWF,** *Shinfield Park, Reading, U.K.* 23-28 Oct.

97. Mobbs, S.D. and Darby, M.S., 1989 : A general method for the linear stability analysis of stratified shear flows. *Q.J.R. Meteorol. Soc.*, **115**, 915-939.

98. Moeng, C.H. and Randall, D A., 1984 : Problems in simulating the stratocumulus topped boundary layer with a third order closure Model. *J. Atmos. Sci.*, **41**, 1588-1600.

99. Moeng, C.H. and Wyngaard, J.C., 1989 : Evaluation of turbulent transport and dissipation closures in second order modelling *J.Atmos. Sci.*, **46**, 2311-2330.

100. Mohanty, U.C. , Dube, S.K. and Singh, M.P., 1983 : A study of the heat and moisture budget over the Arabian Sea and their role in the onset and maintenance of the summer monsoon. *J.Meteorol. Soc. Japan.*, **61**, 208–221.

101. Mohanty, U.C., Parashuram, Venugopal, T. and Parihar P., 1992 : Study of the structure of the surface layer at Kharagpur using MONTBLEX data pp 23-33 in **Workshop on Preliminary Scientific Results of MONTBLEX** *16-17 January, IISC., Bangalore* Department of Science & Technology, Technology Bhawan, New Delhi 110016.

102. Moncrieff, M.W., 1985 : Convective momentum transports. pp 181-203 in **Proceedings, Seminar on Physical Parameterization for Numerical Models of the Atmosphere.** *9-13 September.* ECMWF Shinfield Park, Reading U.K.

103. Moncrieff, M.W. and Green, J.S.A., 1972 : The propagation and transfer properties of steady overturning *Q.J.R. Meteorol. Soc.*, **98**, 336-352.

104. Moncrieff, M.W. and Miller, M.J., 1976 : The dynamics and simulation of tropical cumulonimbus and squall lines. *Q.J.R. Meteorol. Soc.*, **102** 373-394.

105. Narasimhan, M.N.L. and Saibel, E.A., 1989 : Turbulence in journal bearings from a non local point of view. *Int. J. Engng. Sci.*, **27**, 219-236.

106. Neiuwstadt, F.T.M. and Van Dop, H. (eds.) 1984 : **Atmospheric Turbulence and Air Pollution Modelling**. D.Reidel Publishing Company, Dordrecht, Holland. 358 pp.

107. Newton, C.W., 1951 : Note on the mechanisms of Nor'westers of Bengal. *Ind. J. Met. Geophys.*, **2**, 169-186.

108. Pant, P.S., Abbi, S.D.S., Gupta, D.K. and Harish Chandra, 1970: A study of major rainstorms of Assam. *Ind. J. Met. Geophys.*, **21**, 169-186.

109. Pasch, R.J., 1983 : On the onset of the planetary scale monsoon. *Report No. 83-9. Department of Meteorology, Florida State University.* Tallahassee, Florida, 32306. pp 1-220.

110. Pennell, W.T. and Le Mone, M.A., 1974 : An experimental study of turbulence structure in the fair weather trade wind boundary layer *J. Atmos Sci.*, **31**, 1308-1323.

111. Pielke, R.A., 1984 : **Mesoscale Meteorological Modelling.** Academic Press, Orlando, Florida. 612pp.

112. Prahm, L.P., Berkowicz, R. and Christensen, O., 1979 : Generalization of K - theory for turbulent diffusion, Part II : Spectral diffusivity model for plume dispersion. *J. Appl. Meteorol.*, **18**, 273-282.

113. Raghavan, K., 1973 : Break - Monsoon over India. *Mon. Weather Rev.*, **101**, 33-43.

114. Rai Sircar, N.C., 1954 : On the use of tephigrams for forecasting Nor'westers. *Ind. J. Met. Geophys.* **4**, 269 -

115. Ramage, C.S., 1971 : **Monsoon Meteorology**. *International Geophysical Series.* **15**. Academic Press, New York and London. 276 pp.

116. Ramamurthi, K., 1969 : Monsoons of India : Some aspects of the 'break' in the Indian south-west monsoon during July and August. *India Meteorological Department Forecasting Manual, Part, IV*, No. N - 18. 3. pp. 1-13.

117. Ramaswamy, C., 1956 : On the sub-tropical jet stream and its role in the development of large scale convection. *Tellus* **8**, 26-60.

118. Ramaswamy, C. and Bose, B.L., 1953a : On cold pools and their role in the development of Nor'westers over West Bengal and East Pakistan. *Curr. Sci.*, **22**, 103–105.

119. Ramaswamy, C. and Bose, B.L., 1953b : On the importance of the mid-and upper tropospheric thermal systems in the development of weather in northeastern India and East Pakistan during the Nor'wester season. *Curr. Sci.*, **22**, 291-294.

120. Ramaswamy, C. and Bose, B.L., 1954 : On certain new aspects of the thermal patterns associated with nor'westers over Northeastern India and East Pakistan *Curr. Sci.* **23**, 75-77.

121. Rao, Y.P. 1976 : **South West Monsoon.** Meteorological monography, Synoptic Meteorology 1/76, IMD, New Delhi, 140 pp

122. Randall, D.A., 1985 : Parameterization of the interactions between boundary–layer clouds and boundary–layer turbulence. pp 91–120 in: **Physical Parameterization for Numerical Models of the Atmosphere**,Volume I 9–13 September, ECMWF, Shinfield Park, Reading, U.K.

123. Roberts, P.H., 1961 : Analytical theory for turbulent diffusion. J. Fluid. Mech., **11**, 257–283.

124. Rees, J.M., 1987 : The propagation of internal gravity waves in the stably stratified atmospheric boundary layer. *Ann. Geophys.*, **5B** 421–432.

125. Romanof, N., 1982 : Application of Wiener-Hermite expansions to turbulent diffusion. *Meteor. and Hydrology.*, **2** , 25-31.

126. Romanof, N., 1989 : Nonlocal models in turbulent diffusion. *Z. Meteorol.*, **39**, 89-93.

127. Saffman, P. G., 1969 : Application of the Wiener - Hermite expansions to the diffusion of a passive scalar in homogeneous turbulent flow. *Phys. Fluids.* **12**, 1786-1798.

128. Schlesinger, R.E., 1978 : A three dimensional numerical model of an isolated thunderstorm. Part I : Comparative experiments for variable ambient wind shear. *J. Atmos. Sci.*, **35**, 690-713.

129. Schlesinger, R.E., 1980 : A three dimensional numerical model of an isolated thunderstorm. Part II : Dynamics of updraft splitting and mesovortex couplet evolution. *J. Atmos. Sci.* **37**, 395-420.

130. Sikka, D.R. and Gadgil, S., 1980 : On the maximum cloud zone and the ITCZ over Indian

longitudes during the southwest monsoon., *Mon. Weather Rev.* **108**, 1840-1853.

131. Sinha, D.K. and Sen, G.K., 1994 : The Nor'wester scenario : The role of internal gravity waves. *Proc. Indian Natn. Sci. Acad., Ser A,* **60**, 171-179.
132. Stanisic, M.M., 1985 : **The mathematical theory of turbulence. Universitext.** Springer-Verlag, 429 pp.
133. Stull, R.B., 1984 : Transilient turbulence theory. Part I : The concept of eddy - mixing across finite distances *J. Atmos. Sci.* **41**, 3351-3367.
134. Stull, R.B., 1986 : Transilient turbulence theory. Part III : Bulk dispersion rate and numerical stability. *J. Atmos., Sci.* **43**, 50-57.
135. Stull, R.B., 1987 : Transilient turbulence algorithms to model mixing across finite distances. *Environ. Software,* **2**, 4-12.
136. Stull, R.B., 1988 : **Introduction to Boundary Layer Meteorology.** Kluwer Academic Publishers Dordrecht, The Netherlands. 666 pp.
137. Stull, R.B., 1991 : Static stability - An update. *Bull. Am. Meteorol. Soc.* **72**, 1521-1529.
138. Stull, R.B., 1992 : Review of transilient turbulence theory and nonlocal mixing *Bound Layer. Meteorol.,* **45**.
139. Stull, R.B. and Driedonks. A.G.M., 1987 : Applications of the transilient turbulence parameterization to atmospheric boundary layer simulations. *Bound. Layer Meteorol.,* **40** 209-239.
140. Stull, R.B. and Hasegawa, T., 1984 : Transilient turbulence theory. Part II : Turbulent adjustment. *J. Atmos. Sci.,* **41**, 3368-3379.
141. Thorpe, A.J., Miller, M.J. and Moncrieff, M.W., 1982 : Two dimensional convection in non-constant shear : A model of mid-latitude squall lines. *Q.J.R. Meteorol. Soc.* **108**, 739-762.
142. Uccellini, L.W., 1975 : A case study of apparent gravity wave initiation of severe convective storms. *Mon.Weather Rev.,* **103**, 497-513.
143. Wei, M. Y., Johnson, D.R. and Townsend, R.D., 1981: The structure of planetary scale diabatic processes for the atmosphere during FGGE. pp 35 - 42 in : **Int. Conf. on Early Results of FGGE and Large Scale Aspects of its Monsoon Experiments. Tallahassee. U.S.A.** *WMO, Geneva, Session 3.*
144. Wei, M.Y. and Johnson, D.R., 1982 : The spatial and temporal variation of diabatic heating during the summer monsoon pp 1 - 3, in : **Int. Conf. on the scientific Results of MONEX Denpasar., Bali, Indonesia.** *WMO, Geneva, Session 1.*
145. Weismann, M.L. and Klemp, J.B., 1982 : The dependence of numerically simulated convective storms to the vertical windshear and buoyancy. *Mon. Weather Rev.,* **110**, 504-510.
146. Wichmann, M. and Schaller, E., 1986 : On the determination of the closure parameters in higher order closure models. *Bound.– Layer Meteorol.* **37**, 323-3241.
147. World Meteorological Organisation, 1978 : **The South East Asian Monsoon.** 73 pp.
148. Wyngaard, J.C., 1975 : Modelling the planetary boundary layer - extension to the stable case. *Bound.– Layer Meteorol.,* **9**, 441-460.

149. Wyngaard, J.C., 1984 : Boundary layer modelling pp 69-106 in, **Atmospheric Turbulence and Air Pollution Modelling.** F.T.M. Nieuwstadt and H. Van Dop (eds.) *D.Reidel Publishing Company, Holland.*

150. Wyngaard, J.C. and Coté, O.R., 1971 : The budgets of turbulent kinetic energy and temperature variance in the atmospheric surface layer *J. Atmos. Sci.* **28**, 190-201.

151. Wyngaard, J.C. and Coté, O.R., 1974 : The evolution of a convective planetary layer a higher order closure model study. *Bound.– Layer. Meteorol.* , **7**, 284-308.

152. Yamada, T. and Mellor, G., 1975 : A simulation of the Wangara atmospheric boundary layer data. *J. Atmos. Sci.*, **32**, 2309-2329.

153. Yasunari, T., 1981 : Structure of an Indian summer monsoon system with around 40 - day. *J. Meteorol. Soc. Japan.*, **59**, 336-354.

154. Zeman, O., 1981 : Progress in the modelling of planetary boundary layers. *Ann. Rev. Fluid. Mech.*, **13**, 253-272.

155. Zhang, D. and Anthes, R.A., 1982 : A high resolution model of the planetary boundary layer sensitivity tests and comparisons with SESAME - 79 datga *J. Appl. Meteorol.*, **21**, 1594–1609.